An Investigation of Low-Energy Injection for Electron Storage Rings

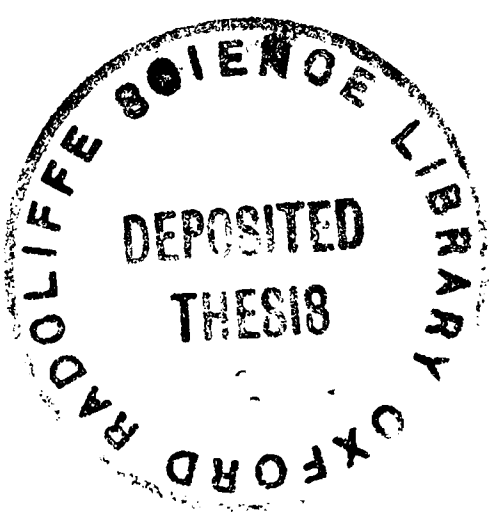
Jan Arie Uythoven

Green College

Von 1

A thesis submitted for the degree of Doctor of Philosophy
at the University of Oxford

March 1991



Part of this thesis is not publicly accessible until April 1993. This concerns sections 5.1, 5.2 and 5.3, the paragraphs in chapter 6 where reference is made to the experimental results mentioned in chapter 5 and the whole of chapter 7.

Voor mijn ouders.

An Investigation of Low-Energy Injection for Electron Storage Rings

Jan Arie Uythoven
Green College

A thesis submitted for the degree of Doctor of Philosophy
at the University of Oxford

March 1991

Abstract

This thesis reports on low-energy injection studies, considering a multi-shot and multi-turn injection method in radial phase space, using only one kicker magnet. A new model is presented in which the coupling between the radial and longitudinal phase space significantly increases the injection efficiency at low energies. Coupling with the longitudinal phase space takes place if the energy of the injected beam is different from the equilibrium ring energy and if there is dispersion at the septum position. Coupling with the vertical phase space, introduced by skew quadrupole fields, also increases the injection efficiency.

A computer program, MCIS, has been written in order to make quantitative predictions from the new model. Calculations are presented for HELIOS, a superconducting synchrotron with a final electron energy of 700 MeV. The present injection energy is 200 MeV. The calculations show that if injection were to take place off-energy by $\delta_m \approx 1$ %, then the injection energy could be lowered to a minimum of about 35 MeV. This prediction only takes into account single particle beam dynamics. The effect of most other parameters on the injection efficiency is also calculated.

Experimental studies of the injection process were performed during the commissioning period of Helios, which was carried out by a team under the author's direction. Data obtained at an injection energy of 100 MeV are compared with calculations. A precise measurement of the relative energy deviation of the injected beam δ_m has been made. The agreement with the model is good and it proves the presence of longitudinal coupling for the optimum injection conditions. The measurement of the optimum kicker strength also agrees with the model, as does the general behaviour of injection as a function of several parameters. The measurements lead to a high level of confidence in the model presented.

The belief in the general validity of the model is reinforced by its agreement with the overall injection behaviour of accelerators other than HELIOS, which inject successfully at low energies.

Acknowledgements

The writing of a thesis, and especially the research which has to be carried out first, can not be done without the help of many people. This certainly applies to my past three years in Oxford, and I would like to thank all the people who contributed directly or indirectly to what finally resulted in this thesis. Some of them I would like to mention by name: first I would like to thank John Mulvey and George Doucas, my supervisors at the Nuclear Physics Laboratory, who always found the time to listen to me and help me in every way they could. The life in Oxford and at the lab would have been very boring without the people in room 6.51. Many friends 'lived' in this office, so I have to restrict myself to mentioning only those who also helped me to develop my frisbee skills: Nigel Crosland, Harald Borner, Martin Bates and Christine Beeston. I would also like to thank Peter Gronbech; without his help my jobs would still not have finished running on V1.

The first secrets about electron injection I learned from Vic Suller and I would like to thank him, and many other people at the SRS Daresbury, for the many stimulating discussions.

During my three years at Oxford Instruments I enjoyed a high level of freedom in almost all my work. I think this is essential for any good research and for this I would like to thank Martin Wilson and Vince Kempson. In everyday life at Oxford Instruments Peter Hamilton, David Ockwell, Vince Kempson and everybody else from the synchrotron group were always prepared to help me. I would never have survived the night shifts without the help of Ian Underhay and Chas Archie. I would also like to thank Mark Barton and Chas Archie for the many inspiring discussions.

I will also never forget the love and support from Lidy, my parents and especially Corinne.

Jan Uythoven,
March 1991.

"I do not know what I may appear to the world, but to myself I seem to have been only like a boy playing on the sea-shore, and diverting myself in now and then finding a smoother pebble or a prettier shell than ordinary, whilst the great ocean of truth lay all undiscovered before me."

Sir Isaac Newton.

Contents

Abstract i

Acknowledgements ii

Table of Contents iii

Table of Symbols vi

1 Introduction 1

1.1 Synchrotron Radiation 2

1.2 X-Ray Lithography 6

1.3 Synchrotrons for X-ray Lithography 8

1.4 HELIOS 11

2 General Accelerator Theory 18

2.1 Basic Quantities 18

2.2 The Betatron Motion and Twiss Parameters 20

2.3 Coupling between the two Transverse Directions 27

2.4 The Synchrotron Motion 28

2.5 Synchrotron Radiation Damping 30

3 Electron Injection 35

3.1 General Description 35

3.2 Low-Energy Injection 39

3.2.1 Coupling with the Longitudinal Phase Space 40

3.2.2 Coupling with the Vertical Phase Space 42

3.3 The Injector 43
3.4 Other Injection Methods 46

4 Computer Modelling of the Injection Process **48**
4.1 Description of the Program MCIS 50
4.1.1 Radial and Longitudinal Phase Space 51
4.1.2 Coupling with the Vertical Phase Space 60
4.2 Results of Simulations with MCIS 67
4.2.1 Choice of Software Parameters 67
4.2.2 Simulations for HELIOS 70
4.2.3 Simulations for MAX 91

5 Experimental Results **95**
5.1 Additional Processes in a Real Machine 95
5.2 Experiments at 100 MeV 98
5.2.1 Experimental Conditions at 100 MeV 99
5.2.2 Results at 100 MeV 102
5.3 Results at 65 MeV 111
5.4 Results from other Machines 112
5.4.1 Experimental Results MAX 112
5.4.2 Experimental Results COSY 113

6 Summary, Discussion and Conclusions **115**
6.1 Summary 115
6.2 Discussion 119
6.3 Conclusions 122

7 Experimental Background **124**
7.1 Measurement of the Linac Beam Parameters 125
7.1.1 Emittance and Twiss Parameters 125
7.1.2 Linac Energy Spread 133
7.2 Setting up of the Transport Line and Obtaining Injection 135

7.3 Measurement of the Closed Orbit 140
7.4 Measurement of the Betatron Tunes and Synchrotron Tune 142
7.4.1 Measurement of the Betatron Tunes 142
7.4.2 Measurement of the Synchrotron Tune 143
7.5 Measurement of the Chromaticity 145
7.6 Levelling of the Vertical Beta Function 147
7.7 Measurements of the Dispersion Function 150
7.8 Measurement of the Transverse Coupling 152
7.9 Overview of the Commissioning in Oxford 154

A Equations of Motion up to Second Order **159**

B Input and Output Parameters of MCIS **161**
B.1 Input Parameters 161
B.2 Output Parameters 164
B.3 CPU-time 164

C List of HELIOS Notes and Publications **166**

Bibliography **168**

Summary in Dutch (Samenvatting) **174**

Table of Symbols

Symbols used only in one place and defined in the text are omitted here. SI units are used throughout the report, except the (electron) energy is in eV according to general convention.

$B(s)$	magnetic induction
C, C_0	ring circumference, orbit length and orbit length of reference particle
c	velocity of light in vacuum
E	total energy of the particle
g	coupling strength
h	harmonic number
k	coupling constant of a skew quadrupole
$K(s)$	focusing strength of the magnetic field
M	transfer matrix between two azimuthal positions
$n(s)$	magnetic field index
p, p_0	momentum of the particle and reference momentum
q	charge of the particle
s	longitudinal coordinate, path length
U_0	energy loss per turn
W	longitudinal phase space coordinate related to the energy deviation
x, x'	horizontal transverse coordinate and its derivative towards s
y, y'	vertical transverse coordinate and its derivative towards s
z, z'	horizontal or vertical transverse coordinate and its derivative
α	momentum compaction factor
$\alpha(s)_{x,y}$	Twiss parameter
$\beta(s)_{x,y}$	Twiss parameter, beta-function
$\gamma(s)_{x,y}$	Twiss parameter
δ	relative energy deviation
$\mathcal{E}_{x,y}$	particle emittance
$\mathcal{E}_T$	total particle emittance
$\varepsilon_{x,y}$	beam emittance
$\eta(s)$	horizontal dispersion function
λ_c	critical wavelength of the synchrotron radiation spectrum
$\mu_{x,y}(s)$	betatron phase
$\nu_{x,y}$	betatron tune
ν_s	synchrotron tune
$\xi_{x,y}$	chromaticity
$\rho(s)$	bending radius of the orbit
$\sigma_{x,y,\epsilon}$	equilibrium beam size or energy spread
$\tau_{x,y,\epsilon}$	synchrotron radiation damping time
ϕ	RF-phase in longitudinal phase space
ω_0	angular orbit frequency of the reference particle
Ω_0	angular synchrotron oscillation frequency

Chapter 1

Introduction

HELIOS is a compact synchrotron light source made by Oxford Instruments. The maximum electron energy is 700 MeV. To minimise the size of the synchrotron, it has a race-track design with two 180° superconducting dipole magnets. The synchrotron has just finished its commissioning phase in Oxford and at the time of writing of this thesis (March 1991) it is in the process of being shipped to the I.B.M. laboratories in East Fishkill, close to New York City. There it is going to be used as the light source in an X-ray lithography production plant for integrated circuits.

In this thesis the possibility of using low-energy electrons (around 50 MeV) for injection in HELIOS is investigated. The advantages of a lower injection energy than the present 200 MeV are that the size of the total system can significantly be reduced, the required radiation shielding around the ring can be reduced and the costs of the injector and the transport line are lower. The theory which is developed to study the low-energy injection process is not only valid for HELIOS, but for electron storage rings in general.

The first section of this chapter discusses the general properties of synchrotron radiation. This is followed by a section on the X-ray lithography process and the choice of X-ray source. Section 1.3 concentrates on the kind of synchrotron most useful for X-ray lithography and in section 1.4 the main features of HELIOS, as it has been built by Oxford Instruments, are described.

Chapter 2 is an introduction to accelerator physics, mainly summarising the 'tools' used in the rest of this thesis. A qualitative description of the electron injection process, with a discussion of the function of special injection magnets and

the vital role played by synchrotron radiation damping, is given in chapter 3. In this chapter a definition of *low*-energy injection and a new approach to electron injection calculations at low energies is introduced. It is explained in which way coupling between the different phase spaces and random processes in the electron beam can increase the injection efficiency. A computer program, MCIS, has been written to make quantitative predictions from the new theories. The program is described in chapter 4, together with results of injection calculations using this program. Calculations are presented for HELIOS and the MAX accelerator (Sweden). Chapter 5 describes the injection experiments carried out on HELIOS during the commissioning period in Oxford. Comparisons are made with MCIS calculations, where the experimental conditions are used as input parameters for the program. The low-energy injection results of MAX and COSY (Germany), as reported by their laboratories, are also discussed. Chapter 6 summarises and discusses the calculations and experimental work presented in chapters 4 and 5. Predictions are made about the lowest possible injection energy for HELIOS, using the present system of injection, and the requirements on hardware parameters imposed by the injection system. Finally, chapter 7 describes the commissioning of Helios.

1.1 Synchrotron Radiation

Synchrotron radiation is emitted by charged particles which are accelerated. The bending magnets in a synchrotron accelerate the particles towards the centre of the ring and it is in these magnets where most of the synchrotron radiation is emitted. For a circular accelerator with bending magnets of equal strength, resulting in a bending radius ρ, the amount of energy radiated per revolution by a single particle is

$$U_0 = \frac{4\pi}{3} r_0 m_0 c^2 \beta^3 \gamma^4 / \rho \tag{1.1}$$

where r_0 is the classical radius of the particle ($r_0 = q^2/(4\pi\varepsilon_0 m_0 c^2)$), m_0 the rest mass of the particle, c the velocity of light and β and γ are the usual relativistic quantities: $\beta = v/c$ and $\gamma = E/(m_0 c^2)$. This expression shows the strong dependence of the

energy loss per turn on the rest mass m_0 and the total energy E of the particle. As a consequence, synchrotron radiation is only significant in present day accelerators which accelerate light particles, electrons and positrons. For high energy accelerators which use these particles, synchrotron radiation is considered as a highly undesirable phenomenon. The energy loss of the particle per turn due to synchrotron radiation can be significant, influencing strongly the size of the accelerator or the maximum energy attainable in a certain ring. The recently built LEP accelerator at CERN [LEP84] is a very good example[1]. Synchrotrons were first built almost entirely for use in high energy physics; subsequently dedicated synchrotrons were built for the exploitation of the emitted synchrotron light. Here the aim is not to accelerate the particles to as high an energy as possible, but to obtain synchrotron light of the desired frequency. The frequency can be shifted to different wavelengths by the use of special insertion devices, such as wigglers and undulators, placed in the straight sections of the ring [ELL90]. At the moment synchrotron light sources are used by many scientists all over the world, for research varying from solid state physics to cancer research. Now for the first time synchrotrons are to be introduced in an industrial *production* environment as light sources in the X-ray lithography process.

For relativistic electrons ($\beta \approx 1$) equation 1.1 can be written in more convenient energy units and also the values for r_0 and m_0 can be substituted. This results in

$$U_0[\mathrm{keV}] = 88.47 \frac{E^4[\mathrm{GeV}]}{\rho[\mathrm{m}]} = 26.54 E^3[\mathrm{GeV}] B[\mathrm{T}] \tag{1.2}$$

Here B is the magnetic field in the bending magnets.

The synchrotron radiation emitted by a non-relativistic electron which is travelling in a circular path, as seen by a stationary observer, has a dipole distribution. For a relativistic electron, the observer sees a Lorentz transformed radiation pattern [JAC75], which is peaked forward and highly collimated with a typical half opening

[1]The dipole magnets in LEP have a very small magnetic field of only 0.06 T. Using superconducting dipoles of 6 T, the bending radius in the dipoles is reduced by a factor of 100; without taking into account the long straight section needed around the detectors, the circumference could be reduced from the present 26.7 km to about 300 m (!). But the RF-power, needed to compensate for the energy loss of the beam by synchrotron light, will have to be increased from 16 MW to 1600 MW. This is the output power of a medium sized power station.

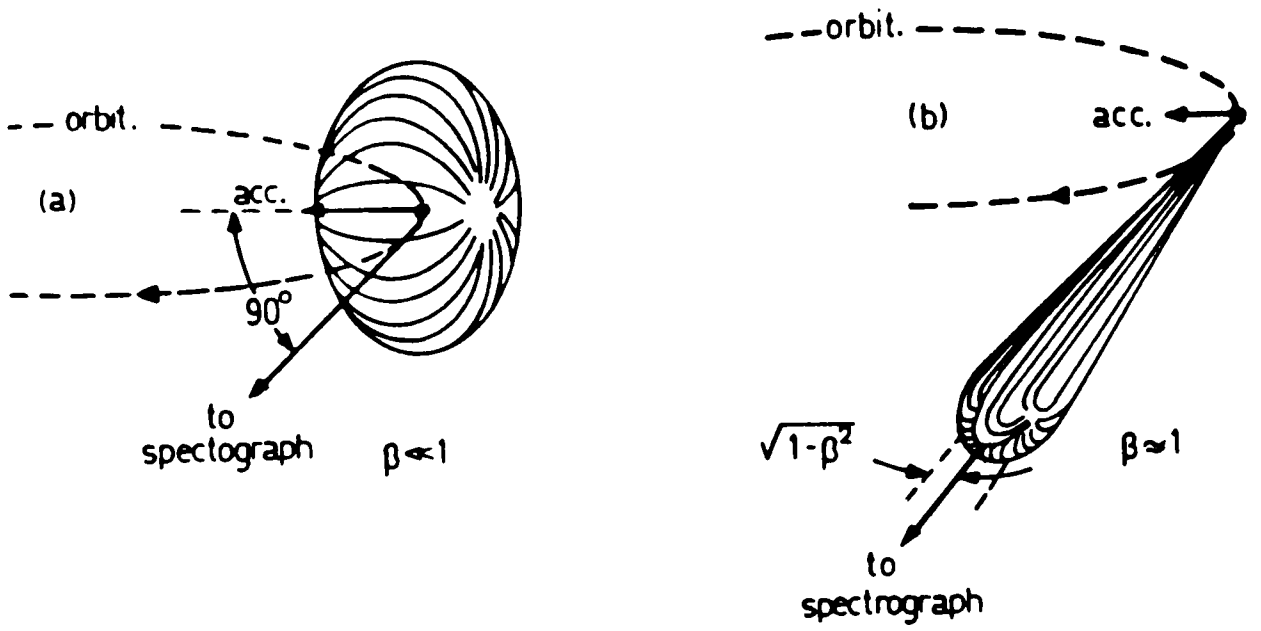


Figure 1.1: The radiation pattern of a slow (a) and relativistic (b) electron in a circular orbit [TOM56].

angle $1/\gamma$, see figure 1.1. It is worth realising that this opening angle depends on the wavelength of the radiation, but in general it is very small because $\gamma \gg 1$ (for example in HELIOS $\gamma \approx 1400$).

Knowing the opening angle of the synchrotron light, an estimate can be made of the typical frequency of the emitted spectrum. Consider the situation of an electron travelling through a bending magnet, emitting synchrotron light which reaches an observer P, see figure 1.2. Because of the small opening angle $1/\gamma$, the observer can only see the synchrotron light emitted from the particle when it is between position A and A'. At position A the angle of the particle orbit with the line of sight of the observer is $1/\gamma$ and at position A' this angle is $-1/\gamma$. The length of the radiation pulse as seen by the observer is the difference in travel time between the electron and the photon going from A to A':

$$\Delta t = t_e - t_\gamma = \frac{2\rho}{\beta\gamma c} - \frac{2\rho \sin(1/\gamma)}{c} \tag{1.3}$$

Because $1/\gamma$ is small, $\sin(1/\gamma)$ can be expanded, leading to

$$\Delta t \approx \frac{2\rho}{\beta\gamma c}\left(1 - \beta + \frac{\beta}{6\gamma^2}\right) \tag{1.4}$$

Now using the approximation

$$1 - \beta = \frac{1-\beta^2}{1+\beta} \approx \frac{1}{2\gamma^2} \tag{1.5}$$

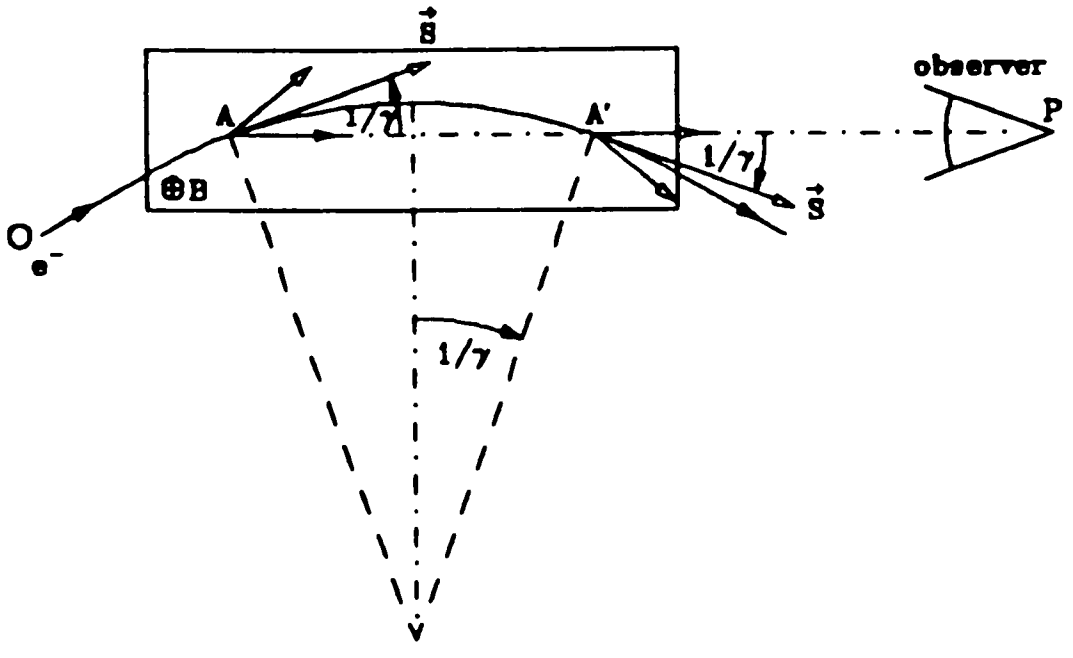


Figure 1.2: Synchrotron light as seen by an observer at position P [HOF90].

the time interval can be written as

$$\Delta t \approx \frac{2\rho}{\gamma c}\left(\frac{1}{2\gamma^2}+\frac{1}{6\gamma^2}\right) = \frac{4}{3}\frac{\rho}{c\gamma^3} \tag{1.6}$$

In accordance with Fourier analysis the emitted spectrum of the particle consists of frequencies up to

$$f = \frac{1}{\Delta t} \approx \frac{c\gamma^3}{\rho} \tag{1.7}$$

The radiation spectrum is conventionally characterised by the *critical wavelength* λ_c, which divides the power spectrum in two equal halves.

$$\lambda_c = \frac{4\pi\rho}{3\gamma^3} \tag{1.8}$$

In more practical units this can be written as

$$\lambda_c[\text{Å}] = 5.59\frac{\rho[\text{m}]}{E^3[\text{GeV}]} = \frac{18.6}{B[\text{T}]E^2[\text{GeV}]} \tag{1.9}$$

The universal synchrotron radiation spectrum as given in figure 1.3 (in number of photons/s/mrad/mA/GeV in a 0.1 % bandwidth of λ/λ_c) shows the significance of the critical wavelength.

Because the acceleration of the electron mainly takes place in the radial direction, the emitted synchrotron light is highly polarised with the electric field in the median plane.

A more complete treatment of synchrotron light can be found in [SOK66, HOF90, JAC75, PAN62].

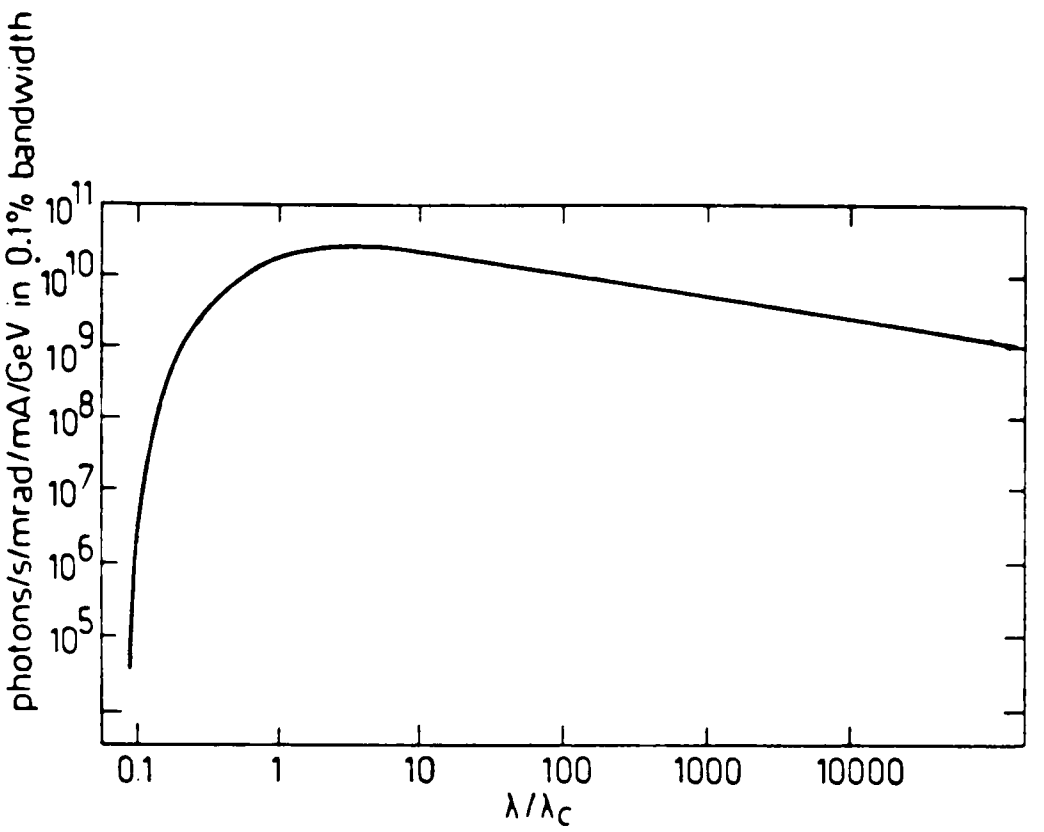


Figure 1.3: Universal synchrotron radiation spectrum [SUL73].

1.2 X-Ray Lithography

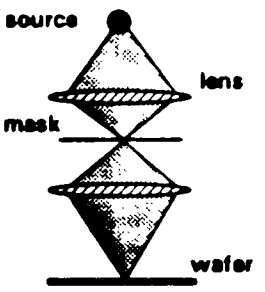
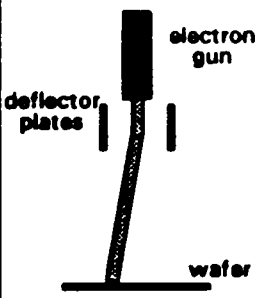
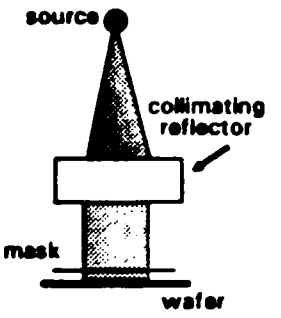
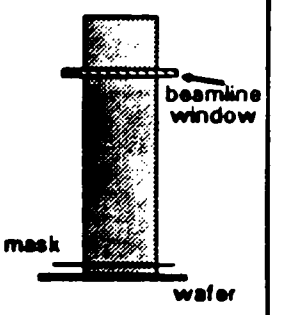
At the moment all mass produced integrated circuits are made by a photo lithography process, in which the image of a 'master' mask is projected onto the surface of a silicon wafer which has been coated with light sensitive 'photo-resist'. Washing the wafer with a solvent dissolves the unwanted resist and leaves a copy of the mask design on the wafer. The 4 Mbit DRAM (Dynamic Random Access Memory), which requires a resolution around 0.8 μm, can now be made routinely. The resolution is generally defined as the width of a valley on the circuit. Research has pushed the limits of optical lithography to 0.35 μm resolution by reducing the wavelength of the light source to the deep ultraviolet and a different choice of the resist material. This moves the 64 Mbit DRAM into the range of optical lithography. The problems related with optical lithography are many: lenses are necessary for the focusing of the light on the mask and again from the mask on the wafer. These lenses have a very small depth of focus (around 1 μm). Because of the small patterns on the mask, there is the danger of diffraction. If the wavelength is shifted in the deep

ultraviolet, the exposure times generally increase, resulting in a smaller throughput of wafers per hour.

Another technique is electron beam writing. With this technique high resolutions can be achieved, but because of the long time required to write one chip, it is not very interesting for mass production.

X-ray lithography solves most of these problems, although some others are introduced. Of course, the main advantage is that because of the few hundred times smaller wavelength there is no danger of diffraction. For X-ray sources a shadow printing technique has to be used, because the light can not easily be focused with optical lenses. The shadow printing process increases the depth of focus typically to 25 – 50 μm, which is about the proximity gap between the mask and the wafer, but a highly collimated beam (around 1 mrad divergence) is necessary for this process. Another advantage is that the process is largely insensitive to dust, because most dust particles are transparent to X-rays. This is of high practical importance, because large amounts of money are spent to make the chip production area dust free. But X-rays introduce new problems. The most important problem is the mask manufacturing: because the substrate of the mask is not completely transparent to X-rays, the masks have to be very thin, and also have an extreme detail with tolerances around 0.1 μm. Because of the complexity of the masks, it is almost essential to develop a mask repair technology. With X-ray lithography the limit of the resolution obtainable is 0.2 μm or less. The first mass produced circuit using X-ray lithography is probably going to be the 256 Mbit DRAM.

There are different X-ray sources proposed for lithography: electron bombardment sources with conventional or rotating anodes, laser plasmas, Z-pinch plasmas and electron synchrotrons. Synchrotrons are favourable because of the natural strong vertical collimation. Most other sources need a large distance between the source and the mask to reduce the divergence, which leads to a large decrease in photon flux. Synchrotrons have a very large photon flux, which reduces the exposure time to less than 10 s (depending on the resist material), and the possibility to connect many lithography ports to one light source. Another advantage of the

Integrated-Circuit Microlithography Techniques				
	optical projection	electron beam writing	laser-generated X-ray *	synchrotron generated X-ray*
exposure source system				
source wavelength (nanometers)	435 (g-line) 365 (i-line) 248 (deep ultraviolet)	20-50 thousand electron-volt beam	2.2 - 0.8	1.1 - 0.8
minimum feature size on wafer (microns)	0.65 0.50 0.35	0.15	0.15	0.15
throughput (wafers/hour)	40 40 20	4	20 - 40	40

Data from Hampshire Instruments

* prototype techniques

Figure 1.4: Comparison of the different micro-lithography techniques.

synchrotron is the almost continuous light beam, so there is no peak in heat load of the exposed system.

The different processes of microlithography are compared in figure 1.4. More information on the different techniques and X-ray sources can be found in [WIL85, HEU86, GRO83, CUL87].

1.3 Synchrotrons for X-ray Lithography

X-ray lithography imposes several constraints on a synchrotron which is intended as a light source.

- The currently available resist and mask technologies require a critical wavelength λ_c between 6 and 12 Å.
- The horizontal and vertical beam dimensions should be around 1 mm and the vertical beam divergence around 1 mrad.

- The requirement on total radiated power is around 5 kW, but significantly different numbers, varying from 1 – 10 kW, are quoted by the various lithography groups, demanding a different throughput of wafers or using a different resist material.

- The size of the accelerator has to be as small as possible, because it is situated in the centre of a high technology X-ray lithography plant, where every square meter of floor space is expensive.

The desired critical wavelength can be obtained by various combinations of ring energy and magnetic field. If iron based magnets with a magnetic field of 1.3 T are used, the required energy for a critical wavelength $\lambda_c = 8.4$ Å is 1.3 GeV (see equation 1.9). This results in a machine with a *bending* radius of 3.3 m, which would probably have a total circumference of more than 50 m. A synchrotron using superconducting dipoles with a magnetic field of 4.5 T needs to have an electron energy of 700 MeV to obtain the same critical wavelength, resulting in a bending radius of 0.52 m. The smallest possible superconducting synchrotron has only one magnet, bending over 360^0, resulting in an orbit circumference of 3.3 m [TAK87a]. A less adventurous machine, which is still very compact, can be made by using 2 dipole magnets, both bending over 180° (race-track design). The circumference of these types of machines is around 10 m, depending on the focusing structure and special devices which have to be fitted in the two straight sections. Many different arrangements can be found for machines with superconducting magnets, but the race-track design with two bending magnets seems to be a good compromise between compactness and risk. It is the solution chosen by most groups (see also table 1.1).

A disadvantage of the superconducting synchrotron is that the total radiated power is less than that from a normal conducting synchrotron with the same critical wavelength. This is because of the dependence of U_0 on energy, see equation 1.2. For the conventional synchrotron mentioned in the example above, the energy loss per turn $U_0 = 76$ keV. For the superconducting example it is 41 keV: almost twice

as much current is necessary in a superconducting light source to obtain the same radiated power. The smaller amount of total power radiated by the superconducting ring can be (partly) compensated; for X-ray lithography the emitted power per unit area is important, which can be increased by a reduction of source size.

An advantage of the superconducting ring is that it can be mounted on a frame and fully tested and commissioned on the manufacturer's site, before it is shipped to the X-ray lithography plant.

There are two main areas in which research on compact superconducting synchrotrons takes place.

- The superconducting dipoles are the most novel and complicated elements of the accelerator, especially if they have a large bending angle of 180°. A high accuracy in the magnetic field is important for stable and repeatable electron orbits (the magnetic field has to be known to an accuracy of $1{:}10^4$), which has to be maintained while the magnetic field is increased from its value during injection to that at the final energy. The fringe fields at the entrance and exit of the magnet have to be well understood; a too large component of higher order magnetic fields can have a large impact on the operation of the machine.

- The other topic of research on compact accelerators is the injection system. To obtain the required radiation power, a current of more than 100 mA has to be stored. The most conventional method of injection is a multi-shot method, in which the synchrotron radiation damping times are very important (see chapter 3). These damping times are ideally close to or smaller than the injection interval. This generally results in an injection energy above 200 MeV, for a superconducting 700 MeV synchrotron, with the extreme being full-energy injection. The cost and size of a full energy injection system are similar to the storage ring itself; also a 200 MeV linear injector, together with the transport line between injector and ring, is in size comparable with the synchrotron. It is of great interest to decrease the injection energy.

1. The size of the total system can be significantly reduced if injection takes place at a lower energy. Not only is the injector smaller, but it is very often possible to place the injector close to the synchrotron, so one vault contains the total system.
2. The amount of radiation shielding required is determined by particle loss during injection. The radiation shielding can significantly be reduced if injection takes place at lower energies.
3. Because of the reduction in size and energy of the injector and transport line, the total cost of the system is significantly reduced.

The second area of research, injection, is treated in detail in this thesis.

An overview of synchrotrons for X-ray lithography can be found in [WEI90, WIL90, HIR90]. A list of present projects is given in table 1.1.

1.4 HELIOS

Most of the calculations and measurements reported in this thesis are for the Oxford Instruments synchrotron HELIOS (High Energy Lithography Illumination by Oxford's Synchrotron). This chapter gives an overview of the machine and its performance during the commissioning period in the summer and autumn of 1990. Currents of more than 500 mA have been injected at the injection energy of 200 MeV. More than 100 mA has been stored at full energy (700 MeV). The design current at full energy is 200 mA, which is expected to be achieved after shipment to East Fishkill.

The present injection energy is 200 MeV (HELIOS 1). This is a conservative choice, originating from the time no detailed injection studies had been made and no experimental injection results of compact synchrotrons were available. Because of the theoretical and experimental results mentioned in this thesis, the injector for the next machine, HELIOS 2, will be a 100 MeV microtron. It is very possible that machines following HELIOS 2 will inject at even lower energies. According to the

Table 1.1: Overview of present compact synchrotron projects worldwide (data are taken from [WIL90]).

	Superconducting magnets					
Name	Aurora	COSY	HELIOS 1	NIJI 3	SuperALIS	SXLS
Location	SHI	IMT	OI	ETL	NTT	BNL
	Tokyo	Berlin	Oxford	Tsukuba	Atsugi	Long Island
	Japan	Germany	England	Japan	Japan	USA
Orbit perimeter	3.14 m	9.6 m	9.6 m	15.54 m	16.8 m	8.5 m
No. of dipoles	1	2	2	4	2	2
Electron energy	650 MeV	592 MeV	700 MeV	615 MeV	600 MeV	700 MeV
Bending field	4.33 T	4.47 T	4.5 T	4.1 T	3.0 T	3.87 T
Critical wavelength	1.02 nm	1.2 nm	0.84 nm	1.2 nm	1.73 nm	0.98 nm
Injection energy	150 MeV	50 MeV	200 MeV	180 MeV	15 MeV	200 MeV
Injector type	Microtron	Microtron	Linac	Linac	Linac	Linac
Injector current	7 μA (5 mA)	30 mA	20 mA	50 mA	200 mA	?
Achieved current at full energy	45 mA	1 mA	100 mA	70 mA	100 mA	–

	Iron based magnets			
Name	CAMD	Luna	NAR	Soretec 1
Location	University	IHI	NTT	Sortec
	Louisiana	Tsukuba	Atsugi	Tsukuba
	USA	Japan	Japan	Japan
Orbit perimeter	55.2 m	23.5 m	52.8 m	45.7 m
No. of dipoles	8	4	8	8
Electron energy	1200 MeV	800 MeV	800 MeV	1000 MeV
Bending field	1.37 T	1.33 T	1.44 T	1.2 T
Critical wavelength	0.95 nm	2.2 nm	2.02 nm	1.55 nm
Injection energy	200 MeV	45 MeV	15 MeV	1000 MeV
Injector type	Linac	Linac	Linac	Synchrotron
Injector current	25 mA	100 mA	200 mA	30 mA
Achieved current at full energy	–	15 mA	20 mA	200 mA

Table 1.2: Main parameters of HELIOS 1 for a typical tune point.

Operating energy	E	700	MeV
Dipole field	B	4.5	T
Operating current	I	200	mA
Stored electrons	N_e	$4.0 \cdot 10^{10}$	
Critical wavelength	λ_c	8.44	Å
Magnetic bending radius	ρ	0.519	m
Circumference	C	9.6	m
Orbit period	T_0	32.02	ns
Radio frequency	f_{rf}	499.654	MHz
Harmonic number	h	16	
Peak r.f.-voltage	$\hat{V}_{rf}$	50 – 400	kV
Radiation loss at 700 MeV	U_0	40.9	keV/turn
Emitted power at 700 MeV	$dP/d\theta$	1.303	W/mrad
Total emitted power at 700 MeV	P	8.2	kW
Operating pressure	p_o	$5 \cdot 10^{-9}$	Torr
Beam life time	τ	≥ 5	h
Horizontal betatron tune	ν_x	1.54	
Vertical betatron tune	ν_y	0.58	
Momentum compaction factor	α	0.25	
Beam emittance	ε_x	0.54	mm mrad
Energy spread $\cdot 10^4$	σ_ϵ/E	7.5	
Injection energy	E_i	200	MeV
Injection rate	f	10	Hz
Damping times at injection	τ_x	84	ms
	τ_y	50	ms
	τ_ϵ	21	ms

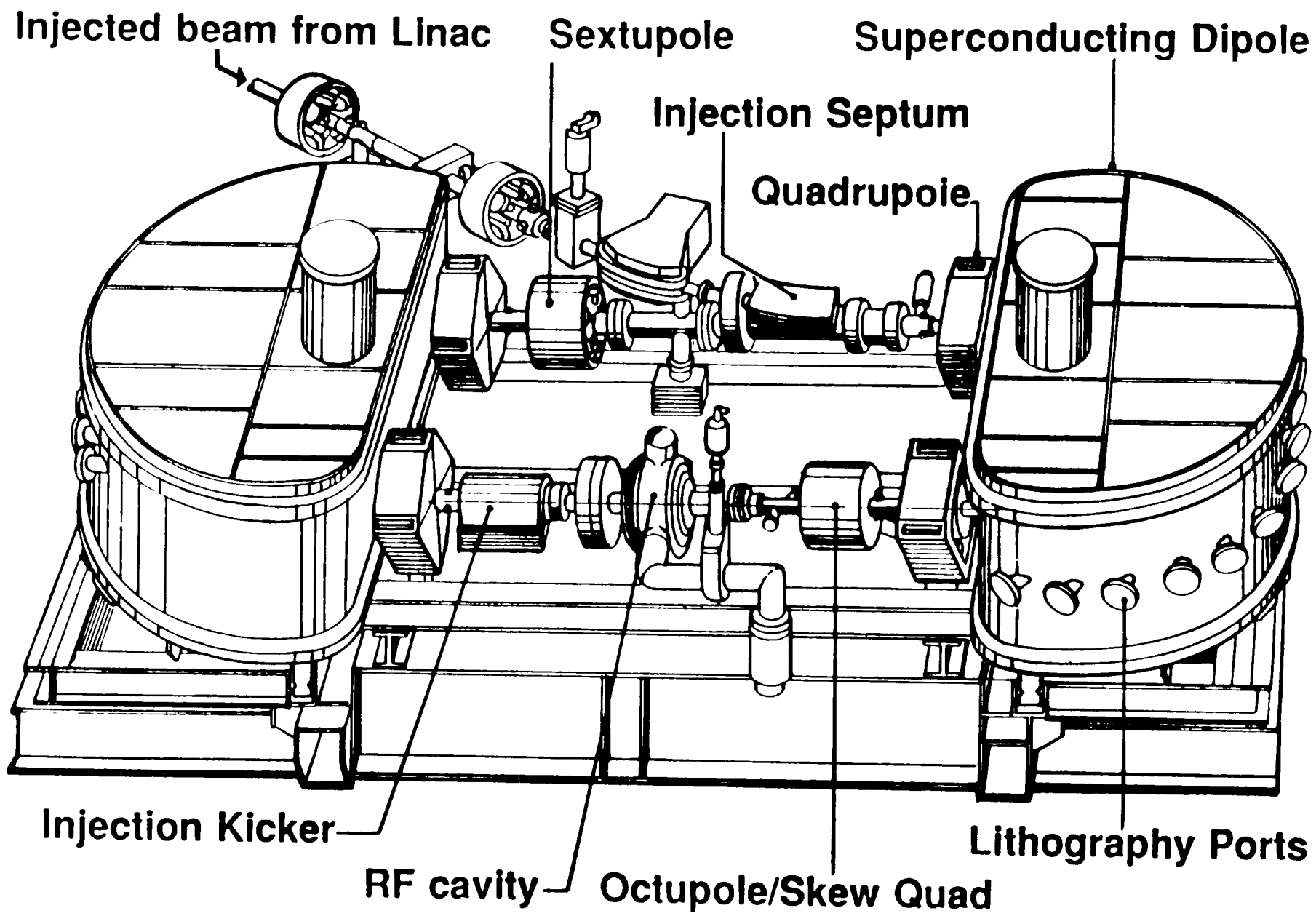


Figure 1.5: Artist's impression of HELIOS.

definition of low-energy injection given in chapter 3, the injection process of HELIOS can be considered to take place at a low energy if it is around 100 MeV or lower.

Table 1.2 lists the main parameters of HELIOS for a typical tune point. The parameters which are not obvious are explained in chapter 2. An artist's impression of HELIOS is given in figure 1.5, which shows the main elements of the synchrotron. There are two superconducting dipole magnets with 10 lithography ports each. Next to the dipoles, there are four conventional quadrupole magnets, which focus the beam in the horizontal direction. By varying the focusing in the ring a wide range of betatron tune points can be achieved (see chapter 2). Capacitive beam position monitors are situated near the quadrupoles. The RF-cavity accelerates the electrons and compensates for the energy loss due to synchrotron radiation. It is fed by a standard television RF power supply. The sextupole magnet can be used to reduce the chromaticity to zero (see chapter 2). There is also a combined skew quadrupole and octupole magnet. The skew quadrupole field can be used to introduce coupling between the horizontal and vertical betatron motion (see chapter 2), while the octupole field can be used to overcome multi-particle instabilities (see chapter 5). The septum and the kicker are pulsed magnets used in the injection system. They are explained in detail in chapter 3.

The injector is a 200 MeV linear accelerator which is built by CGR (France). The accelerating structure consists of two 100 MeV travelling wave structures. They are powered by two klystrons with a peak power of 35 MW each, running at 3 GHz. The linac beam pulse is 100 ns long and has a repetition rate of 10 Hz. The current injected into the synchrotron is around 10 mA. After leaving the linac, the beam is guided through the transport line into the synchrotron. The transport line consists of dipole magnets to bend the beam, quadrupole magnets to focus the beam, slits to select the beam energy and additional diagnostics. The last element of the transport line is the septum magnet.

An overview of the total system, consisting of linac, transport line, synchrotron and lithography stations, is given in figure 1.6. A comparison with the next system, HELIOS 2, is given in the same figure. It clearly shows the reduction in floor space occupied by the new system.

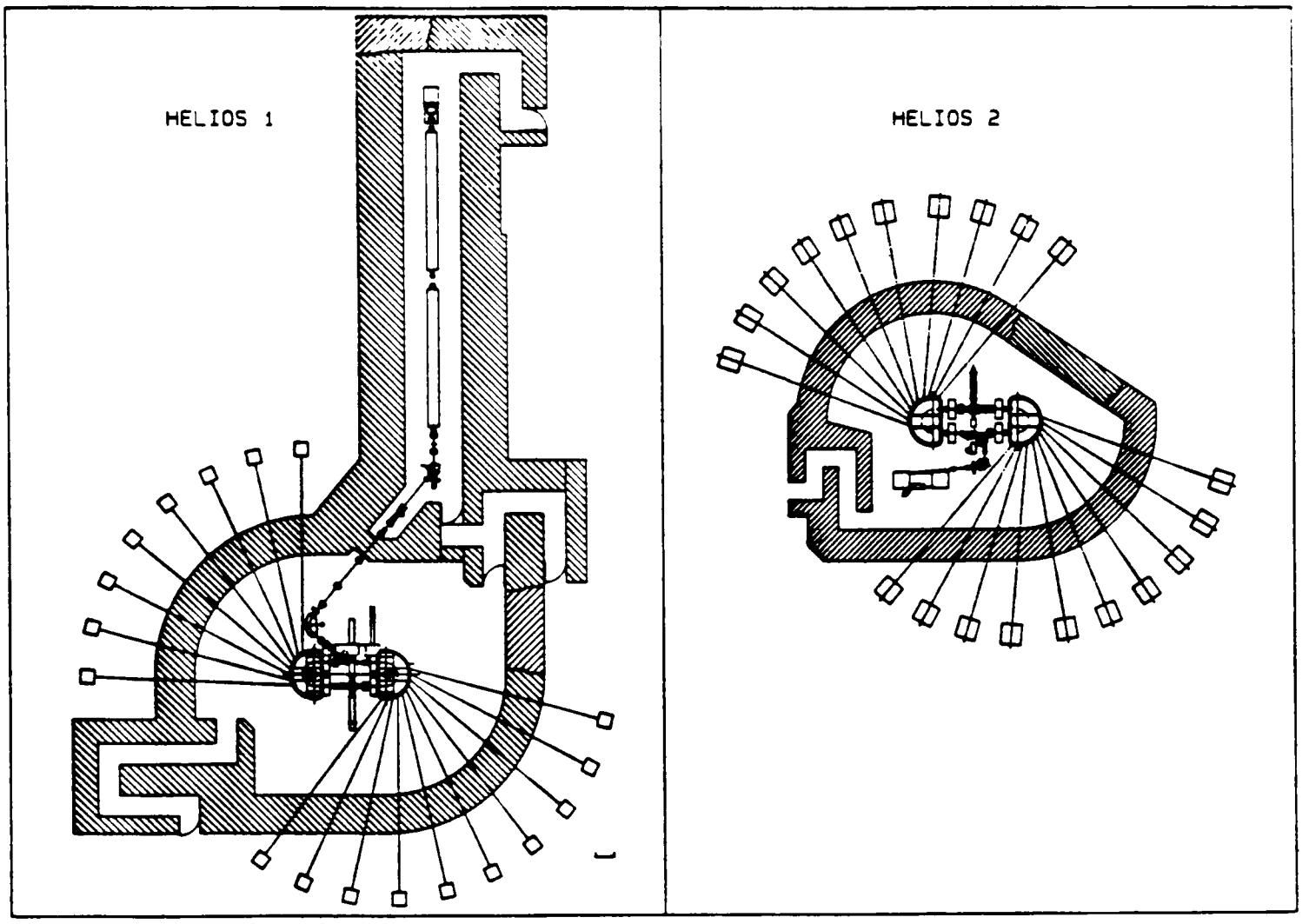


Figure 1.6: An overview of the total system, comparing HELIOS 1 and HELIOS 2.

A 'machine cycle' starts with injection, which should not take longer than about one minute, after which the electrons are stored at the injection energy. This is followed by ramping the magnets to full field, which takes three minutes. The energy of the electrons 'follows' the dipole field and the electrons are stored at full energy. The 1/e lifetime of the beam is designed to be more than 5 hours, which means that after about 5 hours the beam is 'dumped' and the cycle is restarted.

Chapter 2

General Accelerator Theory

This chapter describes the basic principles of single particle orbit dynamics, radiation damping and equilibrium beam size in an electron synchrotron. It is based on the work of Courant and Snyder for alternating gradient synchrotrons [COU58]. The theory is presented extensively in many articles and reports e.g. [SAN70, BRU66, CAS85, BOT86]. For this reason no attempt is made to give a derivation of all the formulae presented in this chapter.

2.1 Basic Quantities

The 'ideal' particle in an accelerator moves along a smooth orbit, the *reference orbit* or equilibrium orbit. This particle is called the *reference particle.* A 'real' particle will describe oscillations around the reference particle in the three normal directions: the two transverse directions and the longitudinal direction. To decouple the longitudinal from the transverse oscillations the position of the particle in the accelerator is given in the curved coordinate system (x, y, s), see figure 2.1. The position s is the distance along the reference orbit from an arbitrary starting point s_0 to the position on this orbit closest to the particle. The coordinates x and y are the distances to the equilibrium orbit in the horizontal and vertical direction, perpendicular to this orbit. The radius of curvature of the equilibrium orbit at position s is $\rho(s)$. The longitudinal oscillation is not normally expressed in position but in phase angle and energy deviation (see section 2.4).

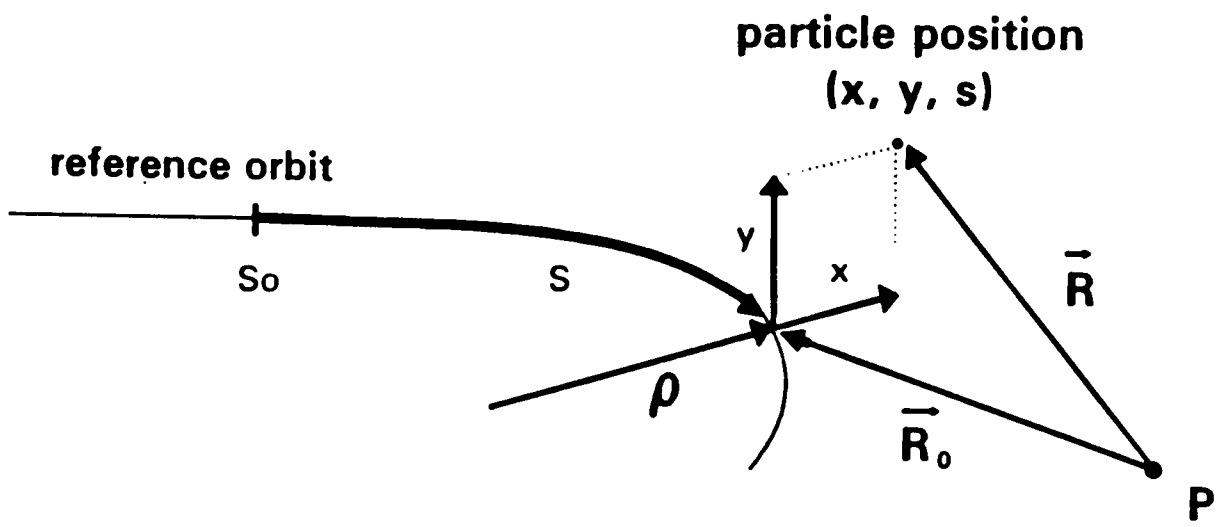


Figure 2.1: Definition of the coordinate system.

The total energy of the particle is

$$E = E_0 + T \tag{2.1}$$

where E_0 is the rest energy of the particle $E_0 = m_0c^2$ and T is the energy added to the particle by the accelerator. With the use of the relativistic quantities β and γ, the momentum of the particle can be written as

$$p = \frac{\beta}{c}E = \frac{E}{c}\sqrt{1-\gamma^{-2}} \tag{2.2}$$

The reference particle has the *reference momentum* p_0.

A useful relation between the magnetic bending field of the dipoles B and the bending radius ρ can be found by setting the Lorentz force equal to the centrifugal force, which results in

$$B\rho = p/q \tag{2.3}$$

where q is the charge of the accelerated particle. The '$B\rho$-value' is often called the *magnetic rigidity* of the particle.

For electron synchrotrons $\beta \approx 1$ and the following practical approximations can be made:

$$p \approx E/c \tag{2.4}$$

$$B\rho[\mathrm{Tm}] \approx \frac{E\ [\mathrm{MeV}]}{300} \tag{2.5}$$

2.2 The Betatron Motion and Twiss Parameters

This section describes the transverse linear motion of the particles caused by dipole and quadrupole magnets. The bending is assumed to take place in the horizontal plane. To start with, no tilted quadrupoles or dipoles are assumed, resulting in independent motions in the x and y direction. The equations are valid for single particles in a paraxial approximation and assume no acceleration by the RF-cavity and no photon emission.

To obtain the equations of motion of a charged particle in a magnetic field, the time derivatives, denoted by $\cdot$, of the unit vectors in the curved coordinate system are written down:

$$\dot{\vec{x}} = \frac{\dot{s}}{\rho}\vec{s}; \qquad \dot{\vec{y}} = 0; \qquad \dot{\vec{s}} = -\frac{\dot{s}}{\rho}\vec{x} \tag{2.6}$$

They are next used to obtain the expressions for position, velocity and acceleration of the particle. The particle position $\vec{R}$ is given relative to some arbitrary point P, with $\vec{R_0}$ the vector from P to the projection of the particle position on the reference orbit (see figure 2.1).

$$\vec{R} = x\vec{x} + y\vec{y} + \vec{R_0} \tag{2.7}$$

$$\vec{v} = \dot{\vec{R}} = \dot{x}\vec{x} + \dot{y}\vec{y} + \dot{s}(1 + \frac{x}{\rho})\vec{s} \tag{2.8}$$

$$\dot{\vec{v}} = \ddot{\vec{R}} = (\ddot{x} - \frac{\dot{s}^2}{\rho}(1 + \frac{x}{\rho}))\vec{x} + \ddot{y}\vec{y} + (2\frac{\dot{x}\dot{s}}{\rho} + \ddot{s}(1 + \frac{x}{\rho}) - x\frac{\dot{s}\dot{\rho}}{\rho^2})\vec{s} \tag{2.9}$$

where $\dot{\vec{R_0}} = \dot{s}\vec{s}$ is used and ρ is not assumed to be a constant.

These relations are substituted in the Lorentz equation for the particle motion

$$\dot{\vec{v}} = \frac{q}{m}(\vec{v} \times \vec{B}) \tag{2.10}$$

and the time derivatives of x and y are rewritten in terms of s derivatives, which are denoted by $'$:

$$x'' + \frac{\frac{x\rho'}{\rho^2} - \frac{2x'}{\rho}}{1+\frac{x}{\rho}}x' - \frac{1}{\rho}(1+\frac{x}{\rho}) =$$

$$\frac{q}{p}\sqrt{x'^2+y'^2+(1+\frac{x}{\rho})^2}\left(\frac{x'y'}{1+\frac{x}{\rho}}B_x - (1+\frac{x}{\rho})\left(1+\frac{x'^2}{(1+\frac{x}{\rho})^2}\right)B_y + y'B_s\right) \quad (2.11)$$

$$y'' + \frac{\frac{x\rho'}{\rho^2} - \frac{2x'}{\rho}}{1+\frac{x}{\rho}}y' =$$

$$\frac{q}{p}\sqrt{x'^2+y'^2+(1+\frac{x}{\rho})^2}\left((1+\frac{x}{\rho})\left(1+\frac{y'^2}{(1+\frac{x}{\rho})^2}\right)B_x - \frac{x'y'}{1+\frac{x}{\rho}}B_y - x'B_s\right) \quad (2.12)$$

$$\frac{\ddot{s}}{\dot{s}^2} = \left(\frac{x\rho'}{\rho^2} - \frac{2x'}{\rho} - \frac{v}{\dot{s}}\frac{q}{p}(y'B_x - x'B_y)\right) \Big/ \left(1+\frac{x}{\rho}\right) \quad (2.13)$$

The equation of motion in the longitudinal direction (equation 2.13) has been used to eliminate the $\ddot{s}/\dot{s}^2$ terms from the two transverse equations.

The equations 2.11 and 2.12 are generally valid and no approximations are made. They can be used to obtain the equations of motions up to any desired order. In appendix A this is shown for second order in x, x', y, y' and δ, where δ is defined as the relative momentum deviation $\delta = \Delta p/p_0$, and magnetic fields are included up to sextupole order. The resulting differential equations as mentioned in appendix A include some terms depending on the bending radius ρ which are very often neglected. For accelerators with a small bending radius these terms are significant and have to be taken into account [ARC91].

For the work presented in this thesis it is sufficient to use the differential equations up to first order in x, x', y, y' and δ. To obtain these, the magnetic field up to quadrupole order is substituted in equations 2.11 and 2.12. The longitudinal component of the magnetic field, $\vec{B}_s$, results only in higher order terms (see appendix A), so it can be neglected. The magnetic field quantities are defined in terms of the reference momentum p_0:

$$\frac{q}{p_0}B_x = Ky \quad (2.14)$$

$$\frac{q}{p_0}B_y = \frac{1}{\rho} + Kx \quad (2.15)$$

with

$$K(s) = \frac{q}{p_0}\frac{\partial B_y}{\partial x} \tag{2.16}$$

and because of Maxwell's equation, curl $\vec{B} = 0$, also

$$K(s) = \frac{q}{p_0}\frac{\partial B_x}{\partial y} \tag{2.17}$$

The quantity $K(s)$ represents the focusing strength of the magnet. For a quadrupole which is focusing in the horizontal direction $K(s) > 0$, if it is defocusing $K(s) < 0$.

The off-energy terms are included by substituting $p = p_0 + \Delta p$. The square root in equations 2.11 and 2.12 is expanded and the resulting equations are truncated at first order in x, x', y, y' and δ. This leads to the equations of motion of interest:

$$\frac{d^2x}{ds^2} + \left(\frac{1}{\rho^2(s)} + K(s)\right)x = \frac{1}{\rho(s)}\frac{\Delta p}{p_0} \tag{2.18}$$

$$\frac{d^2y}{ds^2} - K(s)y = 0 \tag{2.19}$$

Very often the field index n is used to express the focusing strength of dipole magnets

$$n = -\frac{\rho}{B}\frac{\partial B_y}{\partial x} \tag{2.20}$$

The field index is related to the focusing strength parameter K by $n = \rho^2 K$.

The functions $K(s)$ and $\rho(s)$ are periodic with period L:

$$K(s + L) = K(s) \tag{2.21}$$

with L the length of one *super period* of the lattice. The maximum value of L is the circumference of the accelerator.

The solution of the homogeneous part of equation 2.18 and equation 2.19 can be presented in matrix form

$$\begin{pmatrix} z_1 \\ z_1' \end{pmatrix} = M \begin{pmatrix} z_0 \\ z_0' \end{pmatrix} \tag{2.22}$$

where z is x or y and $z' = dz/ds$. In this equation M is the *transfer matrix*, which relates the particle's coordinates z_1 and z_1' at position s_1 to the coordinates at position s_0. It describes the periodic solution of the differential equation and only

depends on the magnetic elements and drift lengths between the positions s_0 and s_1. The determinant of M equals 1. The different matrices for each elements i, M_i, can be multiplied to obtain the transfer matrix for a larger section of the machine

$$M = M_j \cdot M_{j-1} \cdot M_{j-2} \cdot \ldots \cdot M_2 \cdot M_1 \tag{2.23}$$

The transfer matrix M can be written as:

$$M = \begin{pmatrix} \cos\mu + \alpha \sin\mu & \beta \sin\mu \\ -\gamma \sin\mu & \cos\mu - \alpha \sin\mu \end{pmatrix} \tag{2.24}$$

The parameters $\alpha(s)$, $\beta(s)$ and $\gamma(s)$ are the so called *Twiss parameters* and fully describe the linear motion around the reference orbit for on-momentum particles. The two relationships between the Twiss parameters are: $\alpha(s) = -\frac{1}{2}\partial\beta(s)/\partial s$ and $\gamma(s) = (1 + \alpha^2(s))/\beta(s)$. The parameter $\mu(s)$ is called the phase advance between positions s_0 and s_1 and relates to the beta function as

$$\mu_z(s) = \int_{s_0}^{s} \frac{1}{\beta_z(s')}\, ds' \tag{2.25}$$

Introducing the *particle emittance* $\mathcal{E}_z$, the motion can be described by

$$z_\beta(s) = \sqrt{\mathcal{E}_z \beta_z(s)} \cos(\mu_z(s) + \varphi) \tag{2.26}$$

From this equation it can be seen that the particle oscillates with a harmonic sine-like oscillation. Each section of the accelerator has a fixed phase advance $\mu_z(s)$ and the particles differ by their phase offset φ. A group of particles, or the total beam, consists of many of these sine-like trajectories, modulated by $\sqrt{\beta_z(s)}$, because $\mathcal{E}_z$ is a constant for each particle. The beta-function $\beta_z(s)$ gives a measure of the beam size along the accelerator.

The coordinates of a particle in phase space (z, z') over successive turns at a fixed position of the accelerator will lie on an ellipse, the so-called *eigen ellipse.* The area of this ellipse divided by π is the already introduced particle emittance $\mathcal{E}_z$. Knowing the Twiss parameters at a certain position s, $\mathcal{E}$ can be calculated from the coordinates in phase space

$$\mathcal{E}_z = \gamma z^2 + 2\alpha z z' + \beta z'^2 \tag{2.27}$$

$$= \frac{\text{Area}}{\pi} \tag{2.28}$$

It is constant over the accelerator and a preserved quantity. This is called *Liouville's theorem* and follows from Hamiltonian mechanics ([BEL87]).

If a particle has a momentum deviation Δp from the reference momentum, the position of the particle will depend on this momentum deviation. The periodic solution of the inhomogeneous differential equation 2.18 for a particle with 100 % momentum deviation ($\Delta p/p_0 = 1$) is called the *dispersion function* $\eta(s)$. The position of a particle with a momentum deviation is the summation of the betatron motion described in 2.26 and the displacement described by the dispersion function

$$x(s) = x_\beta(s) + \eta(s) \cdot \frac{\Delta p}{p_0} \tag{2.29}$$

The transfer matrix M for off-energy particles is a 3×3 matrix, working on the vector $(x, x', \Delta p/p_0)$.

The Twiss parameters and dispersion function strongly depend on the focusing strength of the machine. The focusing strength is expressed by the *tune* of the machine; this is defined as the number of betatron oscillations per revolution

$$\nu_z = \frac{1}{2\pi} \oint \mu_z(s) ds \tag{2.30}$$

where $\oint$ is the integral around the accelerator.

Figure 2.2 shows the beta functions together with the dispersion function for the HELIOS machine for tunes $\nu_x = 1.54$ and $\nu_y = 0.58$. It clearly shows that the horizontal beam size has a maximum in the conventional, horizontally focusing quadrupoles and the vertical beam size has a maximum in the middle of the dipole where focusing takes place in the vertical direction.

At certain combinations of horizontal and vertical tune, resonances can occur. Small field errors generally increase the amplitude of the betatron oscillations and result in a tune spread. If the tunes are close to a resonance, the particle locks on to the resonance and small amplitude increases build up coherently. In this situation the area in phase space described by the particle is not an ellipse any more (filamentation takes place), and the amplitude of the oscillation increases, until the

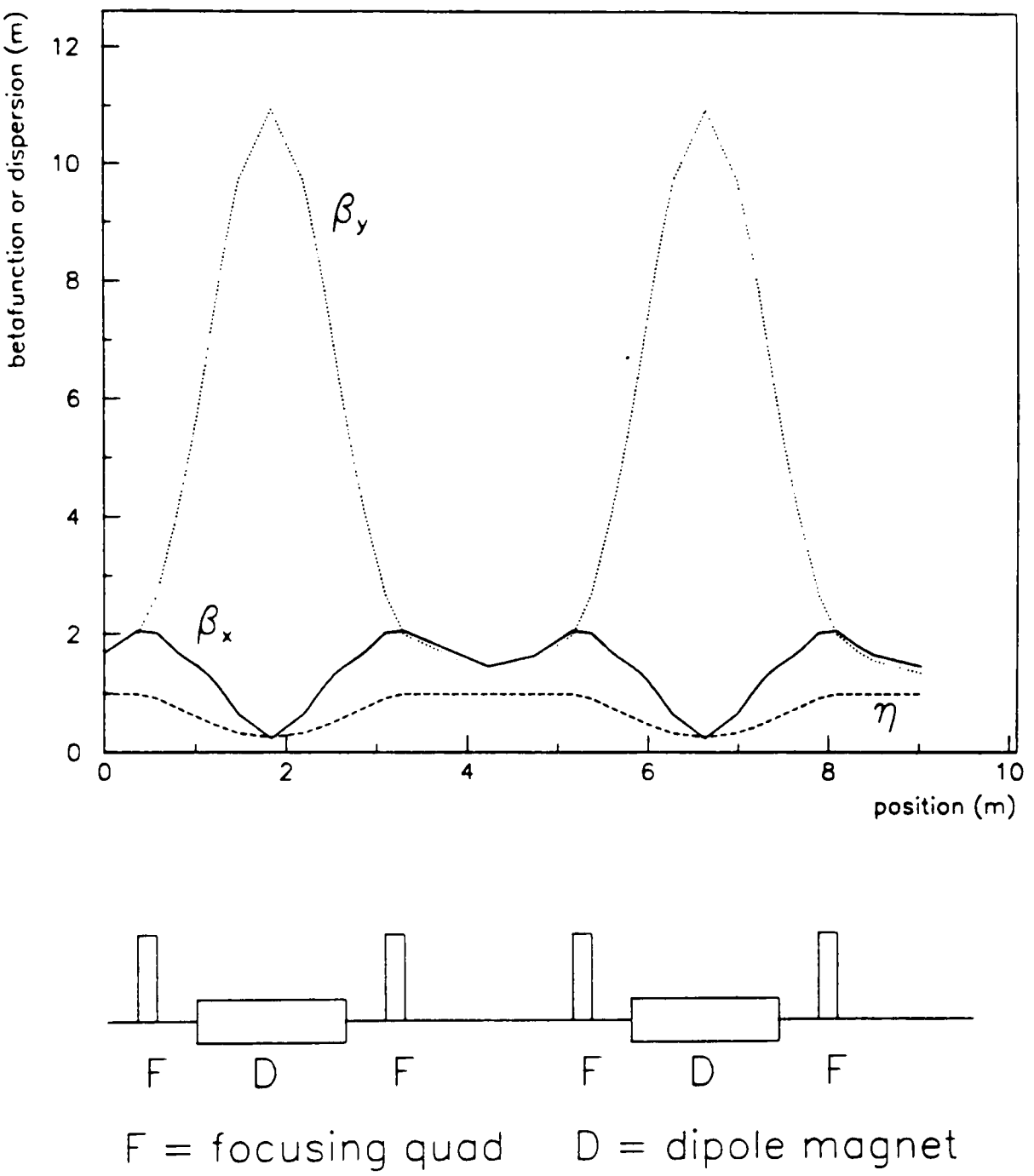


Figure 2.2: Lattice functions of HELIOS, for $\nu_x = 1.54$ and $\nu_y = 0.58$.

particle hits the vacuum chamber wall and is 'lost'. The general resonance condition is

$$k\,\nu_x + l\,\nu_y = m \tag{2.31}$$

where k, l and m are integers. The sum $|k| + |l|$ is called the order of the resonance. Resonances up to third order are seen in most accelerators. Some accelerator groups report having seen resonances up to the fifth order. If m is a multiple of the number of super periods of the machine the resonance is generally stronger and is called a structural resonance.

The *momentum compaction factor* α is the relative change in path length around the accelerator $\Delta C/C_0$ caused by a relative change in momentum $\Delta p/p_0$ (C_0 is the length of the equilibrium orbit):

$$\alpha = \frac{\Delta C/C_0}{\Delta p/p_0} \tag{2.32}$$

It is easy to understand that α depends on both $\eta(s)$ and $\rho(s)$. In linear approximation the length of the particle orbit C depends on the energy deviation as

$$C = \oint \left(1 + \frac{\eta(s)\Delta p/p_0}{\rho(s)}\right) ds = C_0 + \oint \frac{\eta(s)}{\rho(s)} \frac{\Delta p}{p_0}\, ds \tag{2.33}$$

This gives the formula for the momentum compaction factor:

$$\alpha = \frac{1}{C_0} \oint \frac{\eta(s)}{\rho(s)}\, ds \tag{2.34}$$

If a particle has a positive energy deviation it will be focused less strongly by the quadrupole field than a particle with the reference momentum p_0. This will cause a change in tune $\Delta\nu_z$. The *chromaticity* is defined as this change in tune divided by the relative change in momentum:

$$\xi_z = \frac{\Delta\nu_z}{\Delta p/p_0} \tag{2.35}$$

This energy dependent change in tune adds to the tune spread already present in the beam and it is more likely that the particle locks on to a nearby resonance. This tune spread, caused by an energy spread in the beam, can be counteracted by introducing additional focusing, which depends on the energy deviation of the particle. This is

done by placing sextupole magnets at positions with finite dispersion. Because the effect of a certain sextupole on the tune not only depends on the dispersion function, but also on either the horizontal or vertical beta function at the magnet position, it is possible to correct both chromaticities with two families of sextupoles.

The chromaticity also has a strong effect on the *head – tail instability.* This is a multi-particle instability, caused by interaction of the beam with the vacuum chamber wall. To damp this instability the sextupoles will normally be set so that the chromaticity is slightly positive. The chromaticity value without any adjustable sextupoles switched on is called the *natural chromaticity.*

2.3 Coupling between the two Transverse Directions

Up to now uncoupled, transverse betatron motions have been assumed. In the presence of tilted (or skew) quadrupoles, which are the quadrupoles defined previously rotated over 45° around the s-axis, or solenoid lenses the two betatron motions become coupled [GUI76, WIL84, BRY89, EDW73, TEN88]. There is a periodic interchange, or *beating*, of the particle emittance between the horizontal and vertical phase space. If the betatron tunes are close to a coupling resonance

$$\nu_x - \nu_y = p \qquad p = \text{integer} \tag{2.36}$$

the total particle emittance $\mathcal{E}_T = \mathcal{E}_x + \mathcal{E}_y$ is constant. Assuming a particle starting with zero vertical emittance, the total emittance will stay equal to the initial horizontal particle emittance. The amount of coupling can be expressed in the coupling strength g

$$g = \frac{\mathcal{E}_y}{\mathcal{E}_x} \tag{2.37}$$

where $\mathcal{E}_x$ and $\mathcal{E}_y$ are *time averaged* particle emittances, given by

$$\mathcal{E}_x = \frac{1}{1+g}\mathcal{E}_T \quad \text{and} \quad \mathcal{E}_y = \frac{g}{1+g}\mathcal{E}_T \tag{2.38}$$

For a skew quadrupole with magnetic field gradient B_1 [T/m] and length l the coupling constant k is defined as

$$k = \frac{1}{4\pi} \cdot \frac{1}{B\rho} \sqrt{\beta_x \beta_y} B_1 l \tag{2.39}$$

It shows that the skew quadrupole is more effective if it is placed at a position in the accelerator where the beta functions are large. If the distance to the coupling resonance $\Delta = \nu_x - \nu_y - p$ is small, the coupling strength is

$$g = \frac{(\frac{k}{\Delta})^2}{\frac{1}{2} + (\frac{k}{\Delta})^2} \tag{2.40}$$

The particle emittances $\mathcal{E}_x$ and $\mathcal{E}_y$ can be calculated from the phase space coordinates by using the formula of the harmonic betatron motion without coupling (see equation 2.27). The total particle emittance $\mathcal{E}_T$, as calculated with this definition, is only constant close to a coupling resonance. Further away from the coupling resonance $\mathcal{E}_T$ is not constant any more, the motion is not harmonic, and growth of $\mathcal{E}_T$ takes place. Close to a sum resonance this growth is extreme and the motion becomes unstable.

2.4 The Synchrotron Motion

The presence of an RF-system permits a longitudinal oscillation around the reference particle. It is conventional to describe this motion in longitudinal phase space (W, ϕ), with $W = C_0 \Delta p$ and ϕ the RF-phase of the particle relative to the phase of the reference particle, which is always maintained at the synchronous phase ϕ_s. At ϕ_s the energy loss due to the emission of synchrotron radiation over one turn (assuming only one RF-cavity in the accelerator) is exactly compensated by the RF-power from the cavity: $\Delta E = e\hat{V} \sin \phi_s$, in which $\hat{V}$ is the amplitude of the RF-voltage oscillation. For electron synchrotrons ϕ_s is normally on the falling side of the RF sine wave. This can be pictured qualitatively by describing the synchrotron motion in the following simple way: assume a particle with a positive momentum deviation Δp arriving at the cavity at the synchronous phase ϕ_s; because $\Delta p > 0$ the particle's orbit around the accelerator is larger than the reference orbit C_0 (assuming positive

momentum compaction α). The next turn the particle arrives at the RF-cavity later than the reference particle (assuming $v = c =$ constant) at a phase larger than ϕ_s and as a consequence experiences a smaller accelerating voltage. This continues till the particle's momentum is smaller than the reference momentum, but now it will need less time than the reference particle to complete a revolution around the machine; the phase at which it passes the cavity reduces and it will obtain an acceleration at the cavity larger than the reference particle. This process results in a periodic change of energy and longitudinal position and is described by the coupled differential equations (for $\gamma \gg 1$)

$$\frac{dW}{dt} = q\hat{V}(\sin\phi - \sin\phi_s) \tag{2.41}$$

$$\frac{d\phi}{dt} = \frac{1}{C_0}\frac{h\alpha\omega_0}{p_0}W \tag{2.42}$$

where ω_0 is the angular orbit frequency of the equilibrium particle and h the *harmonic number*, which equals the number of bunches in the accelerator:

$$h = \frac{\omega_{RF}}{\omega_0} \tag{2.43}$$

If the energy deviation and the amplitude of the oscillation are small, the motion is harmonic. The frequency of the harmonic oscillation is the angular *synchrotron oscillation frequency* Ω_0:

$$\Omega_0^2 = \frac{\alpha q \left[\frac{dV_{rf}}{dt}\right]_0 \omega_0}{2\pi E} \tag{2.44}$$

In analogy with the transverse phase space the synchrotron tune is defined as

$$\nu_s = \frac{\Omega_0}{\omega_0} \tag{2.45}$$

Generally the synchrotron tune is much smaller than the betatron tunes.

For larger oscillations in longitudinal phase space the synchrotron motion is not harmonic. Particles with an energy deviation larger than the *energy acceptance* will be lost. The energy acceptance $(\Delta p/p_0)_{\max}$ is defined by

$$\left(\frac{\Delta p}{p_0}\right)^2_{\max} = \frac{U_0}{\alpha\pi h E}F(\zeta) \tag{2.46}$$

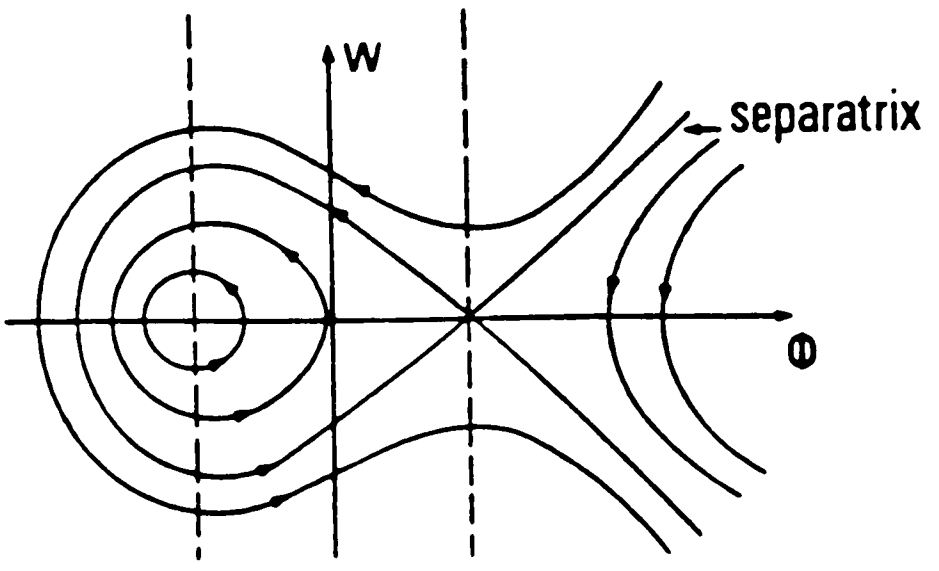


Figure 2.3: Particle motion in longitudinal phase space [CAS85].

with ζ the *over-voltage*

$$\zeta = \frac{q\hat{V}}{U_0} \tag{2.47}$$

used in the function $F(\zeta)$

$$F(\zeta) = 2\left(\sqrt{\zeta^2 - 1} - \arccos\frac{1}{\zeta}\right) \approx 2\zeta - \pi \tag{2.48}$$

A particle with an energy deviation equal to $(\Delta p/p_0)_{\max}$ and phase ϕ_s will move around a fish shaped flow line in longitudinal phase space defining the stable region or *RF-acceptance* of the accelerator. This line is called the *separatrix*, see figure 2.3.

2.5 Synchrotron Radiation Damping

One of the main differences between electron and proton synchrotrons is the damping of the discussed transverse and longitudinal oscillations. The damping is a result of the emitted synchrotron radiation, which gives it the obvious name *synchrotron radiation damping* (although the damping is actually introduced by the RF-cavity and the synchrotron radiation introduces excitation instead of damping).

The damping is characterised by the synchrotron radiation damping time constants for the three directions, τ_x, τ_y and τ_ε, defined by

$$A = A_0 e^{-\frac{1}{\tau_i}t} \qquad\qquad i = x, y, \varepsilon \tag{2.49}$$

where A is the amplitude of the betatron or energy oscillation.

In electron storage rings the energy lost through the emitted synchrotron radiation has to be compensated for by the RF-cavities. In the cavity the electrons will always be accelerated parallel to the reference orbit and the angle with the reference orbit in both transverse directions, x' and y', will be reduced at each passage. This is damping in the transverse phase spaces.

The formula for the vertical damping time τ_y is relatively simple to derive. In this derivation the betatron oscillation is approximated by assuming a constant value of $\beta_y(s) = \beta$, so $\mu = s/\beta$ and the betatron motion can be written as:

$$y = A\cos\mu \tag{2.50}$$

$$y' = \frac{A}{\beta}\sin\mu \tag{2.51}$$

The amplitude of the oscillation can now be obtained from y and y':

$$A^2 = y^2 + (\beta y')^2 \tag{2.52}$$

The phase angle y' before acceleration by the RF-cavity can be written as

$$y'_0 = \frac{p_y}{p} \tag{2.53}$$

After acceleration of the particle in the RF-cavity by δp, the phase angle is changed to

$$y'_1 = \frac{p_y}{p+\delta p} \approx \frac{p_y}{p}\left(1 - \frac{\delta p}{p}\right) = y'_0\left(1 - \frac{\delta p}{p}\right) \tag{2.54}$$

and the change in y' is

$$\delta y' \approx -y'_0\frac{\delta p}{p} \approx -y'\frac{\delta E}{E} \tag{2.55}$$

The corresponding change in amplitude A, obtained by differentiating equation 2.52, is

$$A\delta A = \beta^2 y'\,\delta y' \approx -(\beta y')^2\frac{\delta E}{E} \tag{2.56}$$

The moment of arrival of the particle at the RF-cavity is arbitrary and y' has to be averaged over all phases μ between 0 and 2π. The average of $< y'^2 >= A^2/2\beta^2$. For

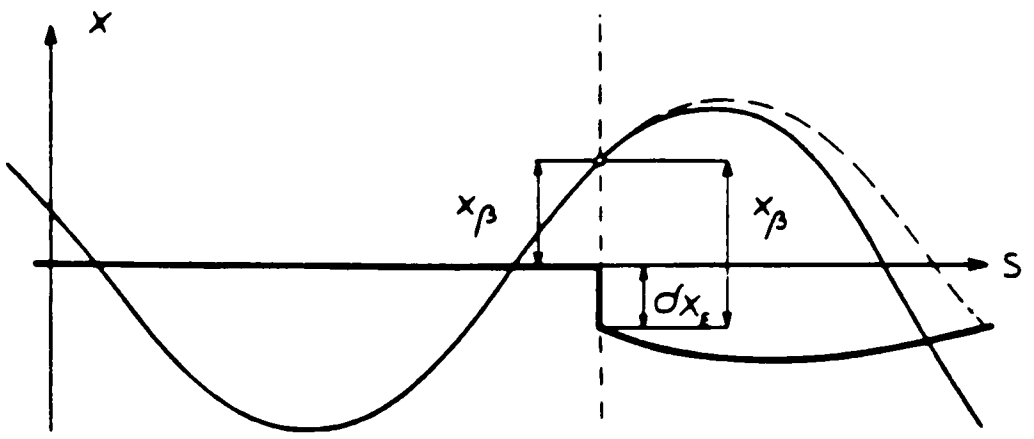


Figure 2.4: The emission of a photon displaces the betatron reference orbit, which excites the horizontal betatron oscillation [CAS85].

the change of the amplitude of the oscillation the average value $< A >$ now has to be considered, which is

$$A < \delta A >= -\frac{A^2}{2}\frac{\delta E}{E} \tag{2.57}$$

Over one complete revolution the total acceleration given to the the particle has to compensate the total energy loss per revolution U_0:

$$\frac{\Delta A}{A} = -\frac{U_0}{2E} \tag{2.58}$$

Now using the definition for the damping times τ_i (2.49), and applying it to one revolution time T_0, the vertical damping time can be written as

$$\tau_y = \frac{2ET_0}{U_0} \tag{2.59}$$

Using a non-constant value of the beta function in this derivation leads to exactly the same equation for τ_y.

The derivation for τ_x is more complicated, because each time a photon is emitted there is a sudden reduction in energy which causes a sudden change in the off-energy orbit (because the emission takes place only in the dipoles where the dispersion is non-zero). Because the particle position can not suddenly change, a small excitation of the radial betatron oscillation takes place, see figure 2.4. This is an additional anti-damping term in $\delta x'$, which has to be added to the formulae as derived for $\delta y'$. Including this anti-damping term in the derivation for the damping time gives for an

isomagnetic lattice (this is a lattice in which all the dipoles have the same magnetic field):

$$\tau_x = \frac{2ET_0}{U_0(1 - \frac{\alpha C_0}{2\pi\rho}(1 - 2n))} \tag{2.60}$$

Generally the anti-damping term is smaller than 1, so damping occurs in the horizontal phase space.

The damping in longitudinal phase space can be derived by taking the dependence of the amount of emitted synchrotron radiation on the relative momentum deviation $\Delta p/p_0$ into account in the equation of motion in the longitudinal phase space (this has been neglected in section 2.4). The damping time for the synchrotron oscillation, again in an isomagnetic lattice, is

$$\tau_\epsilon = \frac{2ET_0}{U_0(2 + \frac{\alpha C_0}{2\pi\rho}(1 - 2n))} \tag{2.61}$$

It is interesting to see that the anti-damping term in τ_x (2.60) reappears as a damping term in τ_ϵ.

Excitation of the oscillations is caused by the stochastic quantum emission of photons (synchrotron radiation). Each time a quantum of energy is emitted, the energy of the electron is suddenly decreased and causes a small energy oscillation. These disturbances occur at a random time and the cumulative effect of many of these disturbances causes the energy oscillation to grow. This is the quantum excitation in the longitudinal direction. In the radial direction the quantum emission causes an excitation of the betatron oscillation; this is the same process which gives the anti-damping term in τ_x, see figure 2.4. This also has to be considered over many randomly emitted quanta, resulting in a radial excitation of the beam. There is no vertical dispersion in the machine and the excitation in the vertical direction is caused only by the variation in angle with which the photon is emitted. This angle is typically very small, around $1/\gamma$, and the resulting vertical oscillations are roughly a factor $1/\gamma^2$ smaller than in the horizontal plane. They can normally be neglected because the effect of coupling between the vertical and horizontal motion caused by magnetic field imperfections is normally much larger.

In the horizontal and longitudinal direction a balance between quantum excitation and synchrotron radiation damping results in an *equilibrium energy spread* of the beam σ_ϵ/E and an equilibrium horizontal beam size. In the vertical direction the equilibrium beam size is determined by the coupling between the horizontal and vertical phase space (see section 2.3).

The equilibrium energy spread for an isomagnetic lattice is

$$\left(\frac{\sigma_\epsilon}{E}\right)^2 = C_q \cdot \frac{\gamma^2}{\rho(2 + \frac{\alpha C_0}{2\pi\rho}(1-2n))} \tag{2.62}$$

where the quantity $C_q = \frac{5}{32\sqrt{3}}\frac{\hbar}{m_0 c} = 3.84 \cdot 10^{-13}$ m. The equilibrium in the radial direction is characterised by the horizontal *beam emittance* ε_x, which for isomagnetic lattices is given by

$$\varepsilon_x = C_q \cdot \frac{\gamma^2}{\rho(1 - \frac{\alpha C_0}{2\pi\rho}(1-2n))} < H(s) >_{\mathrm{m}} \tag{2.63}$$

where γ is the relativistic factor. The quantity $< H(s) >_{\mathrm{m}}$ is the mean value over the bending magnets of H, with H defined as

$$H = \gamma(s)\eta^2(s) + 2\alpha(s)\eta(s)\frac{d\eta(s)}{ds} + \beta(s)\left(\frac{d\eta(s)}{ds}\right)^2 \tag{2.64}$$

with all quantities taken in the horizontal direction.

The beam emittance ε_z describes the beam size due to betatron oscillation as in equation 2.26:

$$\sigma_{z\beta}(s) = \sqrt{\varepsilon_z \beta_z(s)} \tag{2.65}$$

Combining these results gives the equilibrium beam size in the horizontal direction, as a result of the betatron oscillation and the synchrotron oscillation

$$\begin{aligned} \sigma_x^2(s) &= \sigma_{x\beta}^2(s) + \sigma_{x\epsilon}^2(s) \\ &= \varepsilon_x \beta_x(s) + \eta^2(s)\left(\frac{\sigma_\epsilon}{E}\right)^2 \end{aligned} \tag{2.66}$$

Chapter 3

Electron Injection

Injection is the process by which electrons are transferred from an electron source into the accelerator. After injection the electrons have to be stored in the accelerator for a significant period. This thesis considers the efficiency of the injection process and ways to improve it, especially if the injection takes place at 'low' energies (what is called 'low' is defined in this chapter). There are several possible systems of injection but this chapter will focus on the system used for HELIOS: multi-shot – multi-turn injection in radial phase space with a single kicker magnet. Other injection methods are discussed briefly in section 3.4.

After a general description of the injection process the problems of low-energy injection are discussed. This is followed by an explanation of why injection at low energies should still be possible without changing the injection method. This description is mainly qualitative, leaving the more detailed calculations for the next chapter.

3.1 General Description

The injection system as used for HELIOS has two special magnets: the septum and the kicker magnet. They are both pulsed at the injection frequency (10 Hz). The septum is the dividing point between the injection transport line and the accelerator and bends the injected beam so it is approximately parallel with the orbit of the stored beam (see figure 3.1). The magnetic induction in the accelerator vacuum chamber is screened by eddy currents in the septum box; the septum magnet only

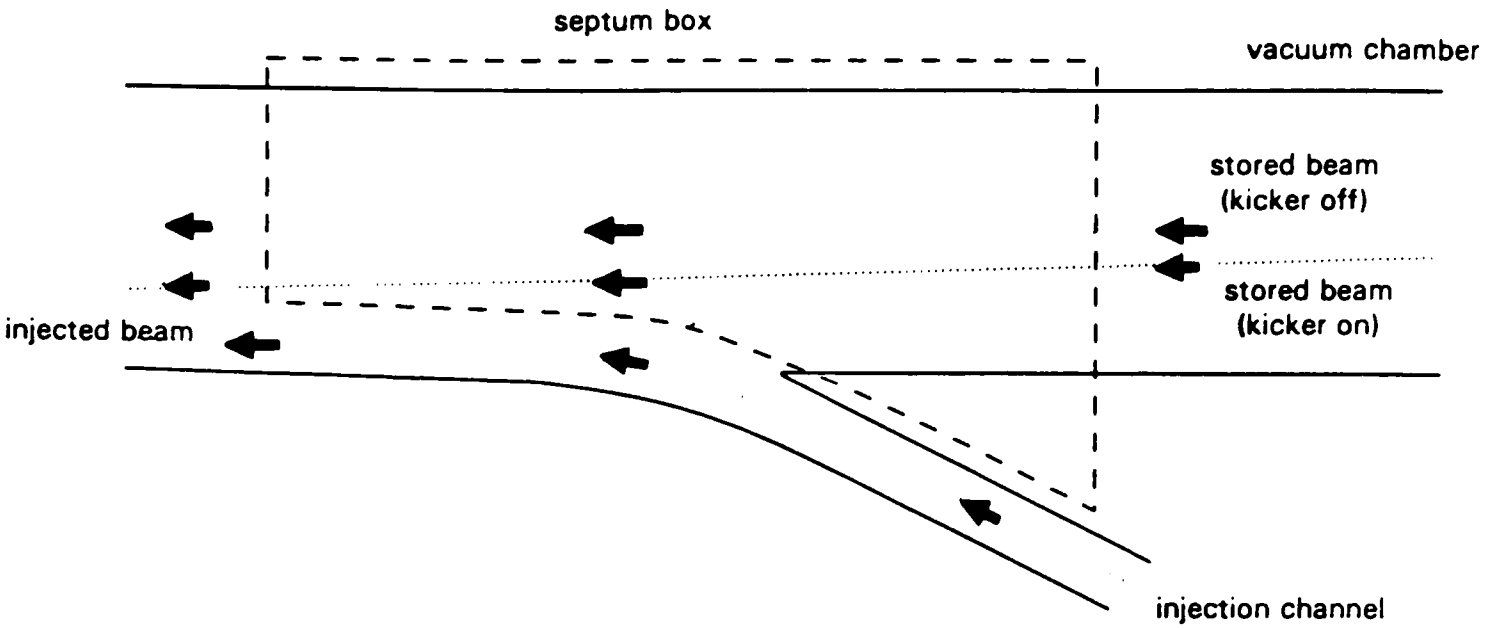


Figure 3.1: Septum box and electron orbits.

has an effect on the injected beam and not on the beam which has previously been stored. The septum magnet pulse is long on an injection time scale, so the septum field can be considered constant during injection. The kicker magnet kicks the newly injected beam in such a way that it is not going to hit the septum box after a few turns, but it also has an effect on the stored beam. The kicker magnet pulse as used for HELIOS, together with the injected beam pulse, is sketched in figure 3.2: the pulse has a half-sine shape and a base width of about 250 ns. For the desired effect, the injected beam is generally injected on the falling side of the kicker pulse and because each particle has to experience a significant kick by the kicker magnet to stay in the machine, it is possible that with a 30 ns orbit period injection can take place over about 3 turns. This means that a 100 ns pulse can be injected. The process of injecting over more than one turn is called *multi-turn injection.* The timing of the injected beam quoted in this thesis is always relative to the start of the kicker pulse at t_0, as given in figure 3.2.

The effect of the kicker magnet on the injected beam is illustrated in figure 3.3a; it shows the coordinates of one injected particle in horizontal phase space on successive turns at the septum position. After 3 turns the particle moves around on an ellipse with area $\pi\mathcal{E}$. The first 2 turns after injection are not on the ellipse, because over these turns the particle receives kicks from the kicker magnet to move it away from the septum. Without any kicks from the kicker magnet this ellipse would go through

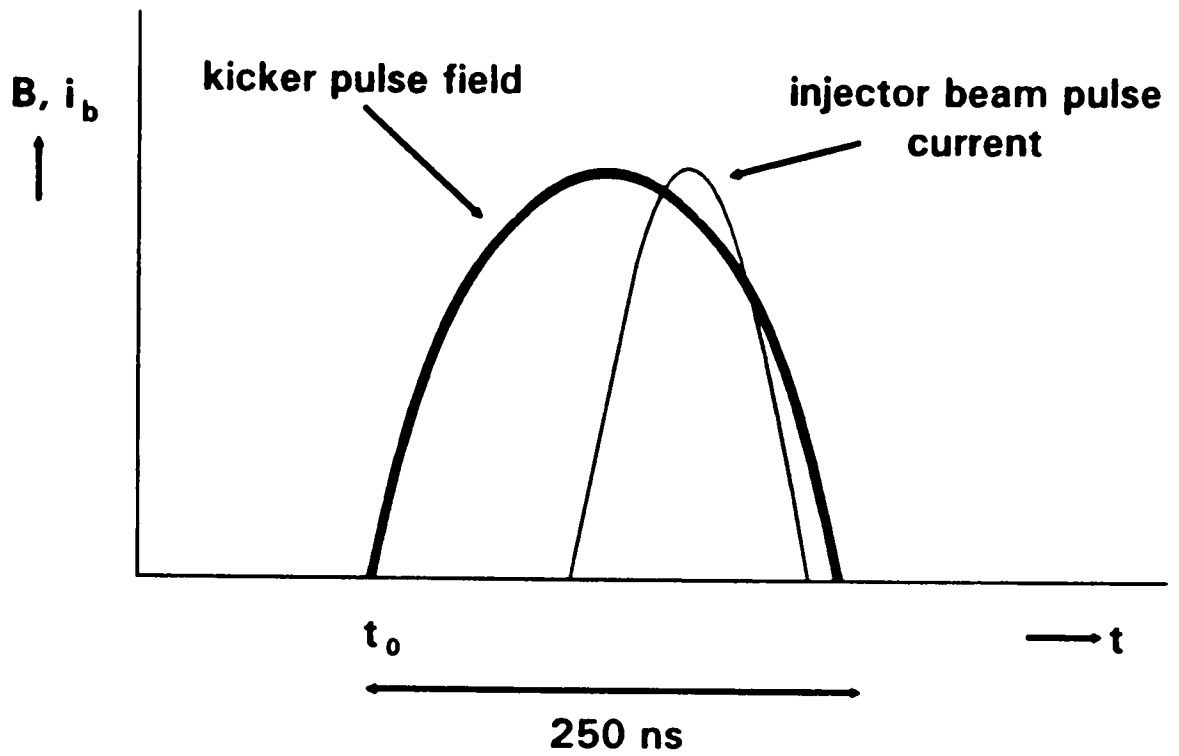


Figure 3.2: The kicker magnet pulse together with the injected beam pulse.

the injection point in phase space, which is outside the accelerator vacuum chamber: the particle would be lost against the septum box wall.

The particle emittance of this ellipse $\mathcal{E}$ is very large. If the kicker magnet is excited again with the particle in the situation as given in figure 3.3a, the particle is kicked outwards in the direction of the septum and would hit the septum box. But after sufficient time, $\mathcal{E}$ will be shrunk to a much smaller emittance because of synchrotron radiation damping. Now the effect of the kicker magnet on a stored particle is as given in figure 3.3b: at the moment a particle at the origin of phase space is excited by the kicker, it will move towards the septum, but will be moved back to the centre of phase space on the falling side of the kicker pulse and eventually end up on a small phase space ellipse around the origin. Generally, $\mathcal{E}$ is a bit larger after excitation by the kicker magnet than before excitation. In this way it is possible to inject many pulses following each other, with a delay between the pulses necessary for radiation damping to shrink the beam. This is called *multi-shot injection.* One of the main topics of this thesis is the calculation of how much radiation damping is needed between successive kicker pulses.

As can be seen from figure 3.3, the kicker magnet must not be too strong, or else it will kick the previously stored beam against the septum wall. But considering the

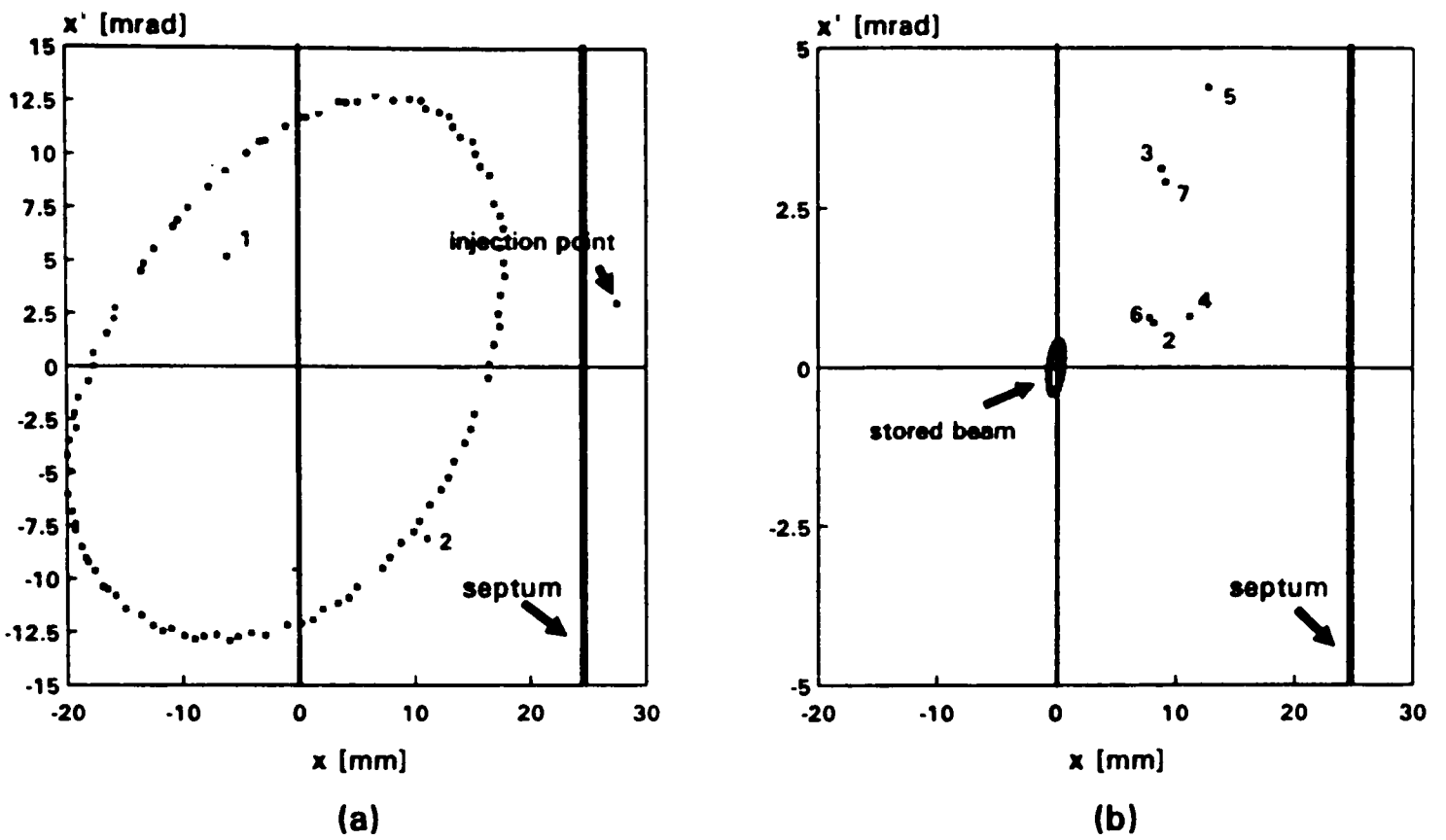


Figure 3.3: Radial phase space plot at the the septum position for a newly injected particle (a) and a previously stored particle (b).

injected beam, the kicker magnet should be relatively strong, to bring the injected beam on a phase space ellipse which is as small as possible. These are counteracting factors and a balance has to be found for the kicker strength.

The use of only one kicker magnet is a special feature of HELIOS: most accelerators use some slow pulsed 'bump magnets', to move the orbit of the stored beam close to the septum, and one or more faster pulsed kicker magnets to move the orbit even closer. In HELIOS there is no space available for more injection magnets than one kicker and one septum. The disadvantage of using a single kicker magnet is that the orbit is distorted through the whole accelerator and not only over a limited part of the orbit around the septum. Because of the short orbit period and the shape of the short kicker pulse, each particle will get a unique set of kicks from the kicker magnet, which can not be approximated by closed orbit error calculations.

3.2 Low-Energy Injection

The synchrotron radiation damping times depend on energy as $1/E^3$ (see 2.59, 2.60, 2.61), since U_0 varies as E^4 (see 1.2). As a consequence a damping time of 0.1 s at 200 MeV increases to 6.4 s at 50 MeV. Assuming that injection still takes place at a repetition rate of 10 Hz, the 'classical' picture as discussed in the previous section is not valid, because the beam will not have time to shrink to a small beam size between subsequent kicker pulses. In this situation, where the synchrotron radiation damping times are much longer than the injection interval, the term *low-energy injection* is used. For HELIOS the radial damping time τ_x at 100 MeV is 0.67 s, which for injection at 10 Hz is about the upper limit of low-energy injection.

The program MCIS (Monte Carlo Injection Studies) has been developed in order to study what happens if the time between the injection pulses is much shorter than the damping times. The main difference of MCIS, compared with conventional studies, is that the program does not assume a clear difference between the newly injected electrons and the stored beam, because the electrons in the previously injected shots can have oscillation amplitudes almost as large as the newly injected beam: *over the first few seconds after injection there is no clear difference between previously injected electrons and the newly injected beam.* Whether an electron is lost over the first few kicker pulses or not depends on random factors such as the position of the electron in radial phase space at the time the kicker is pulsed. It is also possible that the particle is lost within the first few turns after injection, depending on the starting parameters of the particle and the injection time relative to the kicker magnet pulse.

Until now only injection in the radial phase space has been considered, without any coupling with the longitudinal or vertical phase space. This is standard in the 'classical injection picture'. If no coupling with these other phase spaces is taken into account, it is indeed very difficult to inject at energies where the damping time is much larger than the injection intervals. With MCIS it is for the first time possible to give a good quantitative estimate of the effect on the injection efficiency of coupling between different phase spaces. Also the physical explanation of the

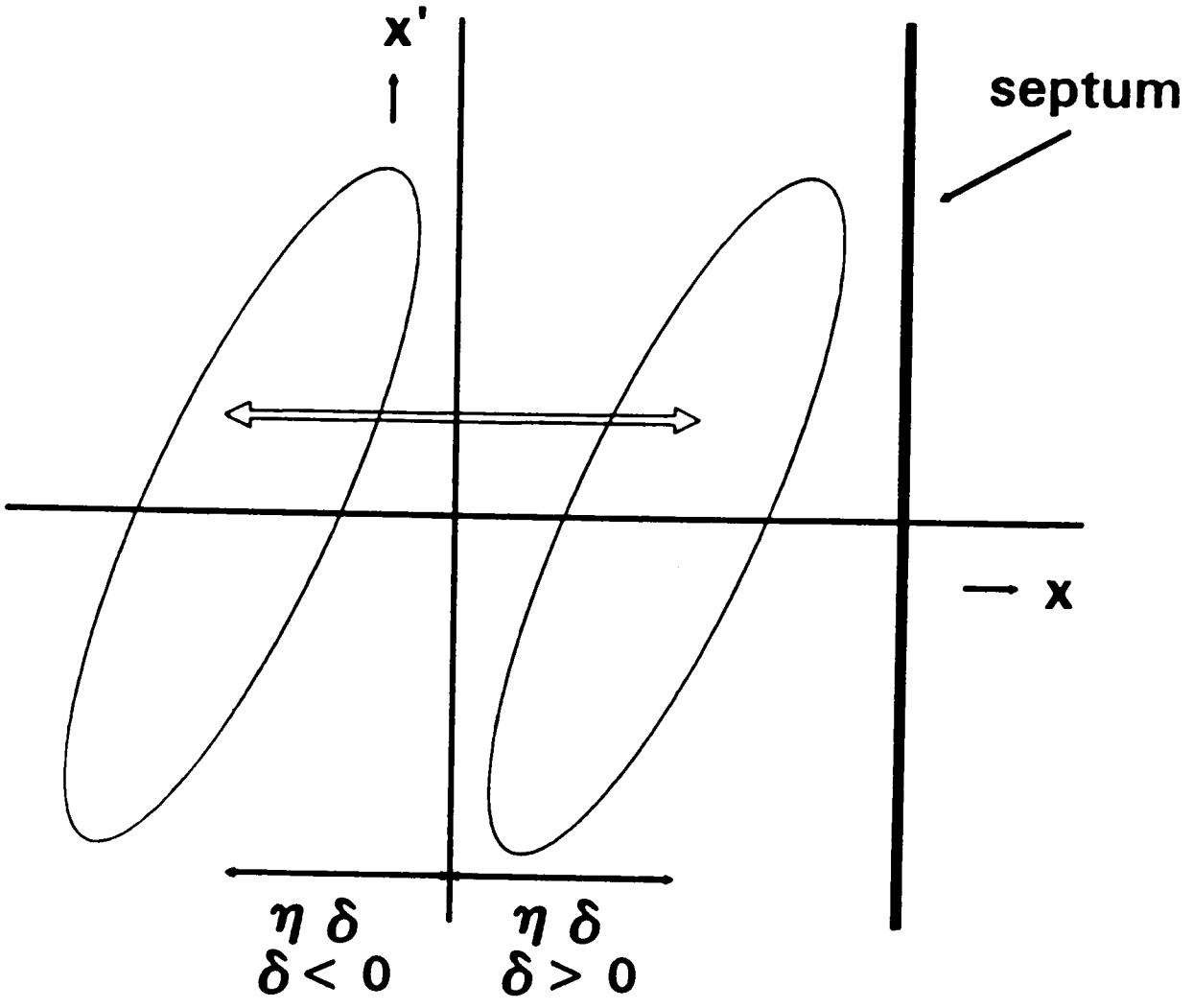


Figure 3.4: Coupling of energy oscillations with the radial phase space.

process by which coupling between the different phase spaces increases the injection efficiency has not been published before.[1]

The effect of coupling of the radial phase space with the other two phase spaces is explained qualitatively in this chapter. Calculations with the program MCIS are presented in the next chapter.

3.2.1 Coupling with the Longitudinal Phase Space

Coupling of the longitudinal with the radial phase space takes place through the dispersion function η, as given in formula 2.29. Assuming a constant energy deviation $\delta = \Delta p/p_0$ and $\eta' = 0$, the eigen ellipse of the particle in horizontal phase space is not centred around the origin but around $(\eta\delta, 0)$. Now considering the longitudinal energy oscillations, the centre of this ellipse will move along the horizontal axis with the synchrotron oscillation tune ν_s, see figure 3.4.

[1] M. Eriksson has made qualitative suggestions about such a mechanism in [ERI90].

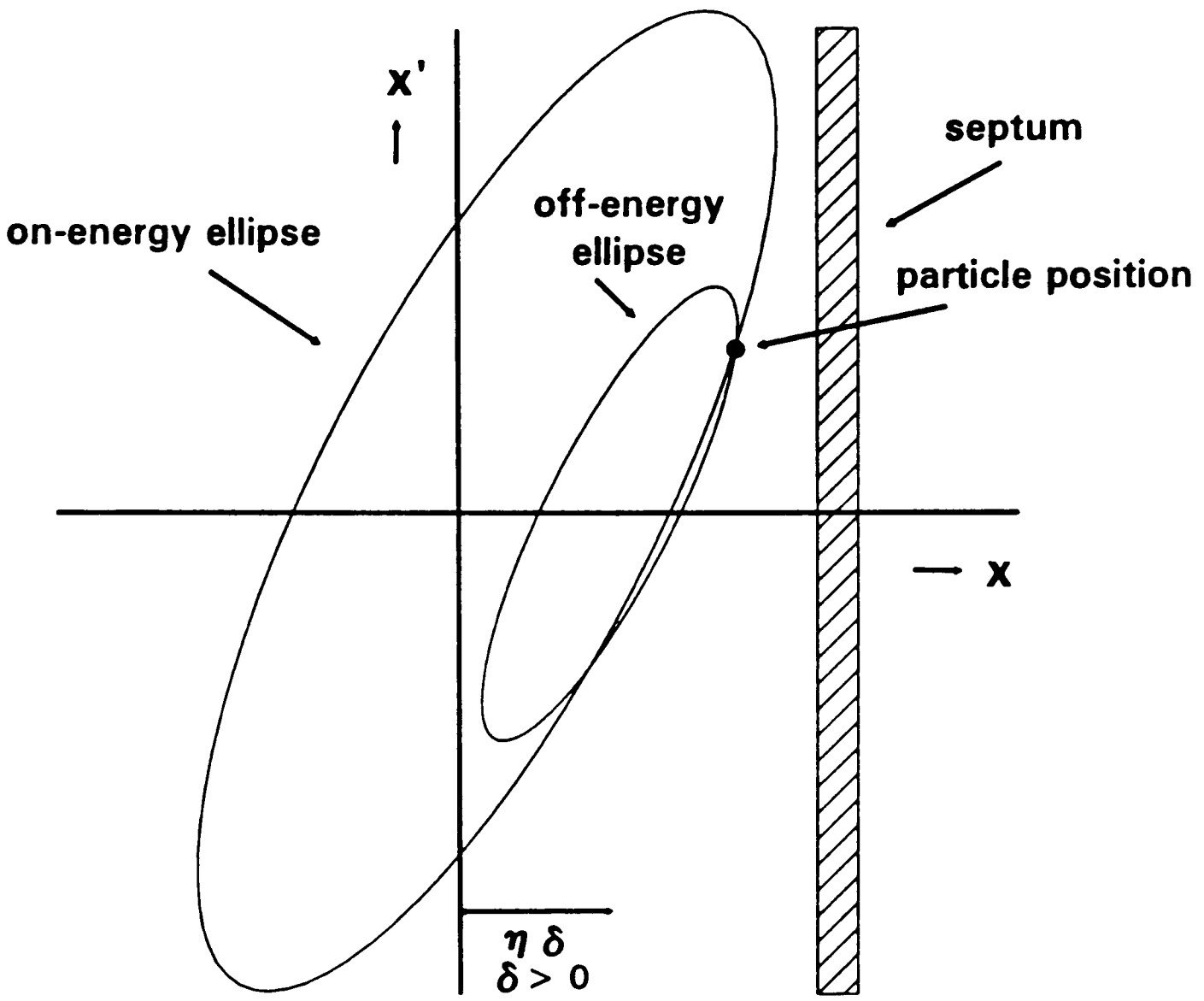


Figure 3.5: Reduction of initial emittance in horizontal phase space by injecting off-energy.

To get a quantitative idea of the effect of longitudinal coupling, the relevant numbers for HELIOS are taken as an example: at the septum the dispersion is about 1 m and by injecting off-energy with $\delta = 1\%$, the centre of the horizontal phase space ellipse starts off displaced to the septum side by about 10 mm. The displaced ellipse has the same orientation of its axes as the ellipse from an on-energy particle. Because the septum position is at $x = 25$ mm, the initial particle emittance in radial phase space is reduced significantly, see figure 3.5. This smaller emittance is damped with the horizontal radiation damping time τ_x. The energy oscillation is damped by the longitudinal oscillation damping time τ_ϵ. Because the anti-damping term in τ_x appears as a damping term in τ_ϵ, see formulae 2.60 and 2.61, τ_ϵ will generally be smaller than τ_x. For HELIOS, at 50 MeV, $\tau_\epsilon = 1.3$ s and $\tau_x = 5.4$ s

(depending on tune).

The smaller energy oscillation damping time is one of the reasons to inject off-energy, but an even more important reason comes from random processes within the electron beam: the time the kicker magnet is pulsed to inject another pulse is random on the time scale of the betatron and energy oscillations. The radial betatron number is around 1.5 for HELIOS, but the synchrotron tune is much smaller, around 0.05 depending on the RF-voltage in the cavity. The particle which is kicked out by the kicker magnet is normally lost over the first few turns after the magnet is pulsed, so for simplicity δ can be taken as a constant over these few turns. Now it can be seen that if at the time the kicker magnet is pulsed δ is negative, the radial phase space ellipse will be centred to the left of the origin of phase space, away from the septum. In this situation it is very unlikely that the particle is kicked against the septum wall by the kicker magnet. Only when δ has the same value as at injection, $\delta = 1$ %, is the chance of kicking the stored beam out the same as when the particle was injected on-energy. For all values of δ smaller than the value at injection the chance of kicking the beam out is smaller.

3.2.2 Coupling with the Vertical Phase Space

The injection efficiency can be further improved by introducing coupling between the horizontal and vertical phase space. This can be done by a skew quadrupole magnet and preferably operating near a coupling resonance (see chapter 2).

The arguments are more or less the same as for coupling with the longitudinal phase space: the vertical oscillation damping time is shorter than for the radial phase space (for the same energy and tune point as in the previous section $\tau_y = 3.2$ s) but not as short as for the longitudinal phase space. But again more important is the effect caused by random processes within the electron beam. The random phase, important for this process, at which the kicker magnet is pulsed is now the phase of the beating between the horizontal and vertical phase space. Working close to a coupling resonance and with a weak skew quadrupole, the beat period is a few hundred turns. If a part of the initial horizontal emittance is transferred to the

vertical phase space, the particle emittance in horizontal phase space is smaller than at the moment of injection and it is less likely that the particle is kicked out by the kicker magnet than it would be with the full emittance in the horizontal phase space. Only in the situation where all particle emittance is transferred back to the radial phase space is the chance of kicking out the particle the same as without coupling. For all other initial beat phases it is less likely that the particle is lost by the kicker pulse acting on the stored beam.

3.3 The Injector

For HELIOS a 200 MeV linear injector, or *linac*, is used. For the following HELIOS machine (HELIOS 2) a 100 MeV microtron will be used. The choice of injector depends on the injection energy: microtrons are made relatively routinely for energies of 50 MeV and 100 MeV, but not for much higher energies; for low-energy injection the quality of the injected beam is more important than at higher injection energies. A 100 MeV microtron is sketched in figure 3.6.

The advantage of a linac is that it is less critical to set up and can produce larger currents than a microtron. A typical linac can deliver currents of more than 20 mA (measured within one pulse) with an energy spread of $\pm$ 0.5 %, using energy selecting slits in the transport line. A well performing microtron has a maximum current of about 10 mA, but with a much better beam quality: the energy spread is around 0.1 % and the emittance is about 20 times smaller in both transverse phase spaces: for 100 MeV $\varepsilon_x \approx \varepsilon_y \approx 2$ mm mrad for a typical linac and 0.1 mm mrad for a microtron. The better beam quality is due to the beam selection process over the turns in the microtron. The beam quality makes the microtron the best choice of injector for low-energy multi-shot – multi-turn injection.

As a 100 MeV injector the microtron is more compact than a linac. Because of the better beam quality no energy selecting slits are necessary and the transport line for a microtron can be made shorter: for energy selecting slits to work well it is necessary to design the optics in the transport line so that at the position of the

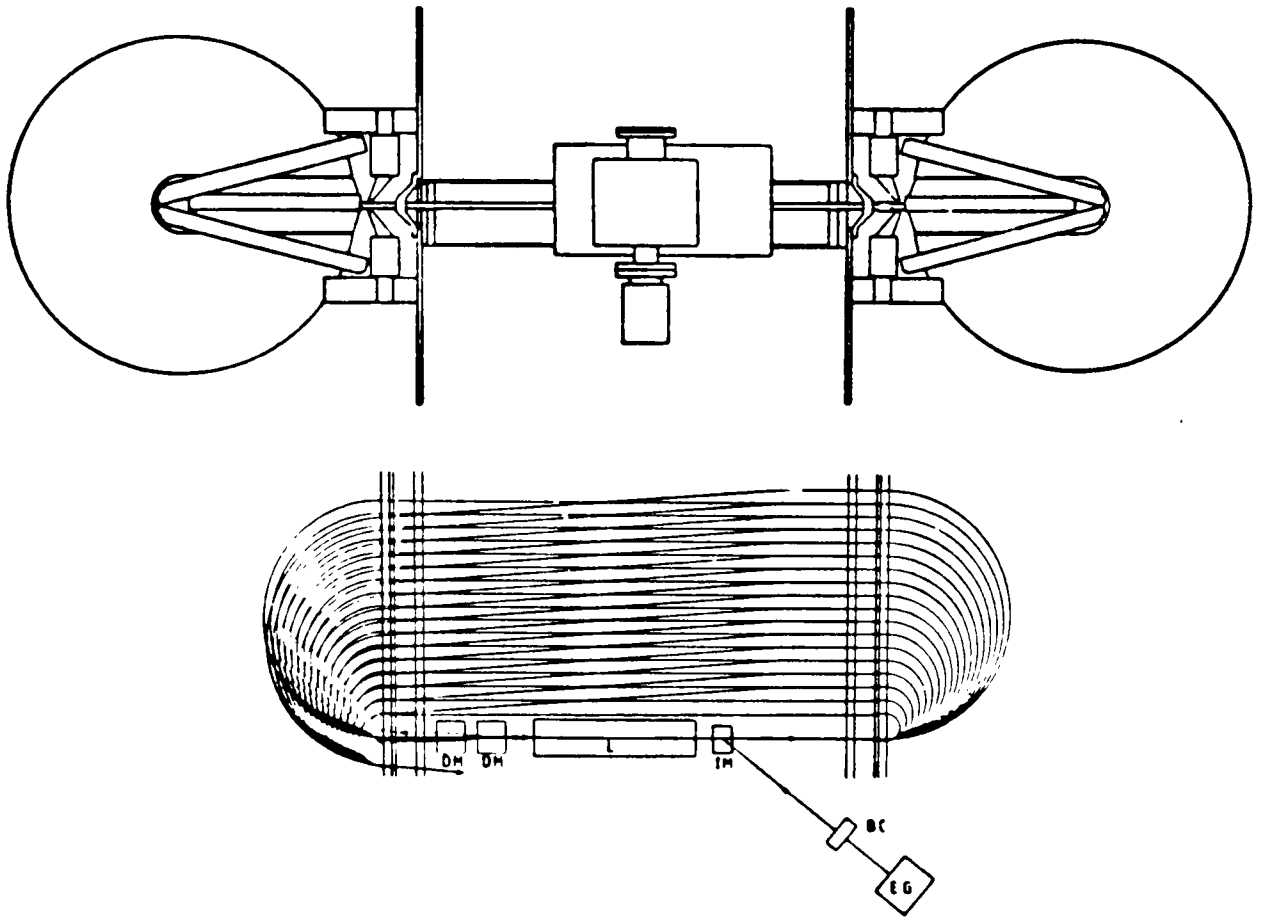


Figure 3.6: Schematic presentation of a 100 MeV microtron [ERI87]. EG = electron gun, BC = pre-buncher, L = linac within microtron.

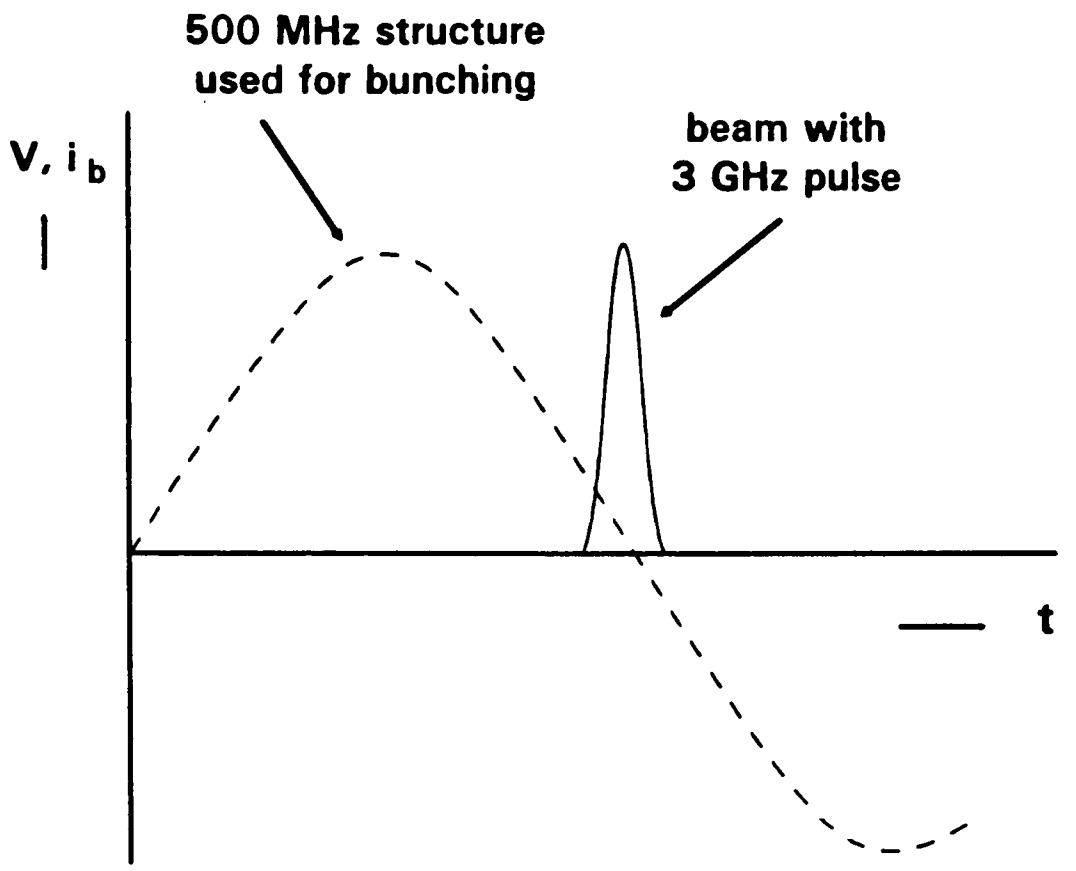


Figure 3.7: Time structure of the microtron beam with the use of a pre-bunching cavity.

slits the beam size is small in the horizontal direction and the dispersion is large. This requires extra drift space and quadrupole magnets.

The fraction of the current injected by a microtron and accepted by the accelerator can be significantly increased by the use of a pre-bunching cavity between the electron gun and the linac within the microtron (see figure 3.6). This cavity runs at the ring RF-frequency and is phase locked with the ring cavity. With the correct drift length between the prebuncher and the first entrance in the microtron-linac, the electrons will only fill one out of the six 3 GHz bunches in the microtron, assuming a 500 MHz ring RF-frequency and a 3 GHz accelerating frequency in the microtron-linac. This is illustrated in figure 3.7. This one bunch can then be injected in the accelerator, close to the synchronous phase ϕ_s. Assuming that most of the beam injected further out of phase will be lost, the useable injector current is effectively increased by a factor of 6. This was experimentally found at the MAX synchrotron in Lund, Sweden (see [ERI82, LIN83, ERI87]), where after installation

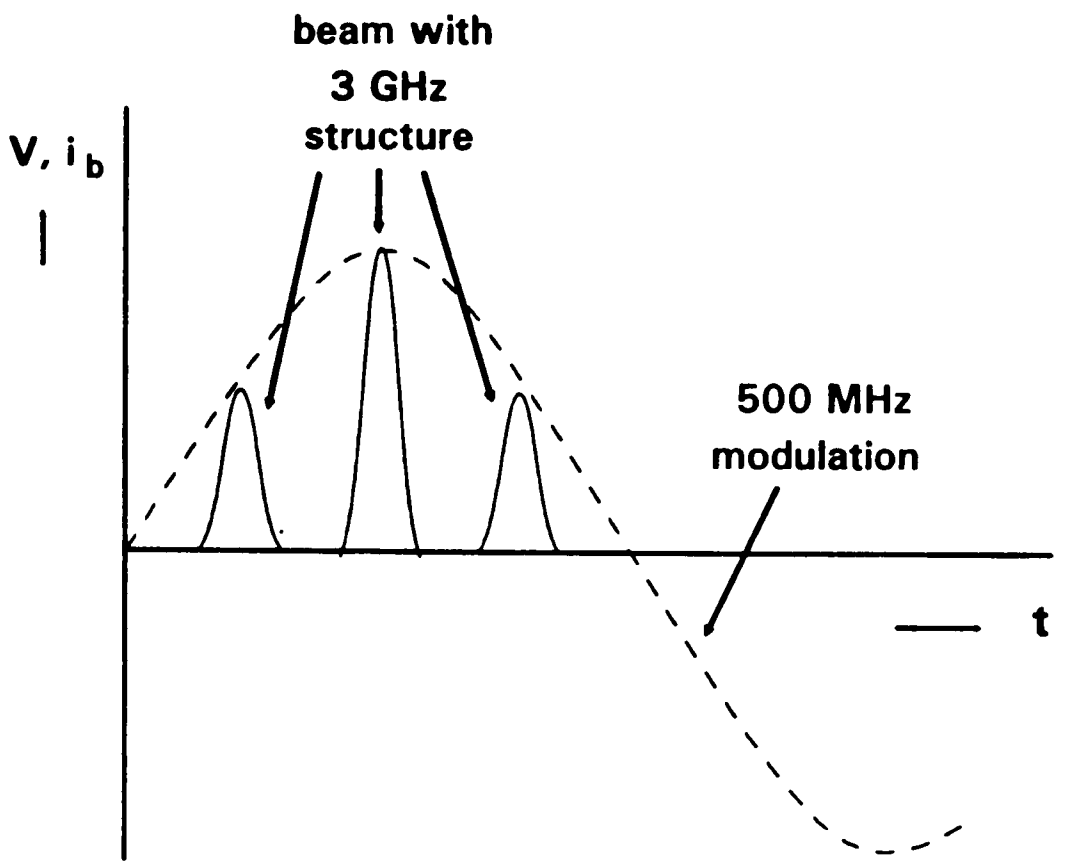


Figure 3.8: Time structure of the linac beam with the use of a pre-bunching cavity.

of a prebuncher in front of their microtron, the injection efficiency increased by a factor of about 6.

The 200 MeV linac as used for HELIOS also has a pre-bunching 500 MHZ cavity, locked to the ring cavity. Because the main accelerating section starts almost immediately after the pre-buncher, the pre-buncher can only give a 500 MHz modulation of the electron beam and does not increase the peak current within a micro-bunch, see figure 3.8.

3.4 Other Injection Methods

Besides the injection method discussed in sections 3.1 and 3.2, there are also other injection methods possible. All other methods of injection which are experimentally realised are briefly discussed in this section.

The multi-turn injection system can be extended to a method where the injection takes place over many, up to a few hundred, turns. The injector has to be able

to deliver a longer beam pulse and the kicker and septum pulse also have to be extended. Very often an exponentially decaying kicker pulse is used instead of the sinusoidal pulse. Depending on the details of the injection system the previously stored beam is more excited by the longer kicker pulse. It is possible to get around this problem by using a very large injector current and injecting all the necessary current in one single shot (single-shot – multi-turn injection). A disadvantage of large current low-energy injectors is that their beam quality is often not very good. At Nippon Telephone and Telegraph in Japan injection in a compact synchrotron similar to HELIOS has been achieved with a single shot method, using a 15 MeV linac ([WIL90]).

Besides injection in the horizontal phase space, it is also possible to inject in the vertical phase space, using a vertical septum and kicker magnet. The reason to choose this system is normally the layout of the accelerator and building or a large horizontal dispersion. If the horizontal dispersion is large, the radial beam size is significantly increased due to energy oscillations (see 2.66), which can be unacceptable if the horizontal emittance ε_x is also large because of injection in horizontal phase space. A disadvantage is that coupling of the vertical phase space with the longitudinal phase space is not possible, because there is no vertical dispersion in the accelerator. For all other processes this system is identical to injection in horizontal phase space. At COSY in Germany vertical injection, using a 50 MeV microtron, has been successful ([WEI88]).

It is also possible to stack in longitudinal phase space ([CAS85]). This is a complicated system, using special RF cycles and is not used for compact synchrotrons such as HELIOS.

A system used by Sumitomo Heavy Industries is resonance injection. It is the time reversal of the more common resonance extraction, operating at a tune point near a betatron resonance and using the movement along the separatrix in the transverse phase spaces to enter the stable regions ([TAK87b]).

Chapter 4

Computer Modelling of the Injection Process

Simulation of the injection process by computer codes becomes more complicated if the synchrotron radiation damping times are much larger than the interval between consecutive injection pulses. This is mainly because there is no clear separation between the previously injected beam(s) and the newly injected beam. In this situation the successful acceptance of a specific electron by the accelerator depends on random processes within the beam. It is also important to take into account the coupling between the different phase spaces, as is explained in the previous chapter.

The code Monte Carlo Injection Studies (MCIS) was written specifically to study the low energy injection process. The main characteristics of the code are:

- Many particles are generated according to a random number procedure, simulating the spread of parameters within a real beam entering the ring from the injector.

- The particles are *tracked* in the three orthogonal phase spaces. In the tracking each particle is followed along the accelerator over many turns, using matrix multiplication for the transverse phase spaces and solving the differential equation for the longitudinal phase space. In the radial phase space a pulsed kicker magnet is modelled.

- Synchrotron radiation damping is simulated for all the three phase spaces. The phase space coordinates after damping are generated according to some

random procedure, which takes into account the random behaviour of the beam during the simulated damping period.

During tracking the particle horizontal position and energy deviation are checked against the physical machine aperture at the septum and the energy acceptance respectively. If the particle is outside the acceptance, it is labelled *lost* and the tracking of another particle starts. Between two kicker pulses the particle makes $3 \cdot 10^7$ revolutions (!) around the accelerator. It is impossible to track the particles over so many turns and a different method is used: the particle is tracked over a few hundred turns, and if the particle is not *lost*, synchrotron radiation damping is simulated. After this simulation the tracking of the particle starts again, with at the beginning of each new tracking series a simulation of the pulsed kicker magnet, exciting the beam. The process of damping – excitation – tracking repeats itself till one can be sure the particle is safely trapped. Normally about 15 simulations of damping and excitation are sufficient[1].

This is repeated for many particles; 2000 particles are sufficient to get a statistically reliable result[2]. The program finally gives two survival percentages. One is for the particles which survive the first series of tracking, but not necessarily any of the tracking after the first simulation of synchrotron radiation damping. This is called *initial capture*. The second is the *final survival* percentage which represents capture by the accelerator, after being excited by all the simulated kicker pulses. Of course the number of particles, the number of turns to track over and the number of kicker pulses necessary for a realistic simulation depend on the actual parameters of the run, such as the damping times and the amount of coupling.

The code originated as a few extra routines added to the SRS Daresbury program ORBIT, used for general beam optics problems in a synchrotron. But during the development of the program the number of new subroutines increased and changes to existing routines had to be made to reduce the computing time. Finally it became easier to handle the program as a separate code: MCIS. A number of routines, like

[1] See page 69.
[2] The statistics are explained on page 67.

calculating basic lattice parameters, were copied from ORBIT. Also the definition of the lattice is according to ORBIT. But many new routines were added to speed up the transverse tracking, track in longitudinal phase space, simulate the synchrotron radiation damping and the generation of many different particles with 'random' starting coordinates. Some of these new routines are discussed in section 4.1.

It is difficult to *guarantee* that any program is error free. Checks have been made for MCIS by studying many phase space plots and running the program over a wide range of most of its parameters. Some of these phase space plots are included in this chapter. The results of these tests are all satisfactory. The results of the program also agree with experiments from different machines (see chapter 5). The theoretical checks and experimental agreement indicate that the code realistically models the assumed situation.

The graphs in this chapter have been made with the Physics Analysis Workstation code (PAW), originating from CERN, see [PAW89]. The plotted data can automatically be written to separate files and in principle may be read in by any other graphics program.

MCIS is written with HELIOS in mind, but can be applied to any accelerator with only one kicker magnet and one skew quadrupole magnet in front of the kicker (in general it is not expected that the number and position of skew quadrupoles have a significant effect on the final survival percentage, assuming that the single quadrupole is not too strong). Only minor modifications to the transverse tracking have to be made to make the program applicable to an accelerator with any number of pulsed and skew quadrupole magnets. Most of the calculations presented in this chapter are for HELIOS (section 4.2.2), but as an example some calculations for MAX (Sweden) are included (section 4.2.3).

The exact format of the input and output data of MCIS is given in appendix B.

4.1 Description of the Program MCIS

This section describes the algorithm used for MCIS in more detail. It is divided into two sections: section 4.1.1 describes the methods of calculation used in radial and

longitudinal phase space, starting with the initialisation of a particle, then tracking in radial and longitudinal phase space and finally the modelling of synchrotron radiation damping. Section 4.1.2 describes the implementation of coupling with the vertical phase space. This division has been made because there are some limitations on the parameters with which the program can be used if there is coupling with the vertical phase space. It is probably also clearer to explain the coupling between the different phase spaces in steps.

4.1.1 Radial and Longitudinal Phase Space

In this section the separate routines for the initialisation of a particle, radial and longitudinal tracking and radiation damping are discussed.

Initialisation of a Particle

The particles are generated with a random spread of their starting parameters according to a specific distribution. The initial values of x, x' and δ are generated according to a Gaussian distribution, with a specified standard deviation σ_x, $\sigma_{x'}$, σ_δ and mean value x_m, x'_m, δ_m.

At the modelled injection energies (below 100 MeV) there is hardly any energy loss because of synchrotron radiation emission over 1 turn so hardly any acceleration by the RF-cavity is needed. This means that the synchronous phase ϕ_s is very close to π rad. The distribution from which the initial particle phase ϕ of the injected particle is generated is described by the *micro-bunch parameter.* If the micro-bunch parameter is set to 1, the particle is always injected at the synchronous $\phi_s = \pi$ rad, which simulates a microtron with a pre-bunching cavity as described in figure 3.7. If the micro-bunch parameter is set to 3, the initial phase will have a probability of 50 % of being equal to π rad, 25 % to be equal to $\frac{2}{3}\pi$ rad and 25 % to be equal to $\frac{4}{3}\pi$ rad. This simulates a linac with a perfectly working prebuncher running at the ring RF-frequency (500 MHz) and a linac accelerating structure running at six times the ring frequency (3 GHz), see also figure 3.8. There is no Gaussian distribution around those initial phase values, because σ_ϕ is very small and some spread in the longitudinal motion is already introduced by the spread in δ.

Under most circumstances the two 'side-bunches' of the injected beam with initial phase $\frac{4}{3}\pi$ or $\frac{2}{3}\pi$ rad are lost over the first few turns because δ increases considerably. As an example consider HELIOS, injecting at 50 MeV and an accelerating voltage of 300 kV: a particle is injected with $\phi = \frac{4}{3}\pi$ or $\frac{2}{3}\pi$ rad and $\delta = 1\%$. After a few turns the particle has obtained its maximum energy deviation, for which $\delta = 1.7$ %. This is an *additional* displacement of 0.7 % $\times\ \eta \approx 7$ mm ($\eta = 1$ m). A movement of 7 mm towards the septum at the beginning of the injection process is normally fatal and the particle is lost. With RF-voltages below 50 kV and δ around 1 % the side-bunches can also be lost in longitudinal phase space.

The timing of injection relative to the start of the kicker pulse (t_0 in figure 3.2) is generated from a flat distribution between a specified upper and lower limit. These limits define the pulse length of the injected beam (macro structure). Depending on the injector a Gaussian distribution can be more realistic. The flat distribution is the more pessimistic approximation from an injection efficiency point of view.

Immediately after generation of the particles x is checked against the defined *outer aperture limit* at the septum. This is the aperture limit at the end of the transport line. For the tracking in the ring the *inner aperture limit* is taken as a selecting criterion. Both aperture limits are fixed by the design of the vacuum vessels in the region of the septum and the septum thickness. By giving these two aperture limits a different value, a finite septum thickness can be modelled. This makes it possible to calculate the effect of injecting a *scraping beam* against the septum; losing part of the beam before it enters the accelerator, but having a higher injection efficiency for the particles which enter the accelerator because they are injected closer to the centre of the vacuum chamber.

The initial value of δ is checked against the energy acceptance of the accelerator before tracking starts, and the particle is considered to be *lost* if δ exceeds the energy acceptance.

Tracking in Radial Phase Space

The tracking in radial phase space is done through first order matrix multiplication. This means that quadrupole fields are the highest order multi-poles which are modelled. Because of this, resonances higher than second order do not appear in the tracking (see formula 2.31). In most accelerator codes tracking takes place over many turns, so that higher than second order resonances can develop. In MCIS tracking also has to be performed over a few hundred turns, but not because of higher order resonances. The number of turns over which tracking has to take place in MCIS is defined by the interaction between horizontal and longitudinal phase space (see page 69).

Tracking with higher order elements for a machine with a small bending radius is complicated. Special care has to be taken in the derivation of the equations of motion, and some terms which are normally neglected become significant if ρ decreases. The derivation of the equations of motion up to second order, this means including sextupole fields, which also has the small bending radius terms, is given in appendix A. Including these terms in the tracking procedure has to be done with care, considering the symplecticity ([BEL87]) and the segmentation of the lattice. The effect of the small bending radius terms on the tracking results for HELIOS is presented in [ARC91]. Including higher than first order tracking in a program to study the injection process is not necessary and should be done by separate tracking studies. The result of the tracking studies can lead to the choice of the injection tune point, which can then be used in the injection studies. Ignoring the higher order magnetic fields significantly reduces the required amount of CPU-time.

For HELIOS the lattice is defined by about 140 elements. The two identical dipoles are segmented in 60 elements each, using the results of TOSCA calculations (see [TOS88]). Because no higher than quadrupole order field components are included in the tracking, the precise field distribution within the dipoles is not expected to have a significant effect on the calculated survival percentages.

After the lattice-data are read, the horizontal betatron tune and the vertical betatron tune are set to the desired value by changing the strength of the focusing

elements in the accelerator. For the calculation of the betatron tunes the 3×3 transfer matrix of each element has already been calculated. The next step is the calculation of the partial matrices from the injection point to the kicker magnet M_{ik} and from the kicker magnet to the injection point M_{ki}. Tracking in the horizontal phase space consists of multiplying the coordinates of the particle with M_{ik}; checking the timing of the particle relative to the kicker pulse and giving the particle a thin lens kick $x' = x' + \Delta x'$ if the kicker is powered[3] and finally multiplying the phase space coordinates with M_{ki}. This is repeated for the specified number of turns.

Because the kicker pulse has the shape of a half-sine wave with a short period, the thin lens kick will normally only take place over the first few turns of the tracking procedure. The pulse length of the kicker magnet and the maximum kick at the top of the pulse $\Delta x'_{\mathbf{max}}$ are specified in the input list of the program.

During tracking the particle position x is checked against the inner aperture limit at the septum, and is considered *lost* if it exceeds the aperture limit.

Tracking in Longitudinal Phase Space

After the particle has been tracked in radial phase space for 1 turn, tracking takes place over the same turn in longitudinal phase space. Before this routine is called, the radial coordinates are translated with respect to the origin of radial phase space by the transformation

$$x_t = x - \eta\delta \tag{4.1}$$

$$x'_t = x' - \eta'\delta \tag{4.2}$$

After tracking the particle in longitudinal phase space the particle is translated back, using the new value of δ.

Tracking in longitudinal phase space consists of solving the two coupled differential equations 2.41 and 2.42 by a simple Runge-Kutta method for a time Δt equal to one revolution period ($\Delta t_{\mathbf{rev}}$). The accuracy of the solution depends on the step-size

[3] A dipole field can in paraxial approximation be modelled by a thin lens kick: if the bending radius in the dipole field is ρ and the magnet length is l, the kick $\Delta x'$ equals the bending angle, which is l/ρ, and is given in the middle of the magnet.

used within the Runge-Kutta method. The maximum Runge-Kutta step-size $\Delta t_{\mathbf{rk}}$ which is acceptable depends on the synchrotron tune and the number of turns over which the tracking takes place. If the $\Delta t_{\mathbf{rk}}$ is not small enough, it leads to a gradual increase of the maximum value of δ and through this to particle loss. The step-size demagnification D defined by

$$D = \frac{\Delta t_{\mathbf{rev}}}{\Delta t_{\mathbf{rk}}} \tag{4.3}$$

is adjusted automatically within the code, depending on the number of turns over which the particle is tracked.

The criterion used is illustrated in figure 4.1. It shows for HELIOS the number of turns required for δ to increase from 1.00 % at injection to $\delta_{\mathbf{max}} = 1.01\%$. This is an error in x of 0.1 mm, assuming $\eta = 1$ m at the injection position. The curve is calculated for HELIOS, injecting at 50 MeV and an RF-voltage of 340 kV. The result depends strongly on the synchrotron tune Ω_0. Larger RF-voltages and lower energies, which increase Ω_0 (see equation 2.44), result in larger steps in δ and ϕ and because of this a larger D is required for the same accuracy in the tracking. Choosing 50 MeV and 340 kV makes the calibration correct for most situations, but if the synchrotron tune is very high, for example because the machine has a very large circumference, it is wise to check the stability of $\delta_{\mathbf{max}}$ and correct D if necessary.

After each turn δ is checked against the energy acceptance of the accelerator. The particle is declared *lost* if it is outside the energy acceptance.

Synchrotron Radiation Damping

The synchrotron radiation damping between two following injection pulses is simulated after tracking for the required number of turns has been successful. The damping in the radial and longitudinal phase space are calculated independently.

The damping calculation in the radial phase space can be divided into 6 steps:

- After the tracking is finished, the initial particle emittance $\mathcal{E}_i$ at the septum position is calculated, using equation 2.27.

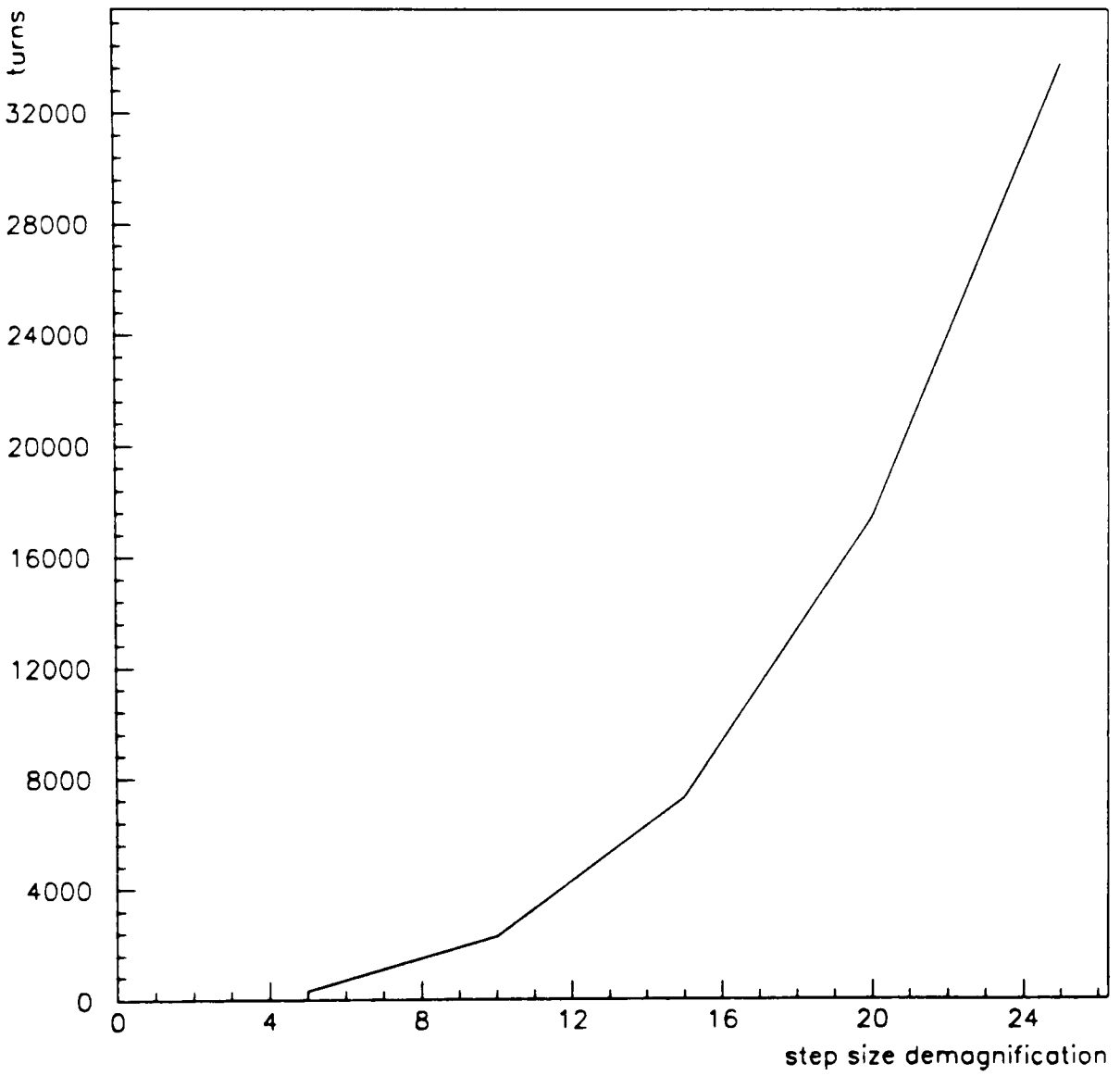


Figure 4.1: Number of turns after which a relative error of 1 % develops in δ, as a function of the step size demagnification D used in the Runge-Kutta integration.

- A particle in the equilibrium state (in equilibrium between synchrotron radiation damping and quantum excitation) is generated in normalised phase space with axes

$$X = \frac{1}{\sqrt{\beta}}x \tag{4.4}$$

$$X' = \frac{\alpha}{\sqrt{\beta}}x + \sqrt{\beta}x' \tag{4.5}$$

In normalised phase space the particle's eigen ellipse is transformed to a circle of which the radius squared equals the emittance. The coordinates (X, X') are generated according to a Gaussian distribution with standard deviation $\sigma_X = \sigma_{X'} = \sqrt{\varepsilon_x}$, where ε_x is the equilibrium beam emittance (see formula 2.63). From the coordinates (X, X') the emittance of this particle in the equilibrium state $\mathcal{E}_e$ is calculated.

- The emittance of the particle after damping is calculated, using

$$\mathcal{E}_f = \mathcal{E}_e + (\mathcal{E}_i - \mathcal{E}_e)e^{-2t/\tau_x} \tag{4.6}$$

where τ_x is the radial damping time and t the time over which the damping is simulated (for 10 Hz injection t= 0.1 s). This is an approximation valid for $\mathcal{E}_e \to 0$.

- At this stage the radius of the circle in normalised phase space on which will be the new particle position is known. The position on this circle is calculated by generating a random angle θ from a flat distribution between 0 and 2π rad and calculating

$$X_f = \sqrt{\mathcal{E}_f}\cos\theta \tag{4.7}$$

$$X'_f = \sqrt{\mathcal{E}_f}\sin\theta \tag{4.8}$$

- Finally the particle position is transformed back to ordinary phase space (x, x').

- Before tracking starts the particle is given a new initial timing relative to the kicker magnet timing t_0, generated from a flat distribution between 0 ns and the orbit period.

The method presented above is only valid for on-energy particles. For off-energy particles the coordinates have to be translated to the correct centre of phase space before the initial particle emittance is calculated and translated back at the end of the routine, using the new value for δ after radiation damping. These translations are the same as described in equations 4.1 and 4.2.

Damping in longitudinal phase space is simulated in almost exactly the same way as in radial phase space. The normalised phase space coordinates are now

$$\Phi = \phi \tag{4.9}$$

$$\Delta = \frac{d\phi/dt}{\Omega_0} = \frac{-\delta h \alpha \omega_0}{\Omega_0} \tag{4.10}$$

The last equality follows from 2.42 and is again only valid if $\gamma \gg 1$. The main difference with radial phase space is that the circle in normalised longitudinal phase space, of which the radius is proportional to the extreme values of δ the particle obtains during one synchrotron oscillation, is an approximation, only valid for ϕ close to π rad, when the motion is harmonic, see figure 2.3. Because of this two additional techniques are necessary:

- To calculate the initial radius of the particle in normalised longitudinal phase space, tracking is continued till ϕ is close to π rad and the radius is calculated at this position.

- If a particle is generated with coordinates (ϕ_f, δ_f) and ϕ_f is not close to π rad, tracking is performed, starting at a point on the same circle with $\phi = \pi$ rad, till δ reaches a value close to the originally generated value δ_f. Now ϕ will have a value a slightly different from ϕ_f because the circle approximation is not used for this tracking. This value is taken as the correct value for ϕ_f.

The damping process in longitudinal phase space is illustrated in figure 4.2. It shows the tracking of one particle, starting at $\delta = 1.75\%$ and $\phi = \pi$ rad, over 200 turns, repeated 20 times after the simulation of damping. The data plotted are a simulation of HELIOS, injecting at 50 MeV with a 10 Hz injection repetition

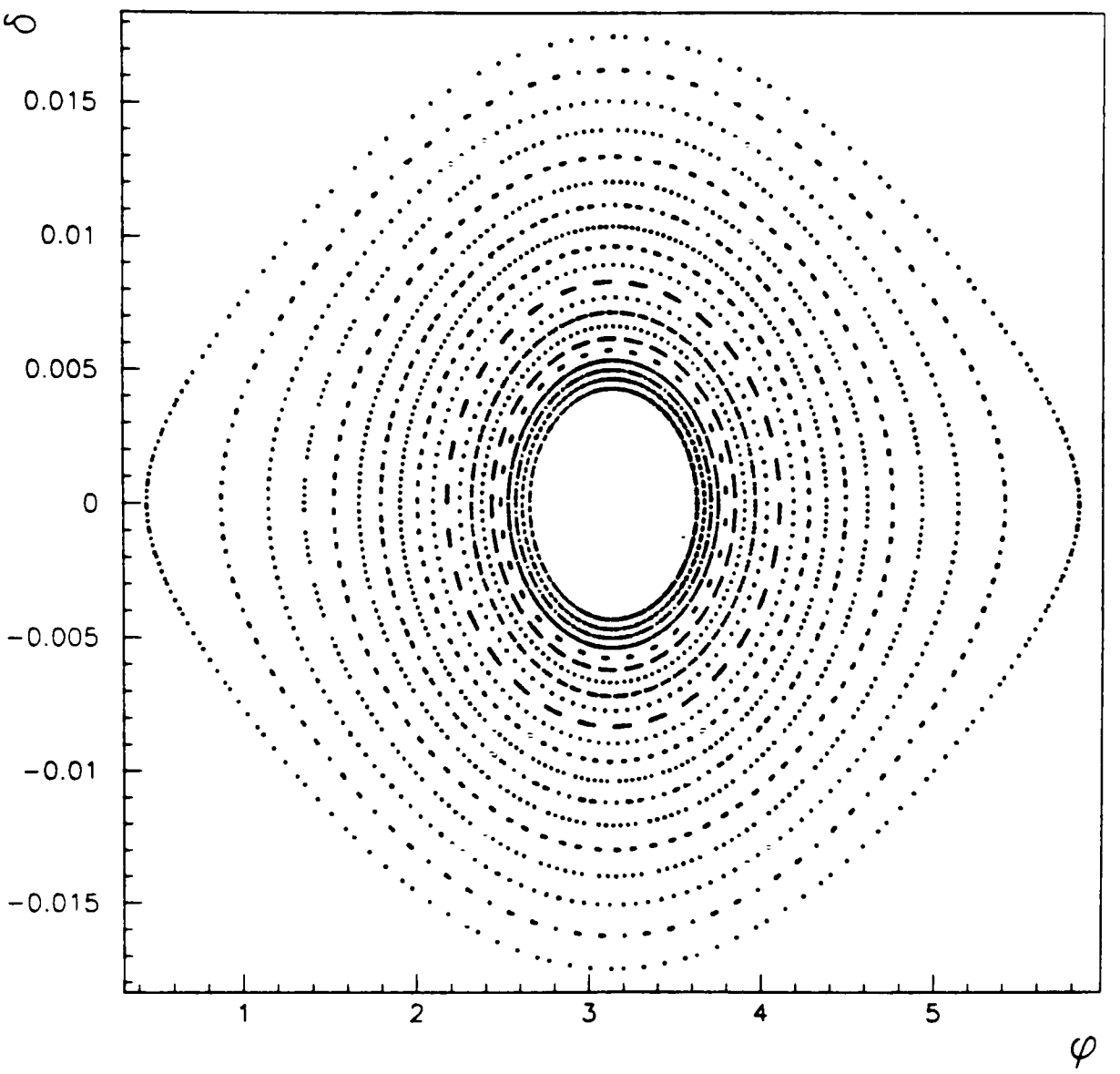


Figure 4.2: Tracking and damping in longitudinal phase space, with ϕ the longitudinal phase and δ the relative energy deviation of the particle.

rate. The initial energy deviation is close to the RF-acceptance $(\Delta p/p_0)_{\max} = 1.8\ \%$ for the arbitrary chosen accelerating voltage of 100 kV, used in this simulation. The figure shows that for large energy oscillations the deviation from the harmonic solution of the differential equations 2.41 and 2.42, which is only valid for $\phi \approx \pi$, is substantial and the differential equations have to be solved numerically.

The effects of the longitudinal motion and the longitudinal damping on the motion in radial phase space are illustrated in figure 4.3. The calculations are made for the same situation as in figure 4.2, except in (a) the particle is injected on-energy and in (b) the particle is injected with $\delta = 1\%$. Figure 4.3a shows concentric ellipses in radial phase space after consecutive damping simulations. The damping is not as smooth as in longitudinal phase space and there are also a few scattered

particles because of the kicker magnet which excites the beam after each damping simulation. Figure 4.3b shows the more complicated motion of a particle which is injected off-energy. The positive effect of the interaction with longitudinal phase space can clearly be seen: if the particle is injected with $\delta = 1\%$, there are only a few radial positions for which $x > 20$ mm, which is certainly not true if the particle is injected on-energy.

4.1.2 Coupling with the Vertical Phase Space

To include coupling between the horizontal and vertical phase space, it was necessary to make modifications to both the tracking routine and the damping routine in the radial direction. The tracking and damping routines in the longitudinal direction remain unchanged.

Modifications to the Tracking Routine

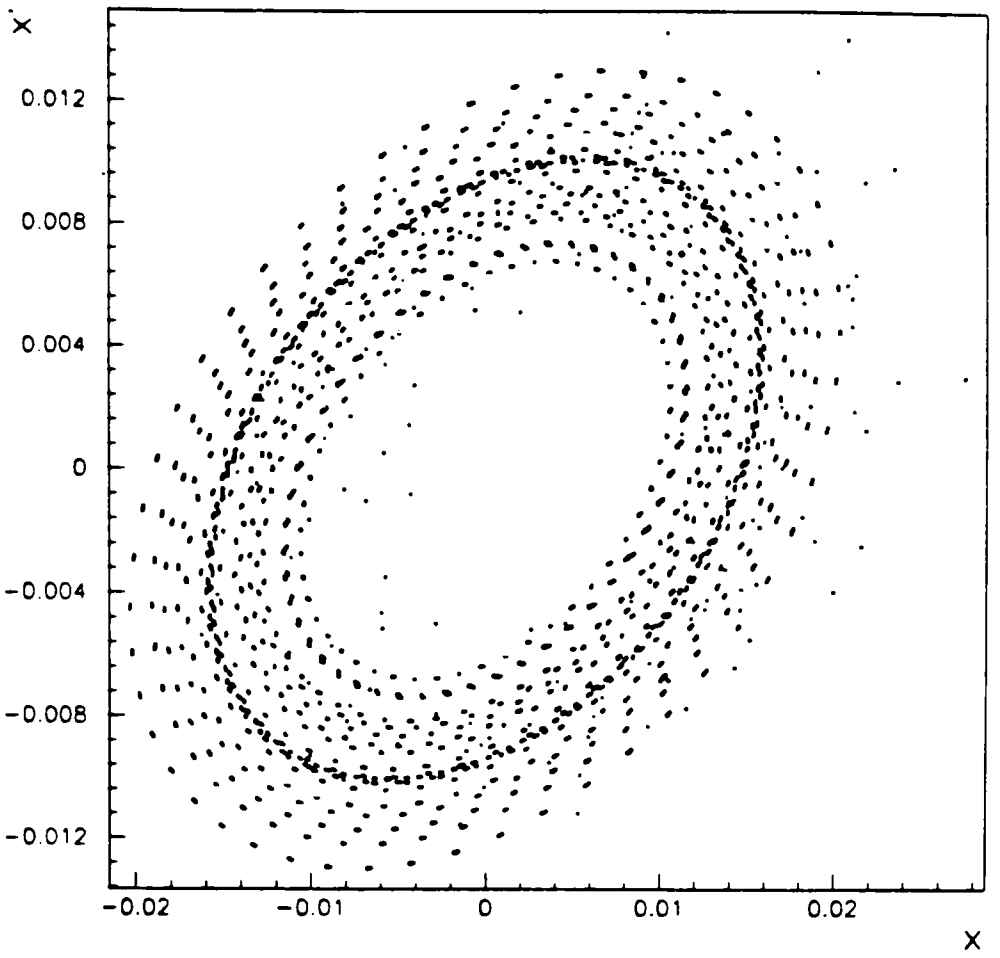
The coupling between the two transverse phase spaces is introduced via a skew quadrupole magnet, which is a normal quadrupole magnet rotated over 45°, modelled as a thin lens. The kick given to the particle in one plane depends on the excursion in the other plane:

$$\Delta x' = -\frac{cB_1 ly}{E[\mathrm{ev}](1+\delta)} \tag{4.11}$$

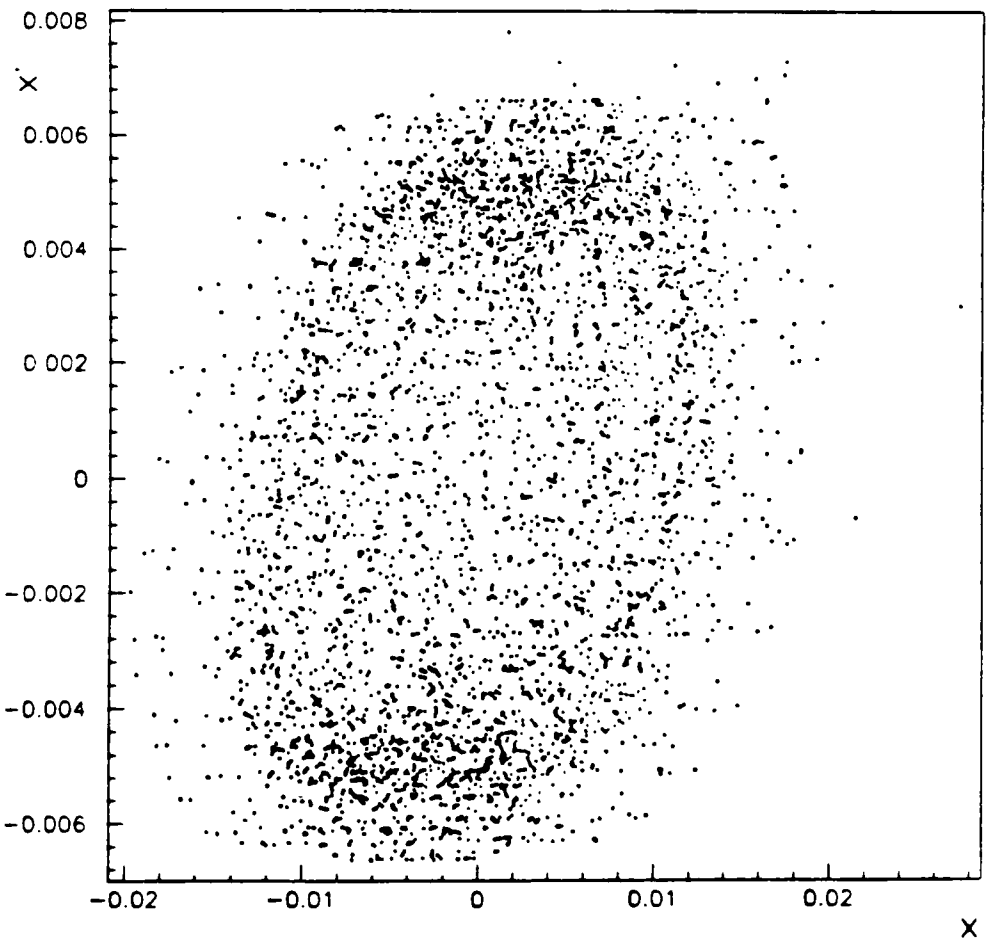
$$\Delta y' = -\frac{cB_1 lx}{E[\mathrm{ev}](1+\delta)} \tag{4.12}$$

where E is the nominal energy, B_1 is the magnetic field gradient of the quadrupole and l is the magnetic length of the quadrupole. The transfer matrix multiplication now takes place in both phase spaces, with a thin lens, skew quadrupole kick every turn.

The effect of the skew quadrupole on the tracking is demonstrated in figure 4.4, in which the position of one particle is plotted for over 600 turns in both phase spaces. This is about half the beat period for the exchange of horizontal and vertical emittance and after more turns the radial beam size would increase again, till it has

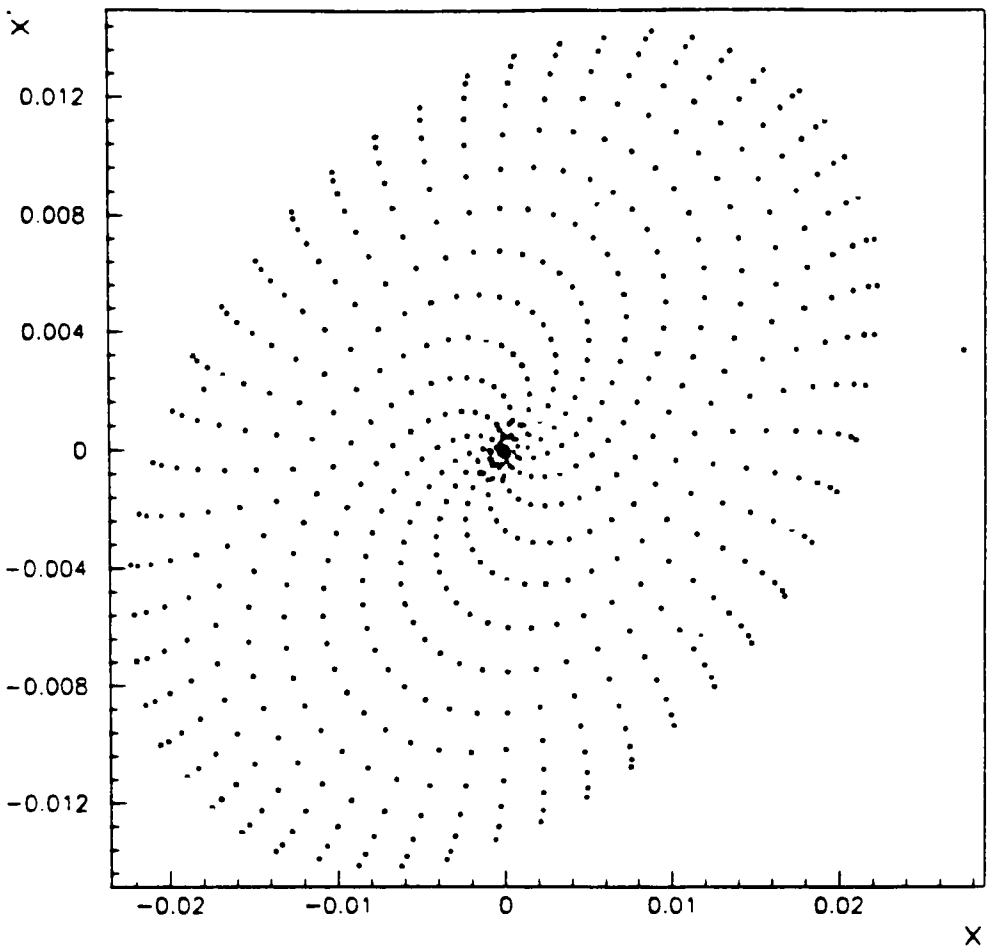


(a)

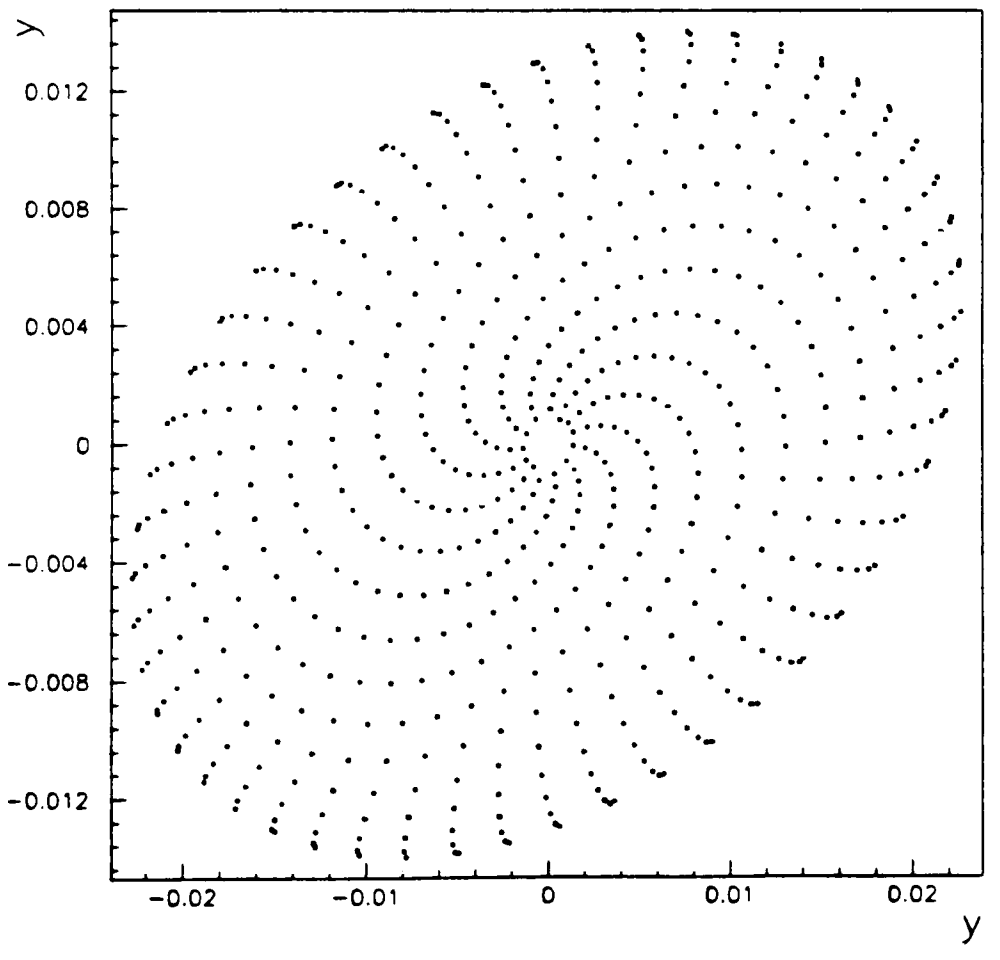


(b)

Figure 4.3: Tracking and damping in radial phase space for an on-energy particle (a) and a particle injected with $\delta = 1$ % (b).



(a)



(b)

Figure 4.4: Simultaneous tracking in horizontal (a) and vertical phase space (b), with coupling introduced through a skew quadrupole magnet.

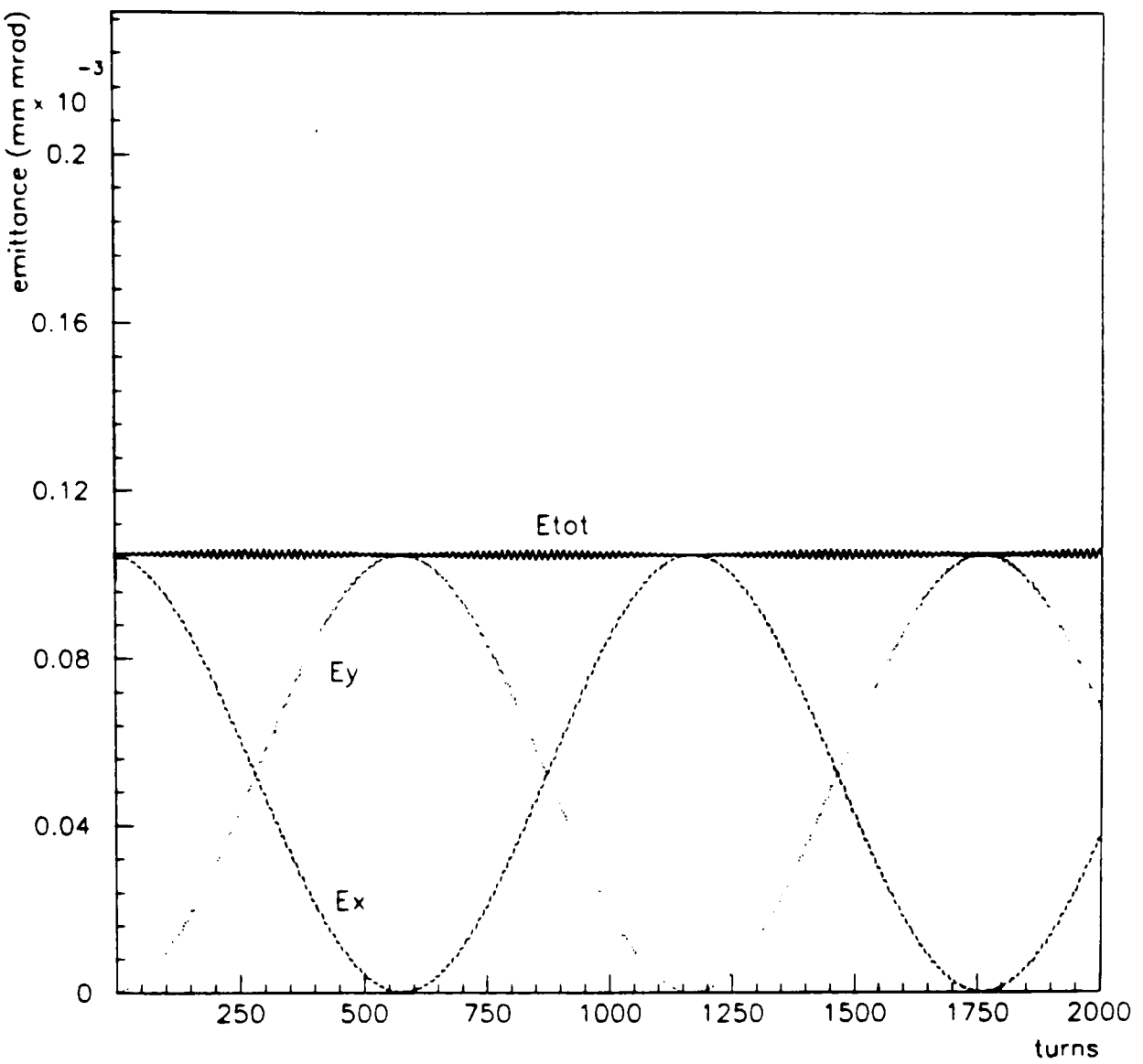


Figure 4.5: Exchange of horizontal and vertical emittance by the use of a skew quadrupole.

reached its initial value. In this example δ is set to zero, because the longitudinal motion would distort the picture in horizontal phase space.

The beating can be shown very clearly if the emittances of the particle in each phase space are plotted as a function of the number of turns over which the particle is tracked. This is shown in figure 4.5. As in figure 4.4 the tune point is exactly on a coupling resonance ($\nu_x = 1.54$ and $\nu_y = 0.54$), and the skew quadrupole has a very small integrated magnetic field strength of 0.0005 T.

The survival of the particle is *not* selected on the vertical physical aperture. This makes it possible to consider the effect of coupling with the vertical phase space without any additional 'hardware limitations'. In the situation of HELIOS, *full* coupling with the vertical phase space results in a critical vertical aperture,

which would in reality decrease the injection efficiency. This is further discussed in chapter 6.

Modifications to the Damping Routine

The method of calculating the emittances is important, because this is used in the damping calculation. The emittances are calculated by using the Twiss parameters as in equation 2.27. These parameters are calculated without any skew quadrupole field present. Introducing a skew quadrupole magnet results in some additional focusing and because of this the Twiss parameters change. To be able to use the standard Twiss parameters, defined without any skew quadrupole field present, the amount of skew quadrupole field has to be kept to a minimum. Assuming full coupling is desired, the best operating tune point is exactly at a coupling resonance. Now any small amount of skew quadrupole field gives full coupling and increasing the field results in a shorter beat period.

As can be seen in figure 4.5 the total emittance is not perfectly constant, but deviates by no more than 1 % from its original value. Decreasing the skew quadrupole field makes the total emittance $\mathcal{E}_T$ more constant, but increases the beat period, which can make tracking over more turns necessary. All calculations for HELIOS presented in this chapter are made at a coupling resonance and an integrated skew quadrupole field of 0.0005 T.

The damping routine within MCIS which includes coupling with the vertical phase space follows the same strategy as the routine described without coupling (see page 55). Now the *sum* of the emittances in the horizontal and vertical phase space is damped towards the emittance of a particle in the equilibrium state. Instead of the radial damping time, a damping time averaged over both horizontal and vertical phase space, τ_a, is used. The weighted average depends on the coupling strength g:

$$\begin{aligned} \frac{1}{\tau_a} &= \frac{\mathcal{E}_x}{\mathcal{E}_x + \mathcal{E}_y}\frac{1}{\tau_x} + \frac{\mathcal{E}_y}{\mathcal{E}_x + \mathcal{E}_y}\frac{1}{\tau_y} \\ &= \frac{1}{1+g}\frac{1}{\tau_x} + \frac{g}{1+g}\frac{1}{\tau_y} \end{aligned} \tag{4.13}$$

Both the integrated skew quadrupole field strength and the coupling strength g can be given as independent input parameters.

After the damped total emittance $\mathcal{E}_f$ is calculated, it is distributed over the horizontal and vertical phase space, by assuming a $(\sin)^2$ modulated beating between the two phase spaces:

$$\mathcal{E}_x = \mathcal{E}_f - \mathcal{E}_f \frac{2g}{1+g} \sin^2 \psi \tag{4.14}$$

$$\mathcal{E}_y = \mathcal{E}_f - \mathcal{E}_x \tag{4.15}$$

where ψ is a random angle generated according to a flat distribution between 0 and 2π rad. The factor of 2 in the formula for $\mathcal{E}_x$ appears because g is defined for *time averaged* particle emittances and is applied to a particle emittance at a specified time.

Within each phase space a random phase angle is chosen to divide the emittance over the normalised phase space parameters as in equations 4.7 and 4.8. The two chosen phase angles θ_x and θ_y do not depend on each other or the values of the partial emittances $\mathcal{E}_x$ and $\mathcal{E}_y$. Because of this the amplitude of the beating between the two phase spaces is sometimes less than the the sum of the two emittances, although the coupling g is still 100 %. This is illustrated in figure 4.6 where the partial emittances and the total emittance are plotted over 400 turns for 9 simulations of synchrotron radiation damping. It can be seen that for example after the first simulation of synchrotron radiation damping the maximum value of $\mathcal{E}_y$ is smaller than $\mathcal{E}_f$. The strength of the modulation depends on the combination of $\mathcal{E}_x$, $\mathcal{E}_y$, θ_x and θ_y. By not always assuming the maximum modulation, some natural variation of the emittances because of multi-particle effects and photon excitation is modelled.

The spikes in figure 4.6 are the sudden change of the horizontal and total particle emittance because of the kicker excitation. In most cases the residual excitation by the kicker magnet is less than the synchrotron radiation damping, which leads to a gradual decrease of the total emittance and a safe capture of the injected electron.

The transformation of the particle back to ordinary phase space and the choice of a random timing relative to the kicker magnet is the same as without coupling with the vertical phase space.

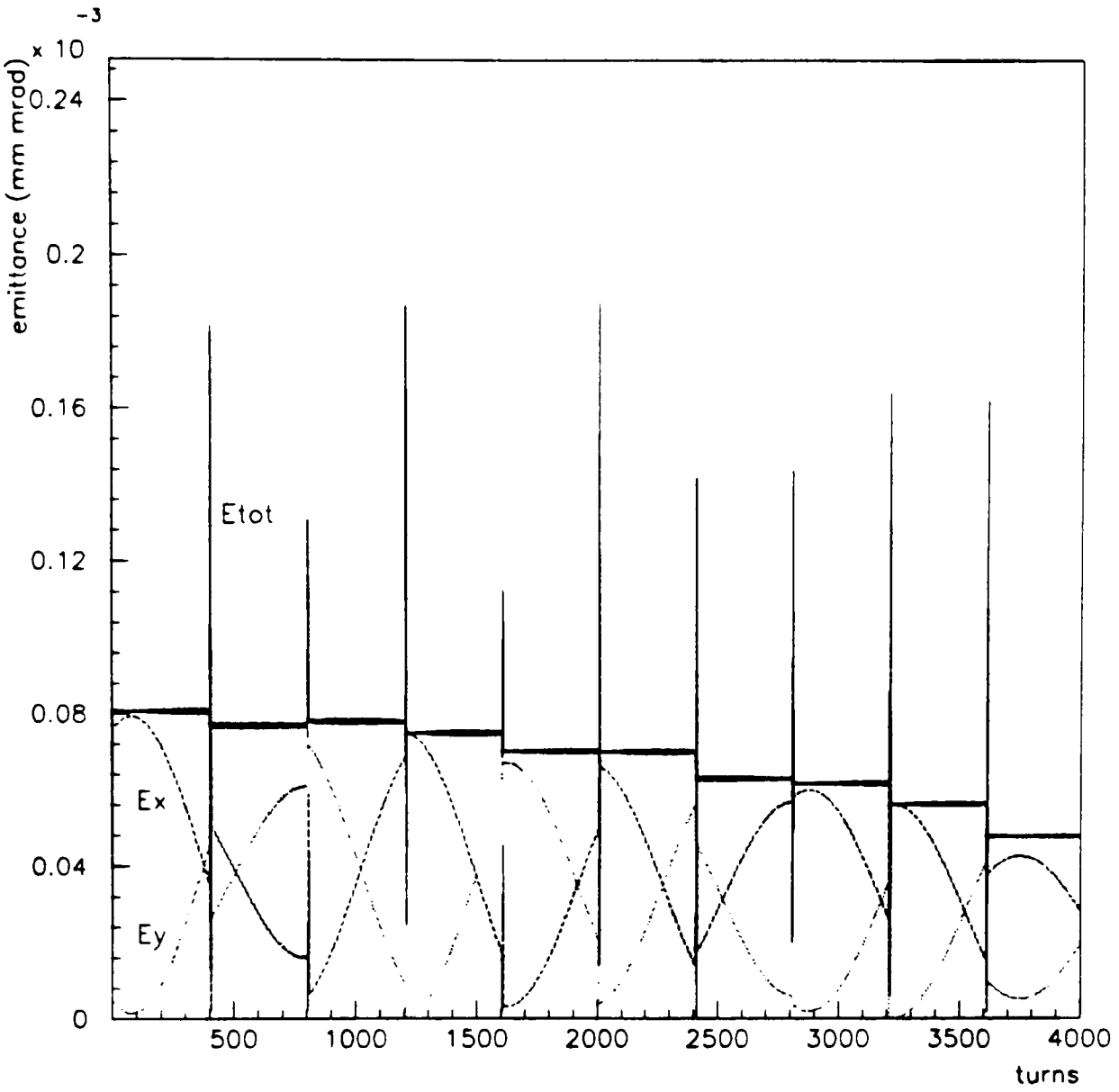


Figure 4.6: Partial and total emittances for 9 simulations of synchrotron radiation damping. Between every damping simulation the particle is tracked over 400 turns, starting with a simulation of the pulsed kicker magnet.

4.2 Results of Simulations with MCIS

MCIS can simulate the injection process over a wide range of variables. These variables can be divided into two groups: the physical parameters, which have a realistic value, for instance injection energy and kicker strength, and the so called 'software parameters' which have a value sufficiently large to guarantee the accuracy and correctness of the calculated survival percentages. Three parameters in the code can be labelled as software parameters: the number of particles that are tested, the number of turns over which the particles are tracked and the number of simulated kicker pulses. The choice of software parameters is first discussed in section 4.2.1, after which scans of the physical parameters are presented for HELIOS (section 4.2.2) and MAX (section 4.2.3). The choice of software parameters is valid for both accelerators.

4.2.1 Choice of Software Parameters

Number of Particles that are Tested

The variance σ^2 of the number of surviving particles S for a binomial distribution is

$$\sigma^2 = \frac{S(N-S)}{N} \tag{4.16}$$

assuming N particles are tested. Applying this to the survival percentage result S/N used in MCIS, the standard deviation in this percentage is

$$\frac{\sigma}{N} = \frac{1}{N}\sqrt{\frac{S(N-S)}{N}} \tag{4.17}$$

Substituting $N = 2000$ and a final survival percentage of $S/N = 25\%$, the standard deviation of the final survival percentage σ/N is 0.97 %. This was tested by calculating the variance over the final survival percentages of 33 simulations with 2000 particles, resulting in $\sigma/N = 0.97$ % for $S/N = 26.4$ %. This shows the very good agreement between the statistical theory and the variance found in the results.

As can be seen from 4.17, σ/N depends on the survival percentage S/N. The theoretical dependency is plotted in figure 4.7 for 2000 tracked particles. The figure

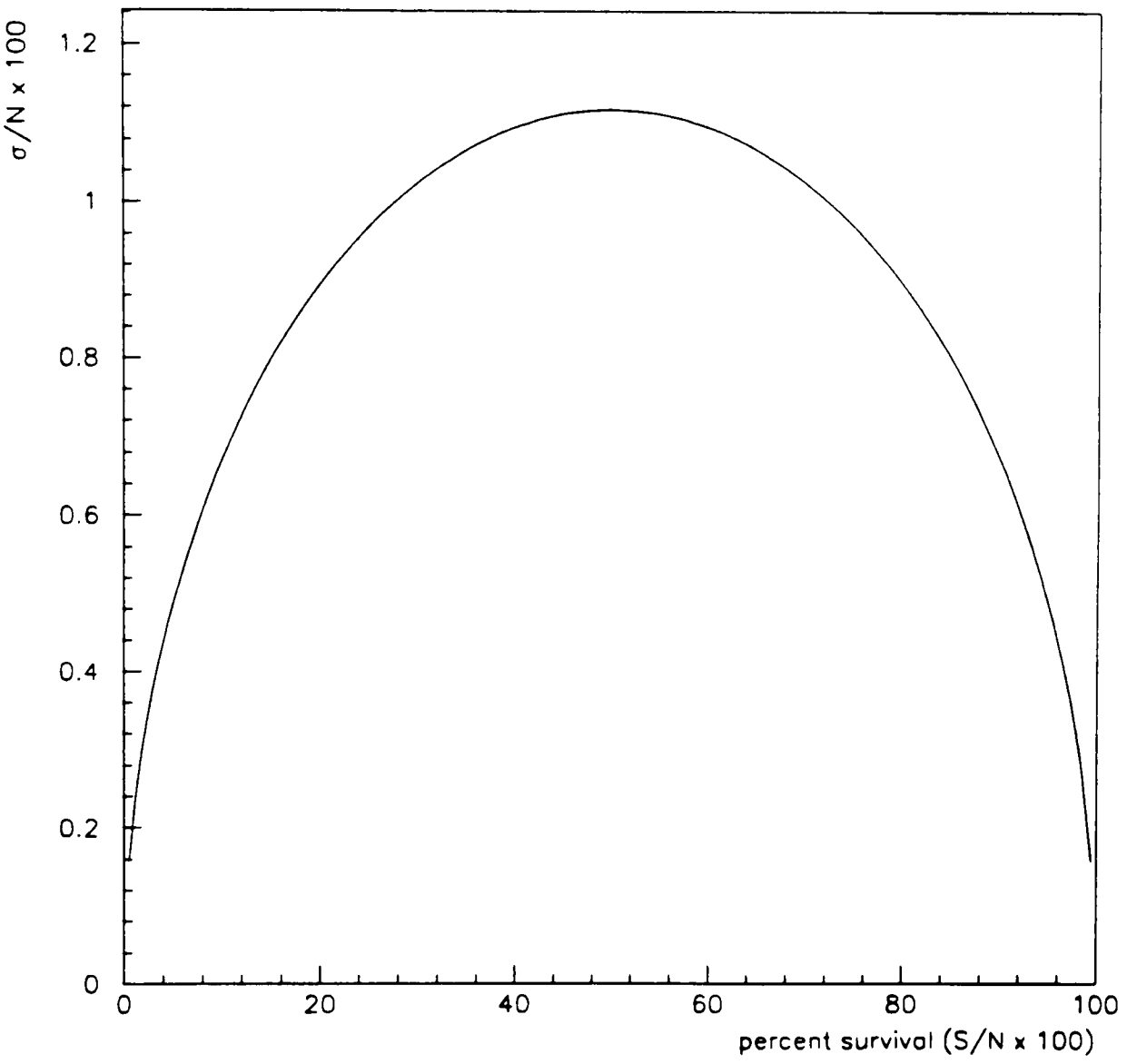


Figure 4.7: The error σ/N as a function of the survival percentage S/N.

shows that the error is the largest at $S/N = 50\%$, but that this is not much larger than 1 %.

All calculations presented in this chapter have 2000 particles in each simulation, which results in an absolute error σ/N in the initial capture and final survival percentage of less than 1 % for most situations.

Number of Turns over which the Particles are Tracked

The particles have to be tracked over sufficient turns between the damping simulations, so that any increase in the number of turns does not lead to a decrease in the surviving percentages. After this number of turns the particles are not only following the eigen ellipse, but also the combination of radial and longitudinal phase leading to the the largest and therefore critical value of x at the septum has taken place. The minimum number of turns necessary depends on the parameters of a specific simulation, but in general 200 turns are sufficient. The results presented in this chapter were obtained by using 500 turns in the tracking.

Number of Simulated Kicker Pulses

The number of kicker pulses equals the number of times synchrotron radiation damping is simulated. After sufficient radiation damping has taken place, the particles are safely trapped in the accelerator and will not be kicked outside the machine aperture by any following kicker pulses. The necessary damping time for final survival depends on the injection energy and also, but less strongly, on the excitation by the kicker magnet.

For the standard settings of HELIOS (presented later in table 4.1), the rate of particle loss, S_{NK}, between successive kicker pulses N_k and N_{k+1} is plotted in figure 4.8. The number of particles plotted for $N_k = 0$ are the particles which are lost over the first tracking period, before any synchrotron radiation damping is simulated. Most particles are lost between the first and second kicker pulse seen by the stored beam (plotted at $N_k = 1$). This is when the particles have had the least synchrotron radiation damping, while being excited by the kicker magnet. For $N_k = 15$, S_{NK} is the number of particles successfully surviving the total number of

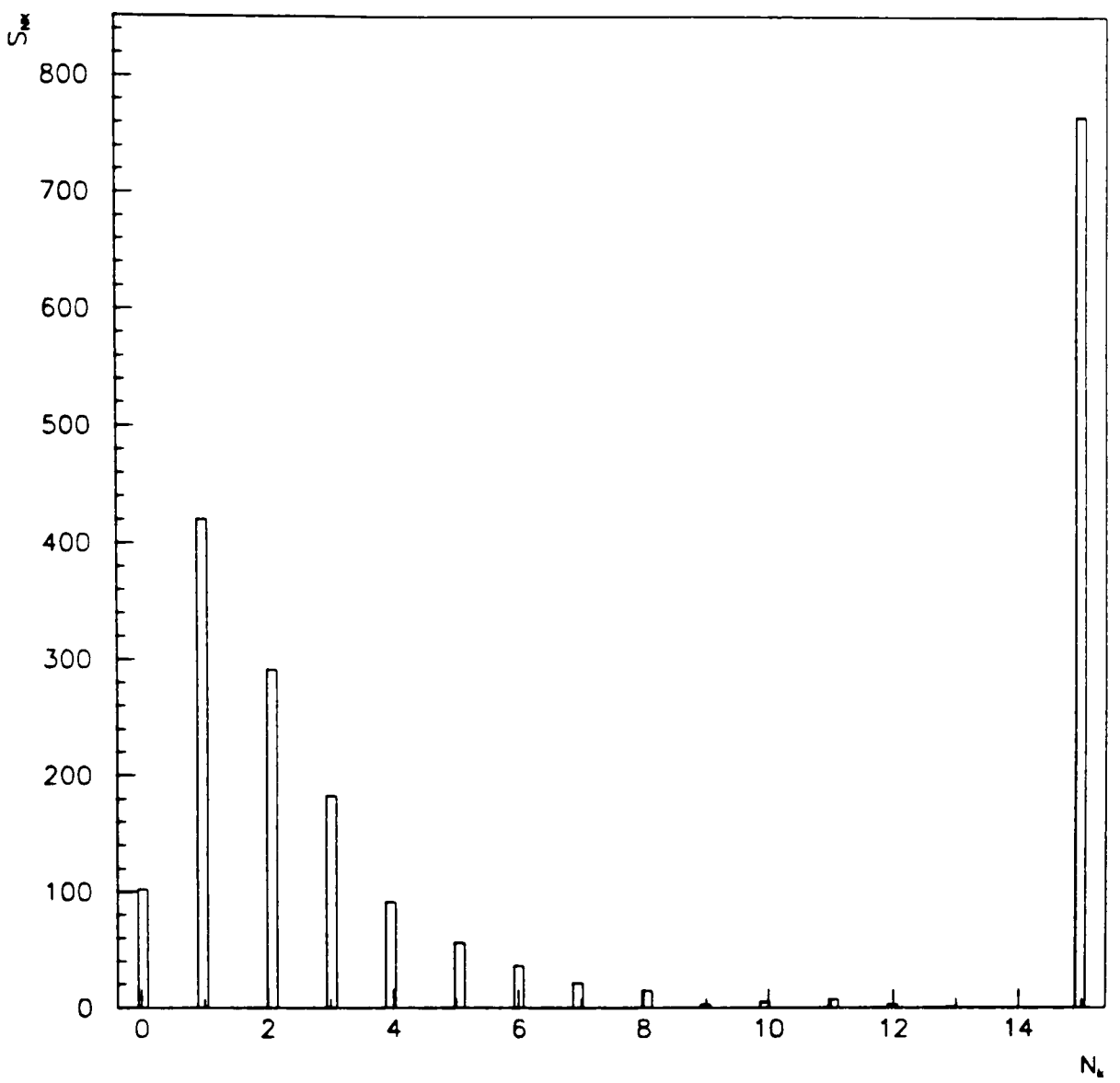


Figure 4.8: Rate of particle loss, S_{NK}, between successive kicker pulses N_k and N_{k+1}, except for $N_k = 15$, where S_{NK} is the total number of surviving particles.

simulated kicker pulses. The figure shows that after about 10 kicker pulses almost no particles are lost by any following kicker pulses. On this basis, the number of kicker pulses in the calculations presented in this section is chosen to be $N_k = 15$.

4.2.2 Simulations for HELIOS

The calculations for HELIOS are divided into two parts: part I models the situation where only coupling with the longitudinal phase space is included, and part II also takes into account the coupling with the vertical phase space.

Table 4.1: Standard settings for MCIS runs for HELIOS.

Injection energy	50	MeV
Betatron tunes ν_x , ν_y	1.54, 0.58	
RF-voltage	200	kV
Injection frequency	10	Hz
Injection position x_m and σ_x	27.5 $\pm$ 0.5	mm
Injection divergence x'_m and $\sigma_{x'}$	3.0 $\pm$ 0.5	mrad
Injection energy deviation δ_m and σ_δ	1.0 $\pm$ 0.25	%
Kicker magnet pulse length	257	ns
Maximum kick by the kicker	-9.0	mrad
Start injector pulse relative to kicker	125	ns
End injector pulse relative to kicker	225	ns
Micro-bunch structure parameter	1	
Outer limiting aperture	25.0	mm
Inner limiting aperture	23.0	mm
Coupling with vertical phase space	No	

I Results Including Coupling with Longitudinal Phase Space only

The results of most calculations are presented as the variation of initial capture and final survival percentages with one variable. The other parameters are kept constant at *standard settings*. These standard settings are listed in table 4.1 and discussed in detail in this section. They are either estimates of a realistic condition or optimum values obtained by scanning the parameters over a range of settings. The synchrotron radiation damping times for these settings (50 MeV) are: τ_x = 5.36 s, τ_y = 3.20 s and τ_ϵ = 1.33 s. It will be shown that although these damping times are much larger than 0.1 s, especially the radial damping time which is 'classically' thought to be the most important one, injection is still very good at the standard injection repetition rate of 10 Hz, taking into account coupling between the different phase spaces.

Survival as a Function of Injection Energy

As standard value of the injection energy a value as low as possible but still giving a good final survival percentage is chosen, so there is sufficient sensitivity to the variation of other parameters. With realistic values for all other parameters, discussed

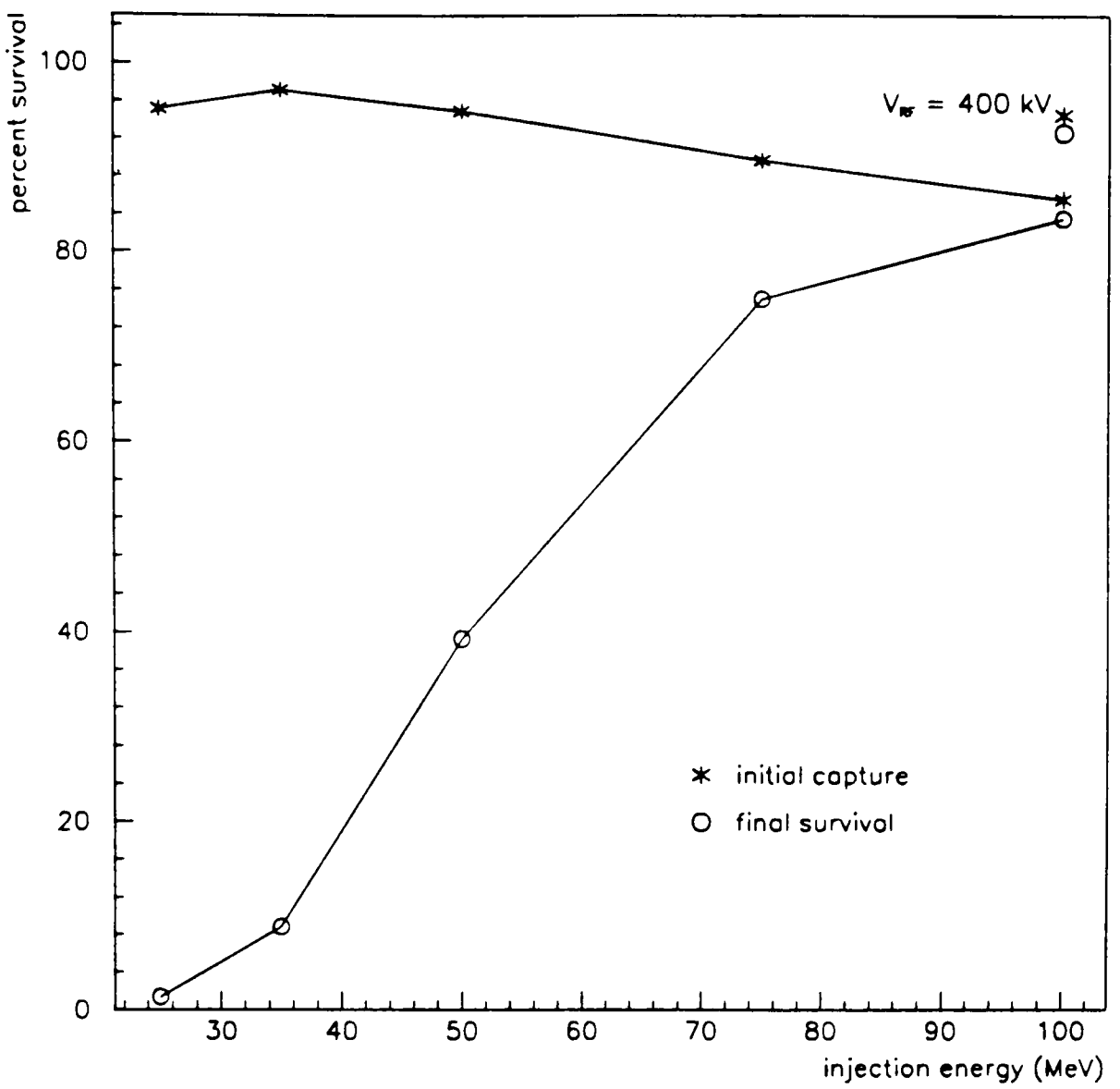


Figure 4.9: Injection efficiencies for different energies.

further on in this section, there is a final survival percentage of 39 % at the chosen standard injection energy of 50 MeV.

Figure 4.9 shows the survival percentages for some energies between 25 MeV and 100 MeV. All parameters, including beam size and RF-voltage, are kept constant and only the injection energy is changed. This leads to a reduced survival percentage at 100 MeV because of a too low RF-voltage. Increasing the RF-voltage at 100 MeV from 200 kV to 400 kV increases the momentum acceptance of the accelerator, which improves the survival, as is indicated by the graph. The change of the size and divergence of the injected beam with energy between 25 MeV and 100 MeV is not larger than a factor of $\sqrt{2}$, relative to the 50 MeV values of σ_x and $\sigma_{x'}$, assuming that the emittance of the injector scales as $1/E$. This only results in a small change of the final survival percentage of the order of 1 %. But increasing the injected beam

size and divergence at 100 MeV to those values valid for the linear injector as used in the experiments reported in the next chapter ($\sigma_x = 1.4$ mm and $\sigma_{x'} = 1.4$ mrad), gives a significant decrease in the final survival percentage from 84 % to 77 % (this is with an increased kicker strength but the same standard RF-voltage of 200 kV).

It is difficult to reach a definite conclusion on the lowest possible injection energy for a specific machine by considering only single particle beam dynamics. Many other, mainly multi-particle, processes play an important role in the injection process. They are briefly discussed in chapter 5. Most of them reduce the injection efficiency, so the injection efficiencies calculated within the single particle model have to be considered as about the maximum obtainable value. It also has to be noted that within these single particle beam dynamics calculations, the resulting final survival percentage depends on assumptions such as septum thickness and position of the injected beam. In addition, coupling with the vertical phase space has not yet been taken into account. Taking into consideration experimental results and using the presented model it is expected to be difficult for HELIOS-like machines to inject with a repetition rate of 10 Hz at energies below 35 MeV. At this energy and tune point the final survival percentage is 8.8 % with synchrotron radiation damping times $\tau_x = 15.6$ s, $\tau_y = 9.3$ s and $\tau_\epsilon = 3.9$ s. The lower limit on the injection energy is discussed further in chapter 6 by considering additional arguments based on experiments and calculations including coupling with the vertical phase space.

Survival as a Function of Off-Energy Percentage

A very important parameter is the energy deviation of the injected particle relative to the ring energy. As before this quantity is called $\delta = \Delta p/p_0$. The effect of off-energy injection on the capture percentages is illustrated in figure 4.10. These calculations are made for a micro-bunch structure number of 1. If 3 GHz side-bunches are simulated, both the initial and final survival percentages are reduced by a factor of 2. This indicates that only the central bunch injected at the synchronous phase ϕ_s, which has half the number of electrons of the injected beam, is accepted by the accelerator. This is valid over the full range of δ.

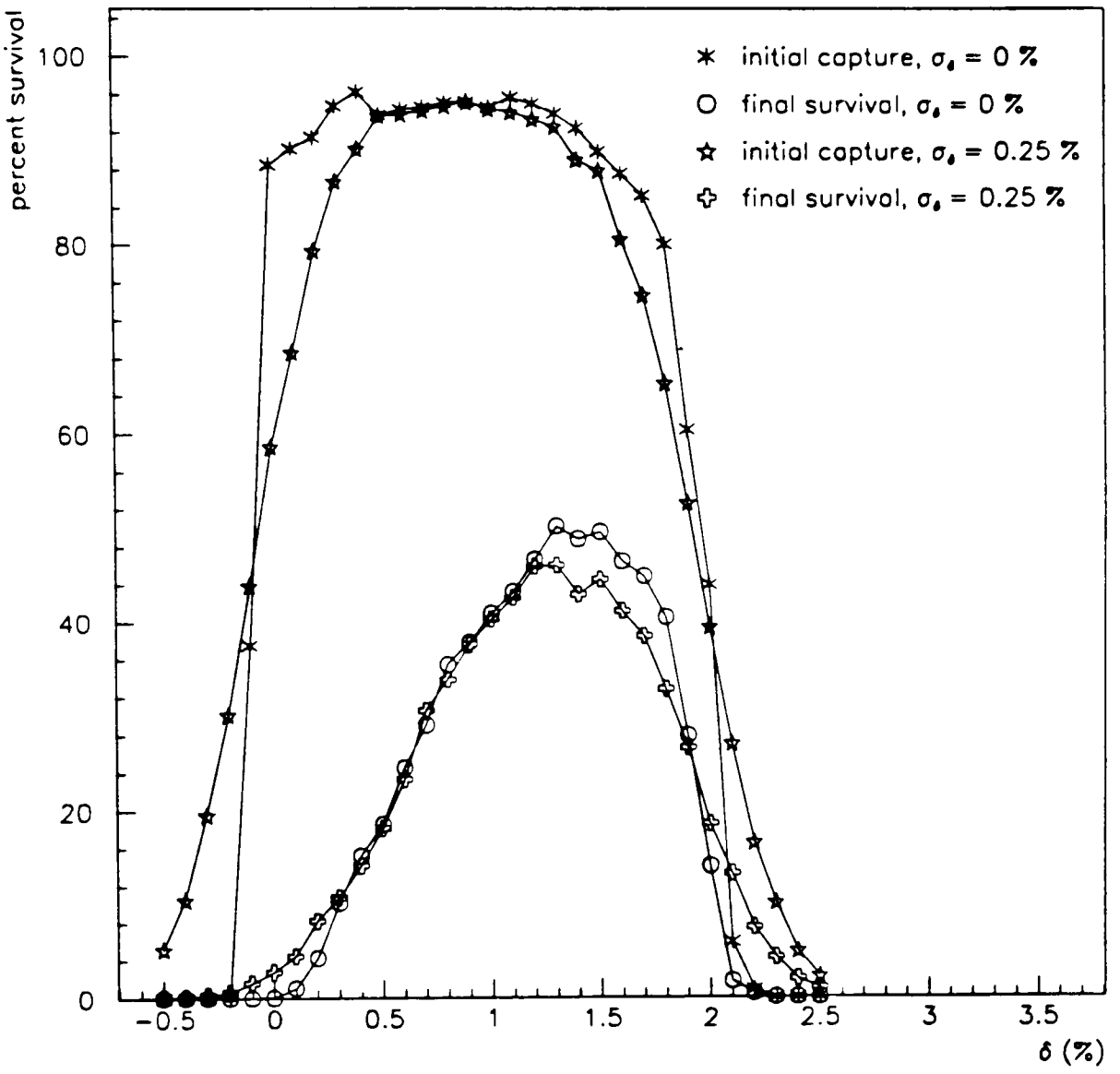


Figure 4.10: The variation of the capture percentages with the relative energy deviation of the injected beam, with and without an energy spread in the injected beam.

The scans are made with and without an energy spread σ_ϵ in the beam. As would be expected some energy spread in the injected beam is not critical and causes an averaging over δ of the curve with $\sigma_\epsilon = 0$.

The centre of the peak of the final survival percentage is at a slightly larger value of δ_m, around 1.3 %, than the standard value of δ_m (1 %), but injection is good for $0.8\% < \delta < 1.8\%$. It is important to realise that with the particles injected on-energy, the final survival percentage at 50 MeV is almost 0 %.

These simulations show for the first time that by injecting off-energy the injection efficiency is significantly increased. They also demonstrate the process by which a multi-shot injection system can operate at low injection energies.

Survival as a Function of RF-Voltage

The standard setting of the RF-voltage is 200 kV, which agrees with the experimentally observed setting for 100 MeV injection. The variation of the capture percentages with RF-voltage is presented in figure 4.11. It is clear that for the maximum final survival percentage it is necessary to have a minimum RF-voltage of 75 kV. At $V_{RF} = 50$ kV the energy acceptance $(\Delta p/p_0)_{\max} = 1.3$ %. Because $\delta_m = 1.0$ % and $\sigma_\delta = 0.25$ % a significant fraction of the injected beam is outside the energy acceptance. For $V_{RF} = 75$ kV, $(\Delta p/p_0)_{\max} = 1.6$ % and almost all the beam is within the energy acceptance at injection. A much larger RF-voltage, above 250 kV, is necessary to obtain the maximum initial capture percentage, but this has no effect on the final survival percentage.

Survival as a Function of the Injected Beam Size and Divergence

The specification of the emittances of 100 MeV microtrons is around $\varepsilon_x = \varepsilon_y = 0.1$ mm mrad. Scaling this with energy for 50 MeV gives $\varepsilon_x = \varepsilon_y = 0.2$ mm mrad. Assuming an upright circular phase space ellipse of the injected beam ($\alpha(s) = 0, \beta(s) = 1$ m at the exit of the transport line), this results in $\sigma_x = \sigma_y = 0.45$ mm and $\sigma_{x'} = \sigma_{y'} = 0.45$ mrad (the values for the vertical phase space are not relevant for this situation where there is no coupling with the vertical phase space, but are used later on when the coupling is introduced). The standard values used

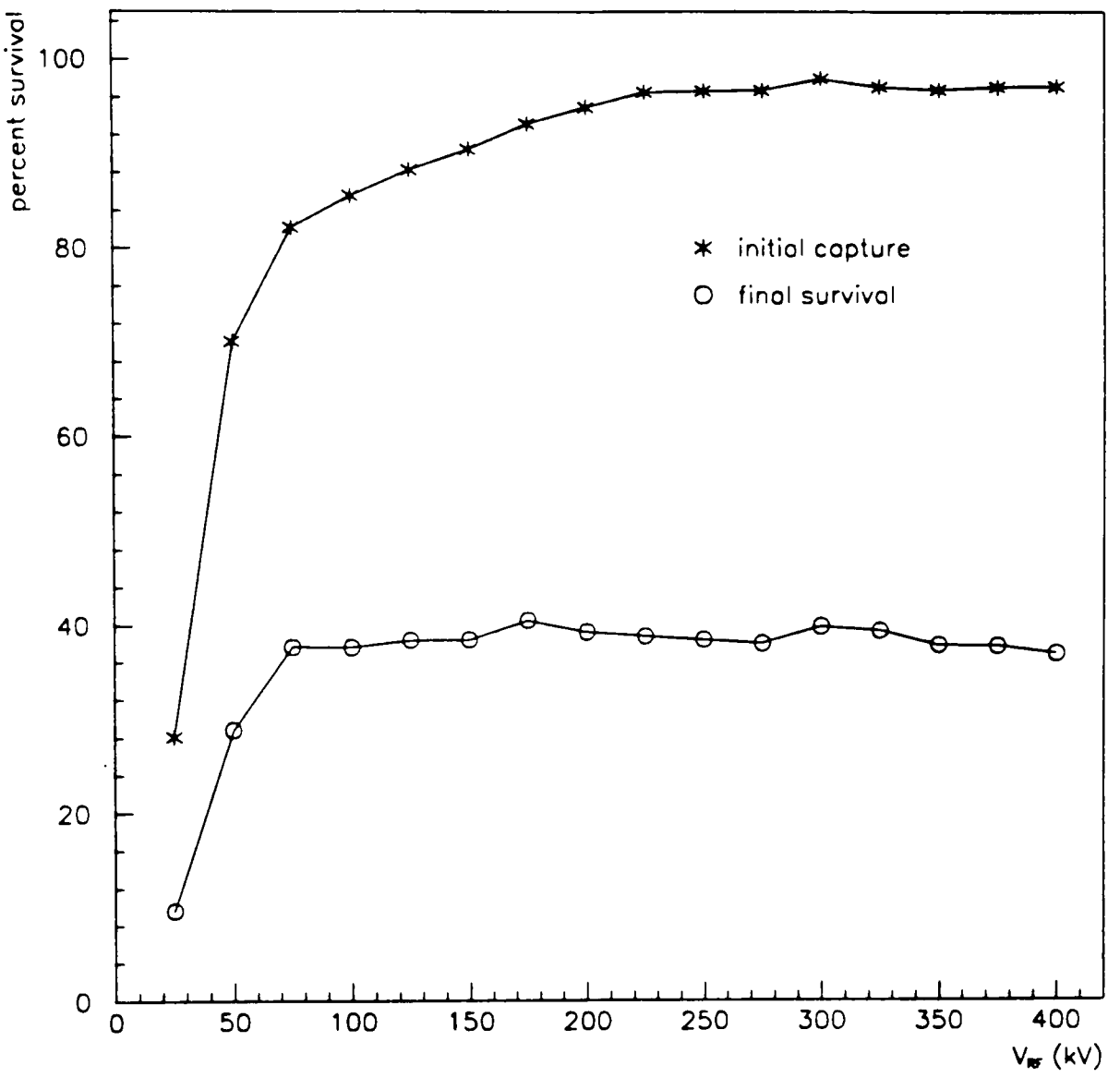


Figure 4.11: Variation of the capture percentages with RF-voltage.

are $\sigma_x = 0.50$ mm and $\sigma_{x'} = 0.50$ mrad. As with a finite energy spread in the beam, the finite beam width and divergence have an averaging effect on the survival percentages over x and x'. This is shown in figure 4.12 where scans are made of the injection efficiencies with no spread and with the standard spread in position and divergence.

For $\sigma_x \rightarrow 0$ mm the initial capture is 50 % if x_m equals the outer limiting aperture of 25 mm. For x_m a fraction of a mm larger, both the initial capture and final survival have their maximum. Using $\sigma_x = 0.5$ mm, the optimum value of x_m is 26 mm. The standard value of x_m is taken to be 27.5 mm, including an estimate of the effects of a not perfectly optimised transport line. For good injection the half-width of the beam should not have a standard deviation much larger than 1 mm.

Figure 4.12(b) shows that the optimum injection angle is slightly positive, around the standard setting of 3 mrad. The resulting position in horizontal phase space, $x = 27.5$ mm and $x' = 3$ mrad, approximately agrees with the direction in phase space in which the kicker magnet kicks the stored beam. An acceptable value of $\sigma_{x'}$ is about 2 mrad.

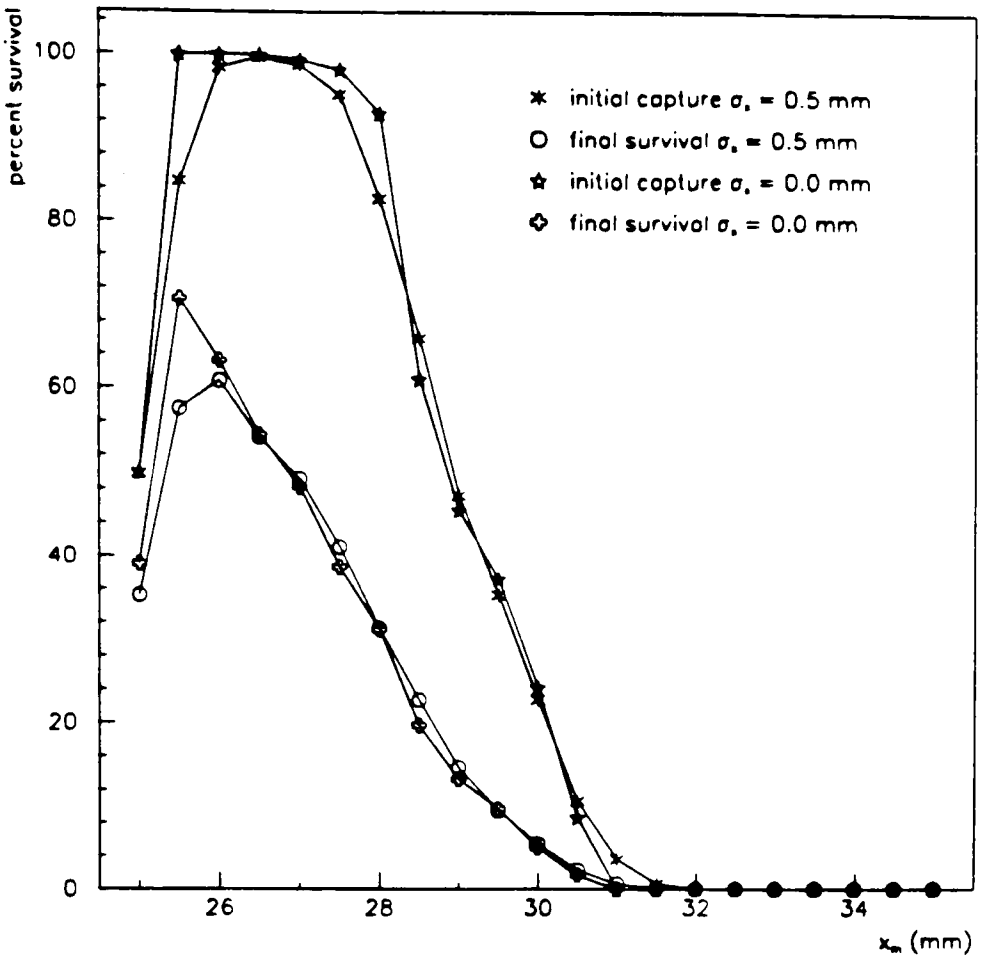
Survival as a Function of Betatron Tune

The variation of the survival percentages with the horizontal betatron tune is complex because two important injection parameters vary significantly with ν_x: the radial damping time τ_x and the sensitivity of the closed orbit to a certain kick $\Delta x'$.

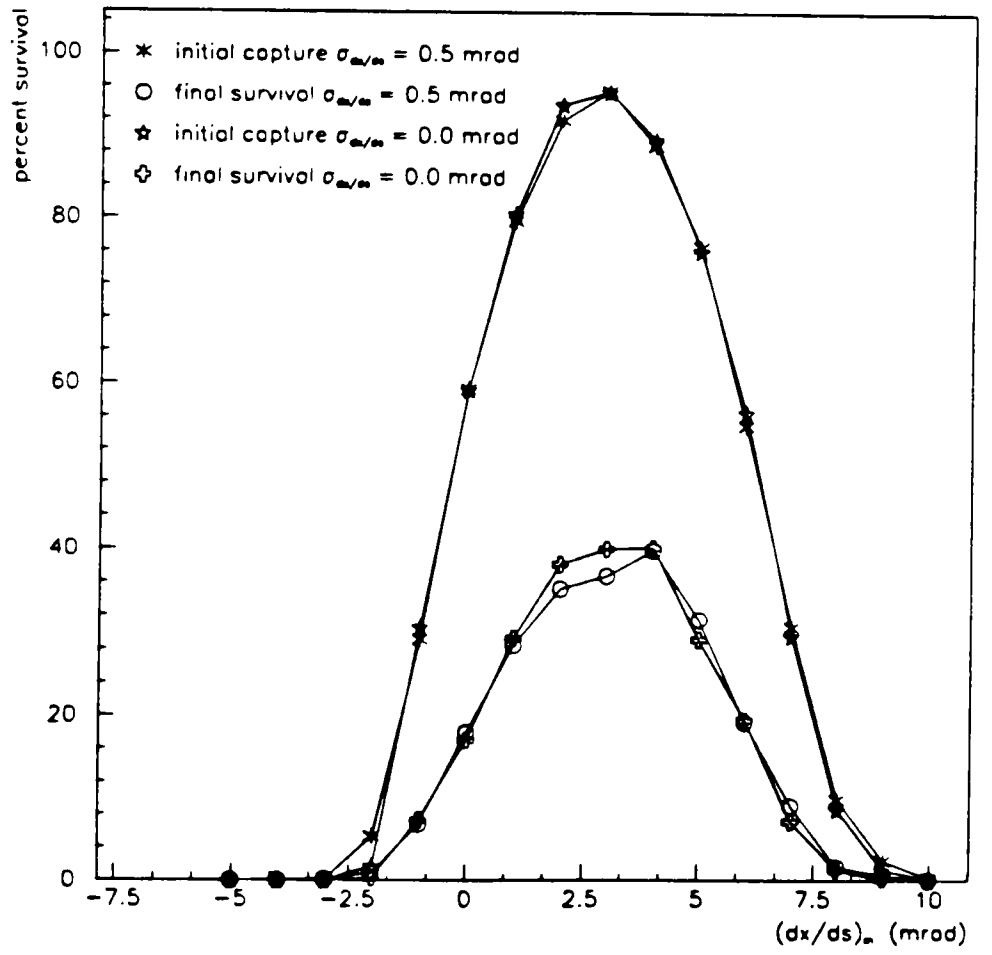
The variation of τ_x and τ_ϵ with horizontal tune is given in figure 4.13. The longitudinal damping time is almost independent of the tune, but the radial damping time decreases almost linearly with a factor of 2 between $\nu_x = 1.2$ and $\nu_x = 1.6$. This results in a better final survival percentage for higher radial betatron tunes.

The effect of a very slowly pulsed kicker magnet on the injected and stored beam is similar to a common closed orbit distortion (cod). The effect of a kick $\Delta x'$ at position $s = 0$, which has betatron phase $\mu_x(0) = 0$, results in a change in x, called $\Delta x_{\mathrm{cod}}(s)$, at position s of ([SAN70])

$$\Delta x_{\mathrm{cod}}(s) = \frac{\Delta x' \sqrt{\beta(0)}}{2 \sin \pi \nu_x} \sqrt{\beta(s)} \cos(\mu_x(s) - \pi \nu_x) \tag{4.18}$$



(a)



(b)

Figure 4.12: Injection efficiencies as a function of the injection position x_m (a) and the divergence of the injected beam x'_m (b), with and without a spread in the beam size and beam divergence.

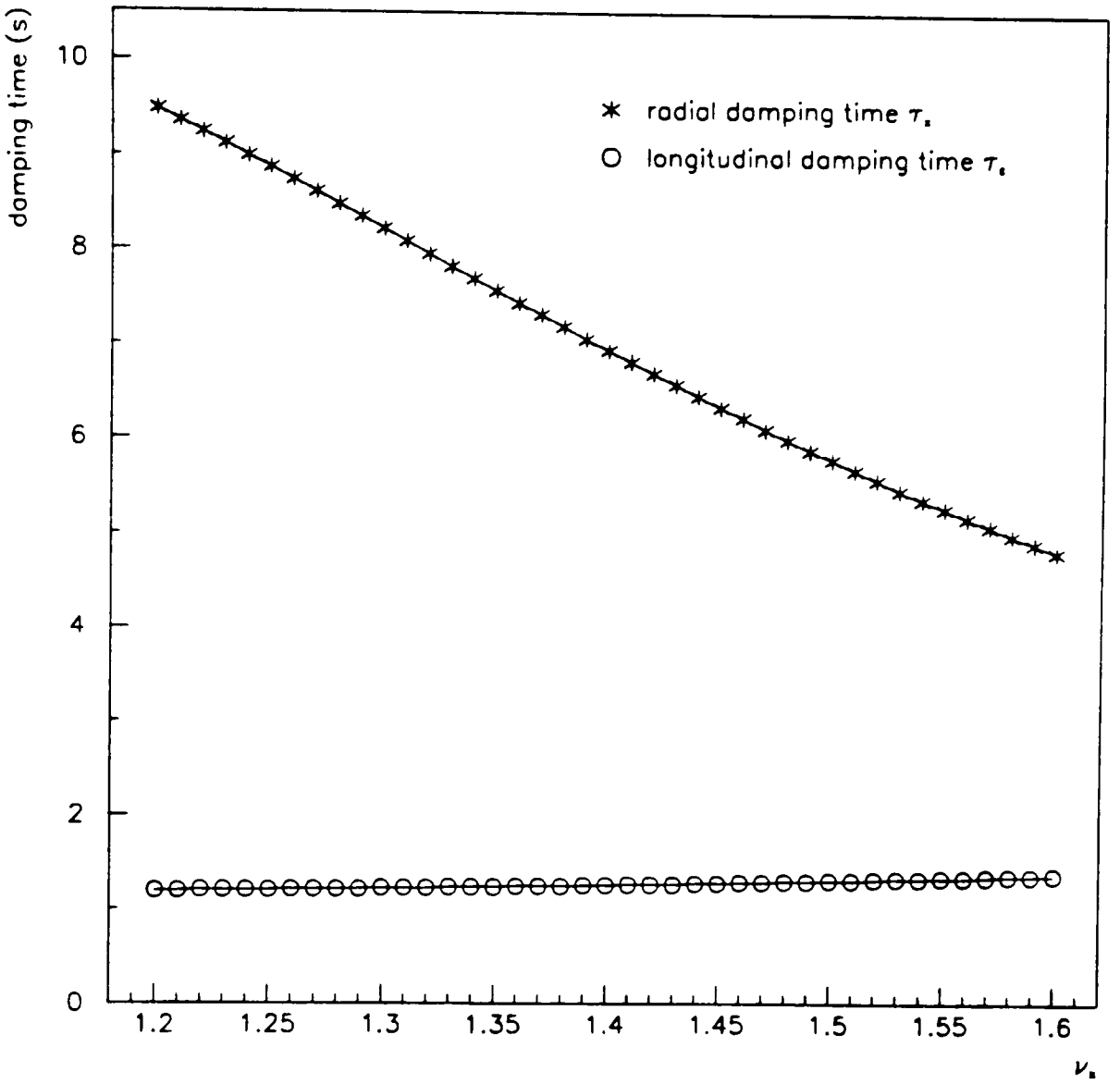


Figure 4.13: Variation of the radial and longitudinal synchrotron radiation damping time with horizontal betatron tune.

This closed orbit distortion is plotted for HELIOS in figure 4.14(a), using a low tune point ($\nu_x = 1.30, \nu_y = 0.58$) and a high tune point ($\nu_x = 1.54, \nu_y = 0.58$). In the calculation a kick of $\Delta x' = -9$ mrad is given at the kicker position. It shows that the size of the cod depends strongly on tune, but that the form is very similar for the two tune points. The variation of the cod at the septum position with horizontal tune is plotted in figure 4.14(b).

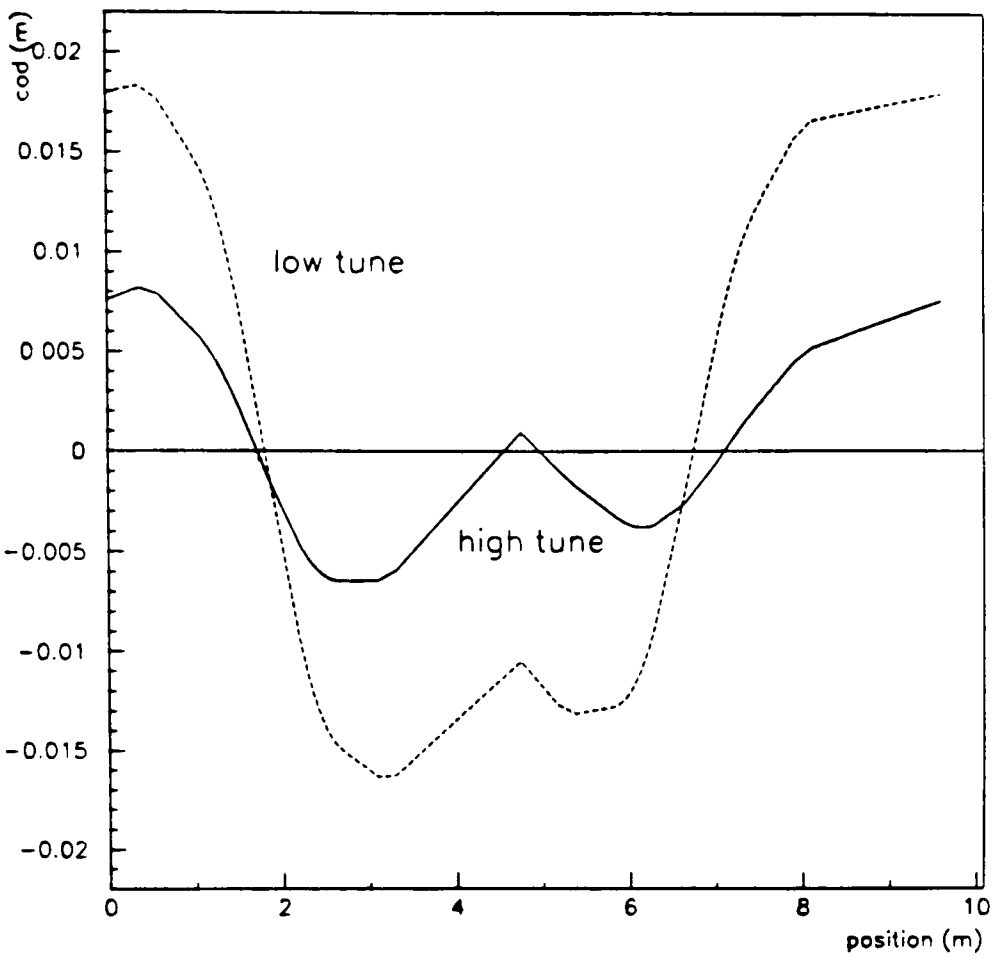
Although the effect of a fast pulsed kicker magnet is different from a common closed orbit distortion, these calculations explain why the kicker strength has to be varied significantly if optimum injection has to be maintained at a different betatron tune point ν_x.

The variation of the ring acceptance with ν_x is plotted in figure 4.15 for the standard maximum kicker strength, -9 mrad, and a reduced maximum kicker strength of -6 mrad. The results agree with the variation of τ_x and the cod with tune: for the reduced kicker strength the maximum final survival percentage takes place at a lower tune point $\nu_x = 1.44$ (38 %). The maximum final survival with the stronger kicker pulse at $\nu_x = 1.55$ is larger because of the shorter synchrotron radiation damping time (44 %). For all curves, including the initial capture percentages, there is a minimum at the half integer resonance $\nu_x = 1.50$.

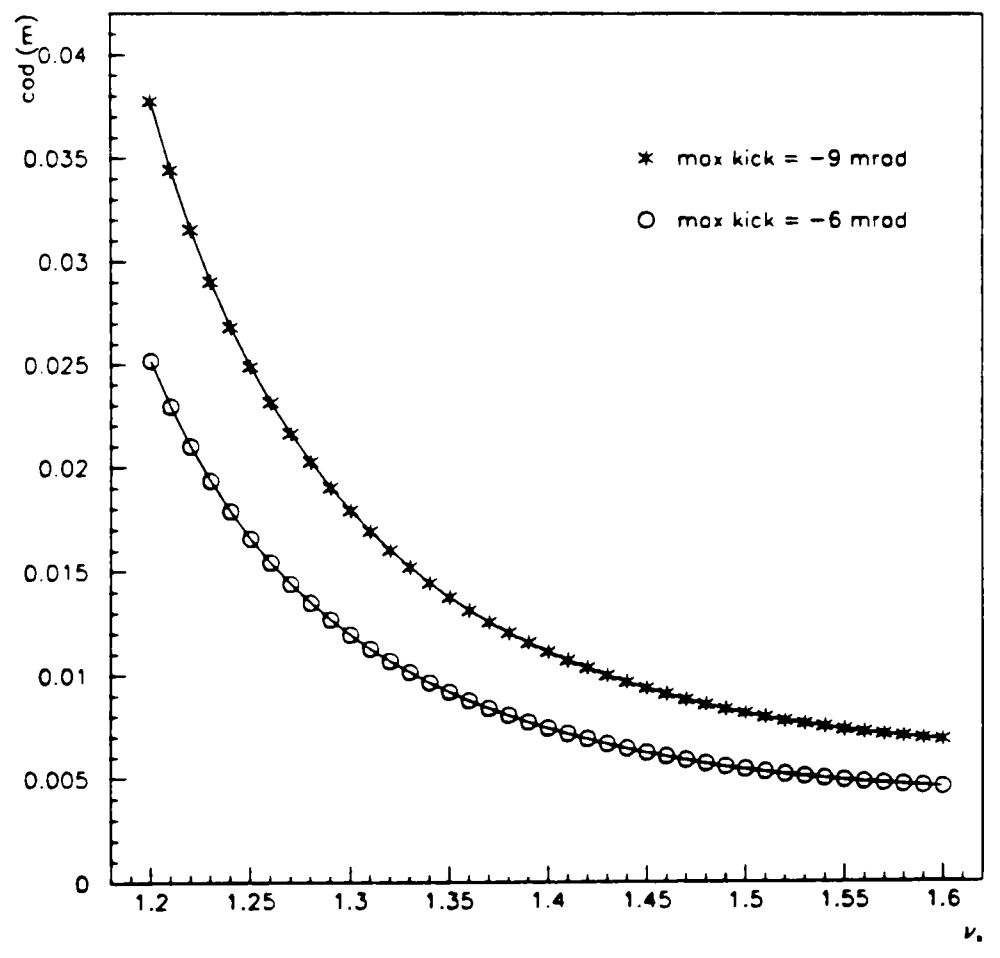
Survival as a Function of Kicker (Related) Parameters

The strength of the kicker magnet is a very important injection parameter. As discussed above, the optimum strength depends strongly on the horizontal betatron tune. For the standard settings the variation of the injection efficiency with maximum kicker strength, $\Delta x'$ at the top of the half-sine pulse, is plotted in figure 4.16. The figure shows a broad maximum of the final survival percentage between -6 mrad and -12 mrad.

The kicker pulse is assumed to be 257 ns long. The time of injection is measured relative to the the start of the kicker pulse t_0. In the simulation a flat 100 ns long injector pulse is injected between 125 ns and 225 ns. Not every part of this pulse has the same chance of survival. This is plotted in figure 4.17. It shows that the



(a)



(b)

Figure 4.14: Closed orbit distortion around the accelerator for a low and high horizontal tune point, with the lattice starting at the septum position (a) and the variation of the closed orbit distortion at the septum as a function of horizontal betatron tune for two different kicker strengths (b).

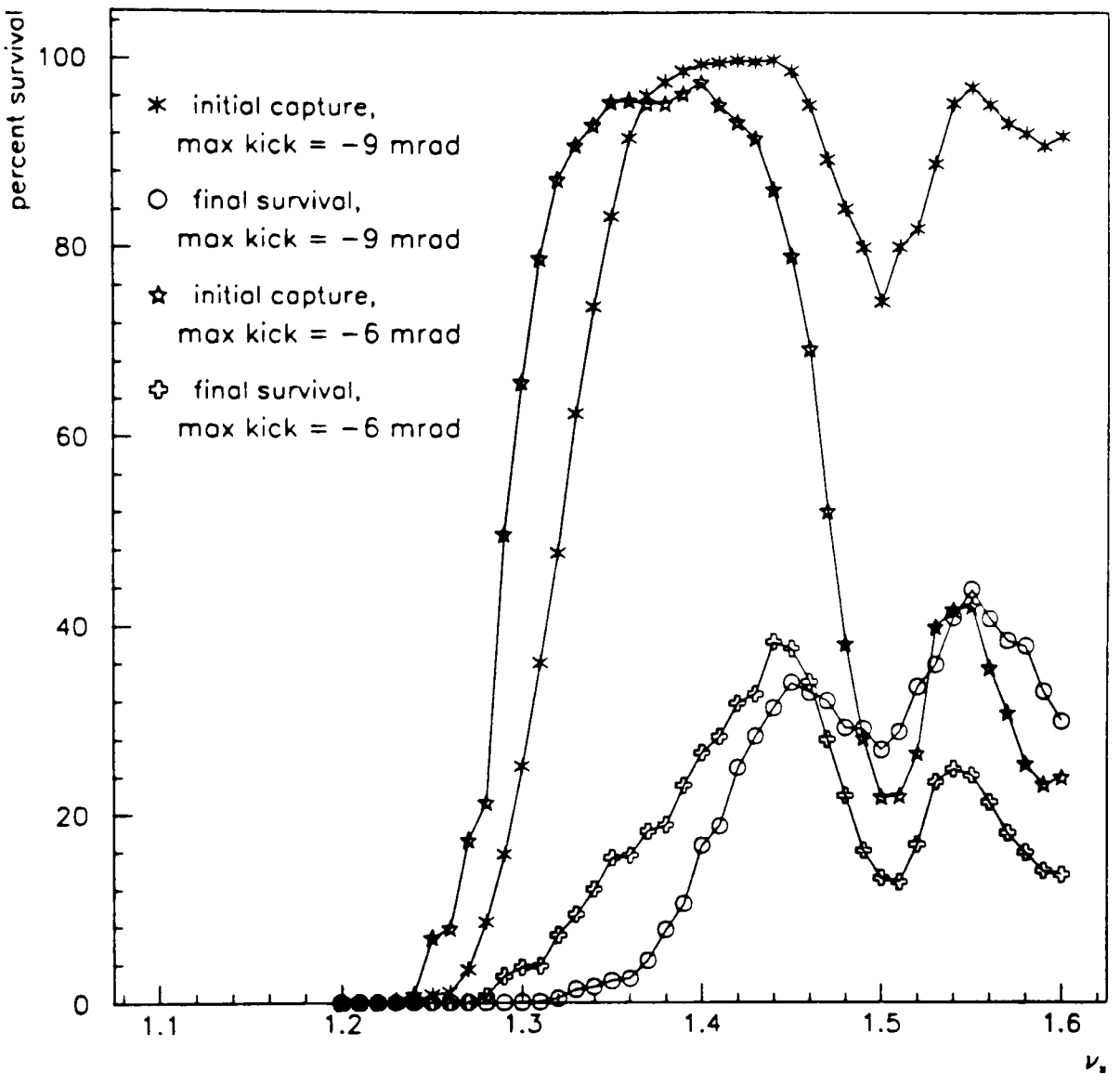


Figure 4.15: The variation of injection efficiencies with horizontal betatron tune for two different kicker strengths.

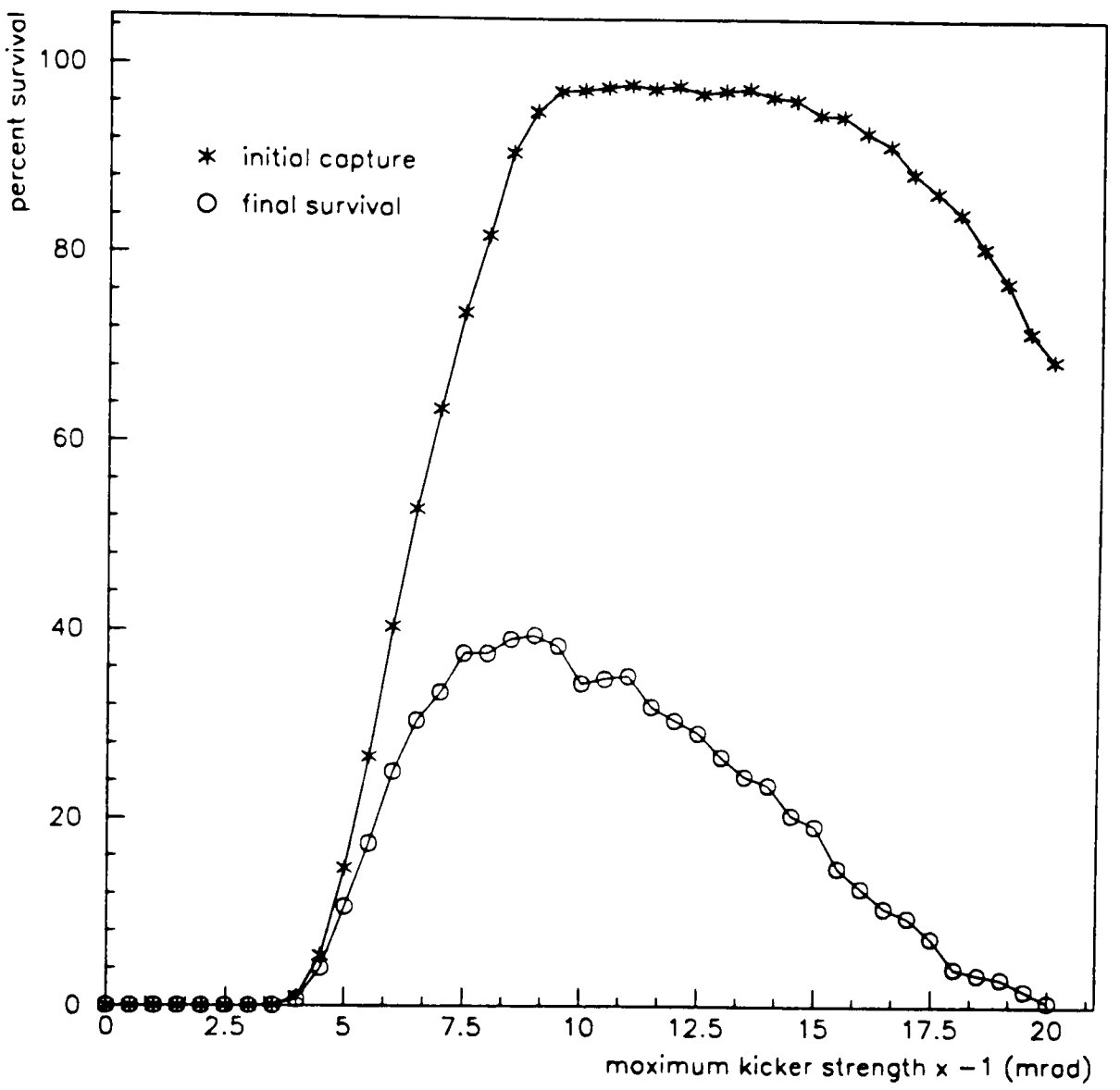


Figure 4.16: The effect of variation of the maximum kicker strength on the ring acceptance.

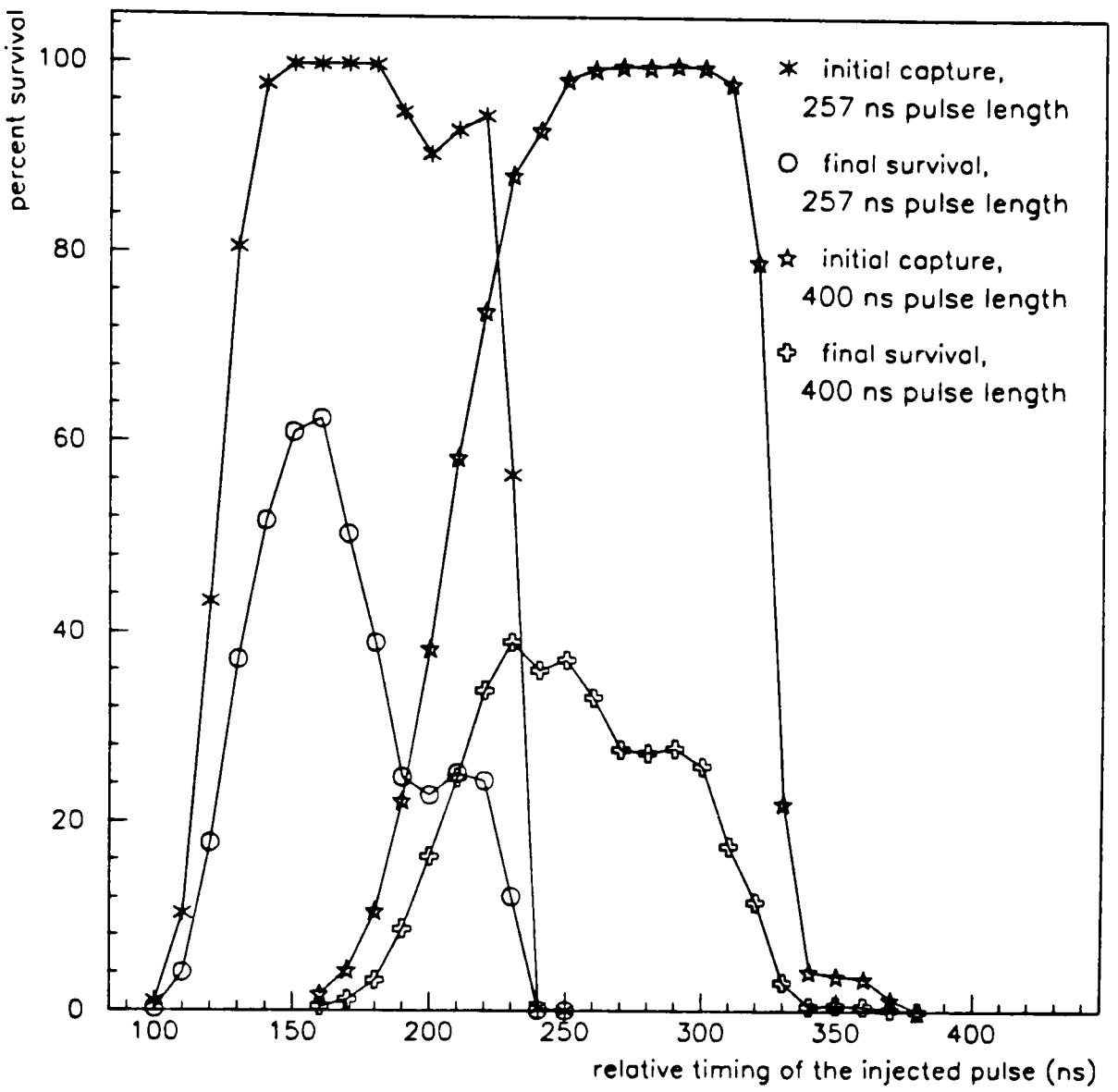


Figure 4.17: Injection efficiencies for a 1 ns long injector pulse, scanning the timing of injection. Calculations are shown for the standard 257 ns kicker pulse length and a 400 ns kicker pulse length.

standard window of injection is between about the full-width half-maximum values of the final survival percentage.

Calculations were also made for a 400 ns kicker pulse length. In general the longer kicker pulse excites the electrons which are already stored in the accelerator more strongly, which reduces the final survival percentage (see also figure 4.17). Using the longer kicker pulse length, the injection timing over which good injection takes places is increased by about 30 % (there is good survival between 190 ns and 320 ns), but the final survival percentage has a relative reduction of about 30 %, comparing it with the shorter kicker and injector pulse. This means that there are 30 % more electrons in the longer injector pulse, assuming the peak current of the injected pulse does not depend on pulse length, resulting in the same number of

successfully injected electrons in the accelerator as for the shorter kicker and injector pulse. This leads to the conclusion that from a radiation safety point of view, it is better not to increase the kicker pulse length above the standard setting. For much longer kicker pulse lengths the survival percentage decreases rapidly: a 1μs pulse length only has a maximum final survival percentage of 6 %. Now the reduction in efficiency because of the longer pulse length can not be compensated by making the injector pulse longer.

The betatron excitation of the stored beam by the kicker magnet can be reduced by choosing the kicker pulse length K so that the excitation of the beam on the rising side of the kicker pulse is counteracted by excitation in anti-phase on the falling side of the pulse. The conditions for this are ([EIN87])

$$K = nT_0 \tag{4.19}$$

$$\nu_x = \frac{m + \frac{1}{2}}{n} \tag{4.20}$$

This is confirmed for HELIOS by single particle tracking, using a particle starting at the centre of all 3 phase spaces [UYT89]. The variation of the kicker pulse length for the standard settings shows no maxima of the final survival percentage for the values of K as given by the formulae 4.19 and 4.20. This can be explained: the given condition leads to a minimum excitation of a small beam (in or near the equilibrium state), but for these beam sizes there is never any danger of beam loss by the kicker excitation, so there is no effect on the final survival percentage. For particles with a larger betatron excitation the conditions as given by 4.19 and 4.20 lead to a *constant* particle emittance, for and after kicker excitation; but this is not necessary for maximum particle survival: if the kicker pulse length is not optimised, the *particle* emittance will sometimes increase and sometimes decrease because of the kicker excitation. For a total beam this effect will average out and this explains why the final survival percentage is not sensitive to relatively small changes in kicker pulse length.

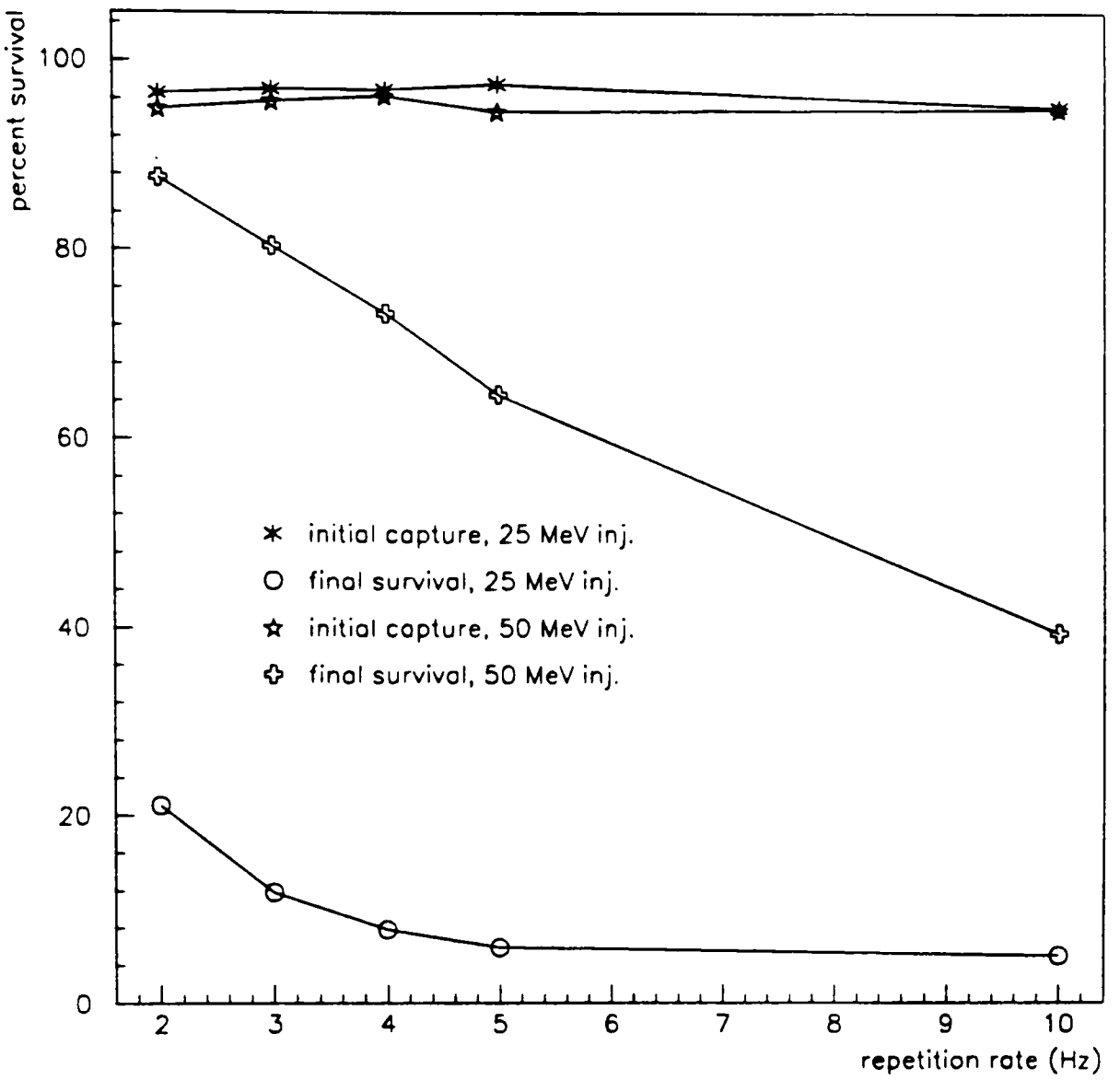


Figure 4.18: Injection efficiencies for 25 MeV and 50 MeV injection, using different injection repetition rates.

Survival for Different Injection Frequencies

The final survival percentage decreases if the injection repetition rate is increased, because there is less time for synchrotron radiation damping between successive kicker pulses. The variation of injection efficiencies with the injection repetition rate is plotted in figure 4.18 for 25 MeV and 50 MeV injection.

For 50 MeV injection the final survival percentage decreases almost linearly over the scanned region between 2 Hz and 10 Hz. Increasing the repetition rate from 5 Hz to 10 Hz reduces the final survival percentage by 25 %. This is a relative decrease of 38 %. Because at 10 Hz twice as much current can be injected in the same time interval, it is better to inject at the high repetition rate.

At 25 MeV the situation is different: there is a very low survival percentage for

repetition rates above 5 Hz. Increasing the repetition rate from 2 Hz to 4 Hz reduces the final survival percentage from 21 % to 7.9 %. This is a relative decrease of 62 % and it is better, and in practice probably even necessary, to inject at a low repetition rate.

There may be a practical lower limit on the injection repetition rate: if the repetition rate is decreased, the injection process takes longer. This can be a problem because of a reduced beam lifetime at very low energies and because the time available to fill the ring has to be minimised.

II Results Including Coupling with Vertical Phase Space

For the code to work correctly when coupling with the vertical phase space is included, the tune point has to be exactly at a coupling resonance, as is explained on page 64. For HELIOS all calculations which include coupling with the vertical phase space are performed at the standard horizontal tune $\nu_x = 1.54$ but a slightly different vertical tune $\nu_y = 0.54$, instead of $\nu_y = 0.58$. This small change in vertical tune has no significant effect on the injection efficiency calculations if coupling with the vertical phase space is not taken into account.

There are two parameters which can be set to model the coupling between the two transverse phase spaces: the integrated skew quadrupole field and the coupling strength g used in the damping simulation. Because the operating point is exactly at the coupling resonance, any small amount of skew quadrupole field results in full coupling: $g = 1$ (see equation 2.40). The integrated field strength is chosen to be 0.0005 T, which gives a beat period of about 1200 turns and an error of less than 1 % in the emittance calculation of the damping routine (see figure 4.5).

The vertical beam size and divergence are taken to be the same as the standard values for the horizontal beam ($\sigma_y = 0.5$ mm and $\sigma_{y'} = 0.5$ mrad) and injection takes place at the centre of vertical phase space. It is assumed that there is no correlation of the initial parameters between the two phase spaces. Because the injection takes place around $x = 27.5$ mm, the initial vertical emittance is only a small fraction of the total emittance; for standard injection positions and divergences, using $\delta = 1$ %, $\mathcal{E}_x \approx 70$ mm mrad and $\mathcal{E}_y \approx 0.47$ mm mrad, a few turns after injection.

Table 4.2: Results of MCIS simulations for HELIOS.

	initial capture		*final survival*	
	$\delta_m = 0$ %	$\delta_m = 1.0$ %	$\delta_m = 0$ %	$\delta_m = 1.0$ %
No vertic. coupl.	59 %	95 %	3 %	39 %
Full vertic. coupl.	61 %	97 %	23 %	73 %

All parameters, except the vertical betatron tune, are kept constant at the standard settings from table 4.1. The previously used 500 turns for the tracking are still more than sufficient (100 turns in the tracking results in the same survival percentages); increasing the number of turns to values much larger than the beat period does not decrease the final survival percentage. This implies that particle loss occurs soon after the kicker magnet is pulsed and a later increase of x, because of an increase in $\mathcal{E}_x$, has no effect on particle survival. Also the number of 15 simulated kicker pulses is still sufficient.

Table 4.2 gives an overview of the different injection efficiencies, with or without coupling between the various phase spaces. Using full coupling between all the three phase spaces results in a final survival percentage of 73 %. Without any coupling with the vertical phase space, but injecting off-energy, the final survival percentage is 39 %, so there is a significant advantage in introducing coupling with the vertical phase space. Using full coupling with the vertical phase space, but injecting on-energy results in a final survival percentage of 23 %. Having no coupling with the vertical phase space and injecting on-energy results in a final survival percentage of only 3 %. These percentages show that coupling with the vertical phase space is very effective if there is no coupling with longitudinal phase space. Coupling with the longitudinal phase space is more effective than coupling with the vertical phase space, which can be explained by the much shorter longitudinal synchrotron radiation damping time ($\tau_\epsilon = 1.3$ s, $\tau_y = 3.2$ s).

Calculations using full coupling have been made for different values of off-energy injection and for different kicker strengths. The calculated efficiencies have a similar

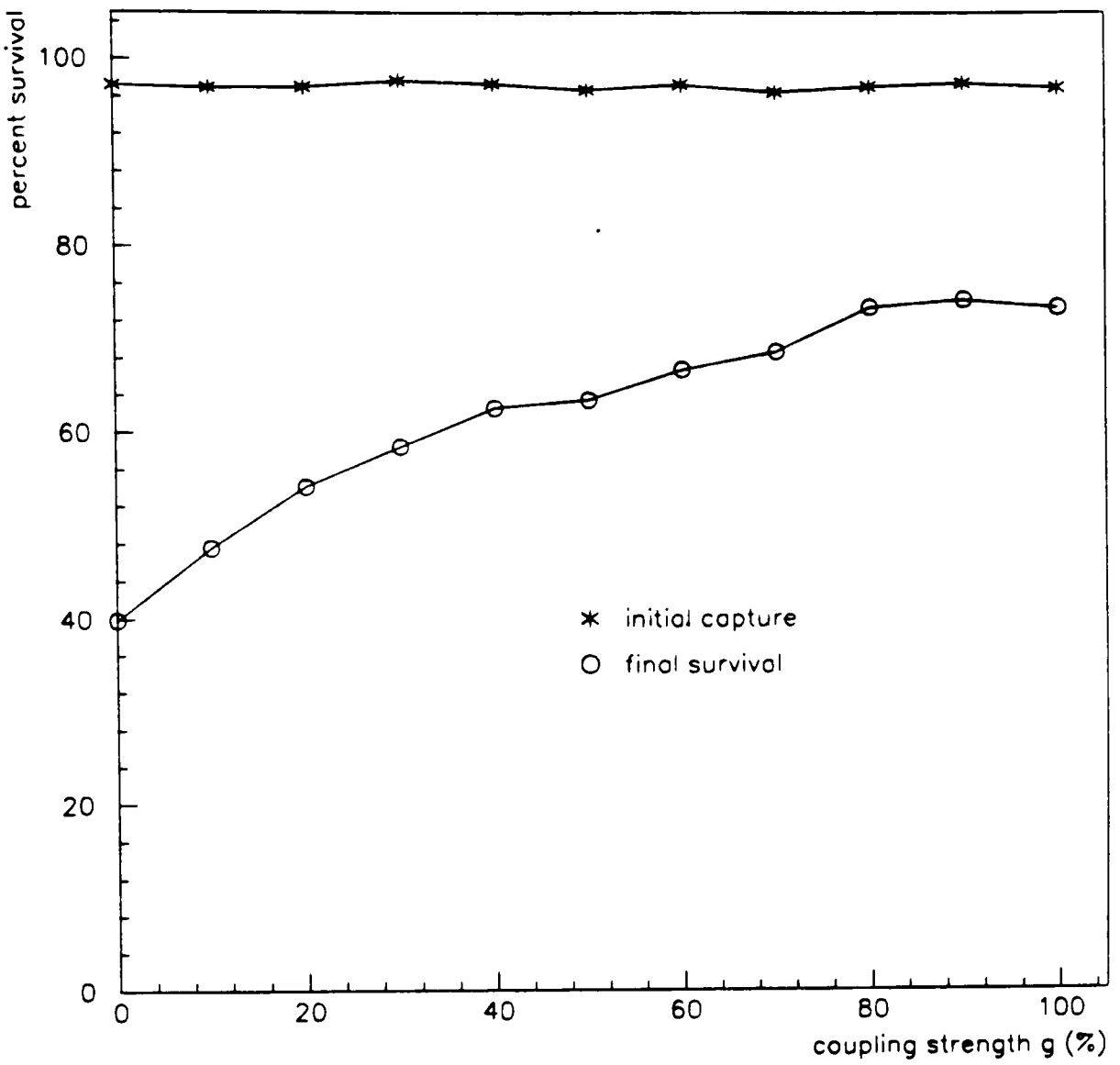


Figure 4.19: Variation of injection efficiencies as a function of the coupling strength g between horizontal and vertical phase space.

variation as without coupling with the vertical phase space and the final survival percentages have their maximum at the same values of δ_m and $\Delta x'_{\mathbf{max}}$.

Because the tune point has to be exactly at the coupling resonance, the only realistic value for g to be used in the damping simulation is 100 %, but it is instructive to see how the ring acceptance varies with g, and obtain a feeling for the effect of the amount of coupling on the ring acceptance. This variation is shown in figure 4.19. The calculations are made with $\delta_m = 1$ %. The figure shows that there is a smooth increase in final survival with g and that the maximum survival is already reached at about $g = 80\%$, after which it stays close to its maximum.

Without coupling with the vertical phase space the final survival percentage at 35 MeV is 9 %. With full coupling with the vertical phase space this increases to

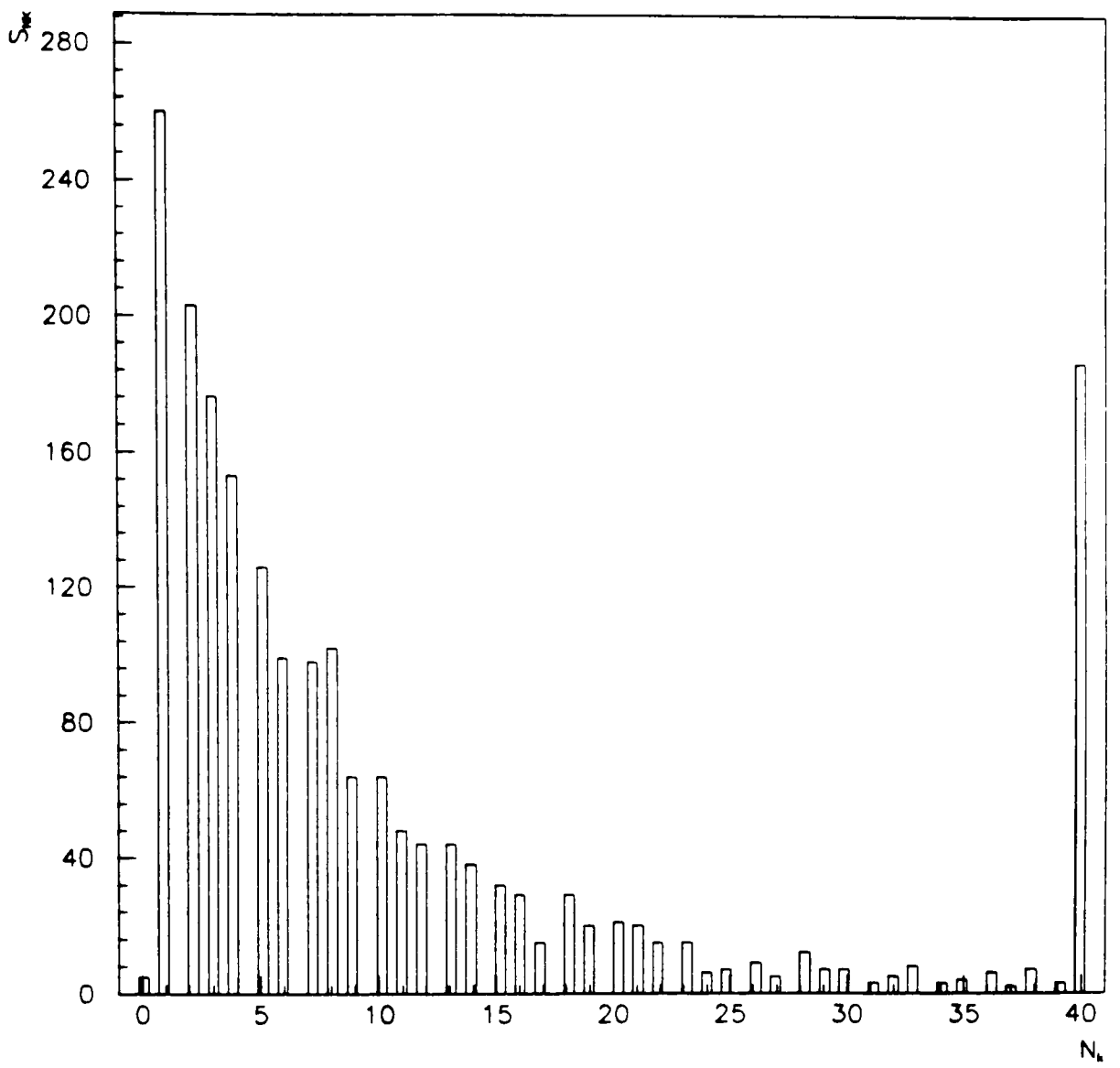


Figure 4.20: Loss of electrons for 25 MeV injection as a function of the number of kicker pulses applied; for 40 kicker pulses S_{NK} is the number of electrons still present in the accelerator.

36 %. For both calculations to be done correctly the number of simulated kicker pulses has to be increased to at least 40 (this is a simulation of synchrotron radiation damping over 4 s, which is about the same as the longitudinal radiation damping time, but only one quarter of the radial damping time). At lower energies the excitation of the betatron oscillation by the kicker magnet is not compensated any more by the synchrotron radiation damping. This is shown in figure 4.20 for 25 MeV injection, where just before the last kicker pulse is applied ($N_k = 40$), electrons are still lost because of kicker excitation. Reducing the kicker strength does not give a large improvement and electrons are still lost after many kicker pulses. It can be concluded that although the injection efficiency is increased at low energies by including coupling with the vertical phase space in the calculations, the predicted

lower limit of the injection energy does not significantly decrease by including coupling between the two transverse phase spaces. This is only valid if the beam is injected off-energy; for on-energy injection the introduction of coupling with the vertical phase space decreases the lower limit of the injection energy.

4.2.3 Simulations for MAX

MAX is a 550 MeV conventional electron storage ring with a circumference of 32 m. There are 8 dipole magnets and different families of focusing and defocusing quadrupole magnets. Injection takes place in the horizontal plane from the inside of the ring (x is negative) at an energy of 100 MeV using a repetition rate of 10 Hz, although the synchrotron radiation damping times are $\tau_x = 2.8$ s, $\tau_y = 2.9$ s and $\tau_\epsilon = 1.5$ s. The injector is a 100 MeV race-track microtron. The storage ring is described in detail in [ERI82, LIN83] and the microtron injector in [ERI87].

Injection is very similar to the system used for HELIOS: it is a multi-turn – multi-shot system and only a single kicker magnet is used. The kicker pulse also has a half-sine pulse shape. At the septum the dispersion function has its maximum, which is approximately 1 m; this introduces the possibility of coupling with the longitudinal phase space by injecting slightly off-energy.

The injection conditions, as modelled within the program MCIS, are listed in table 4.3. They agree with the routinely used injection conditions for MAX, although the septum thickness is doubled and a value considered to be realistic has been chosen for the injection position x_m . For the calculations where coupling with the vertical phase space is included the vertical tune is slightly changed to 1.11, so that the calculations take place exactly at a coupling resonance.

The results of MCIS calculations with and without coupling are listed in table 4.4. Again coupling with the longitudinal phase space is more effective than coupling with the vertical phase space because of the shorter longitudinal damping time. The variation of the injection efficiencies with δ_m is shown in figure 4.21. If the injection efficiencies are calculated for different coupling strengths g, as is shown for

Table 4.3: Standard settings for MCIS runs for MAX.

Injection energy	100	MeV
Betatron tunes ν_x , ν_y	3.11, 1.16	
RF-voltage	170	kV
Injection frequency	10	Hz
Injection position x_m and σ_x	-22.5 $\pm$ 0.32	mm
Injection divergence x'_m and $\sigma_{x'}$	0.0 $\pm$ 0.32	mrad
Injection energy deviation δ_m and σ_δ	-0.7 $\pm$ 0.1	%
Kicker magnet pulse length	3000	ns
Maximum kick by the kicker	0.5	mrad
Start injector pulse relative to kicker	1200	ns
End injector pulse relative to kicker	2200	ns
Micro-bunch structure parameter	1	
Outer limiting aperture	22.0	mm
Inner limiting aperture	20.0	mm

Table 4.4: Results of MCIS simulations for MAX.

	initial capture		*final survival*	
	$\delta_m = 0$ %	$\delta_m = -0.7$ %	$\delta_m = 0$ %	$\delta_m = -0.7$ %
No vertic. coupl.	17 %	61 %	2 %	29 %
Full vertic. coupl.	20 %	67 %	12 %	57 %

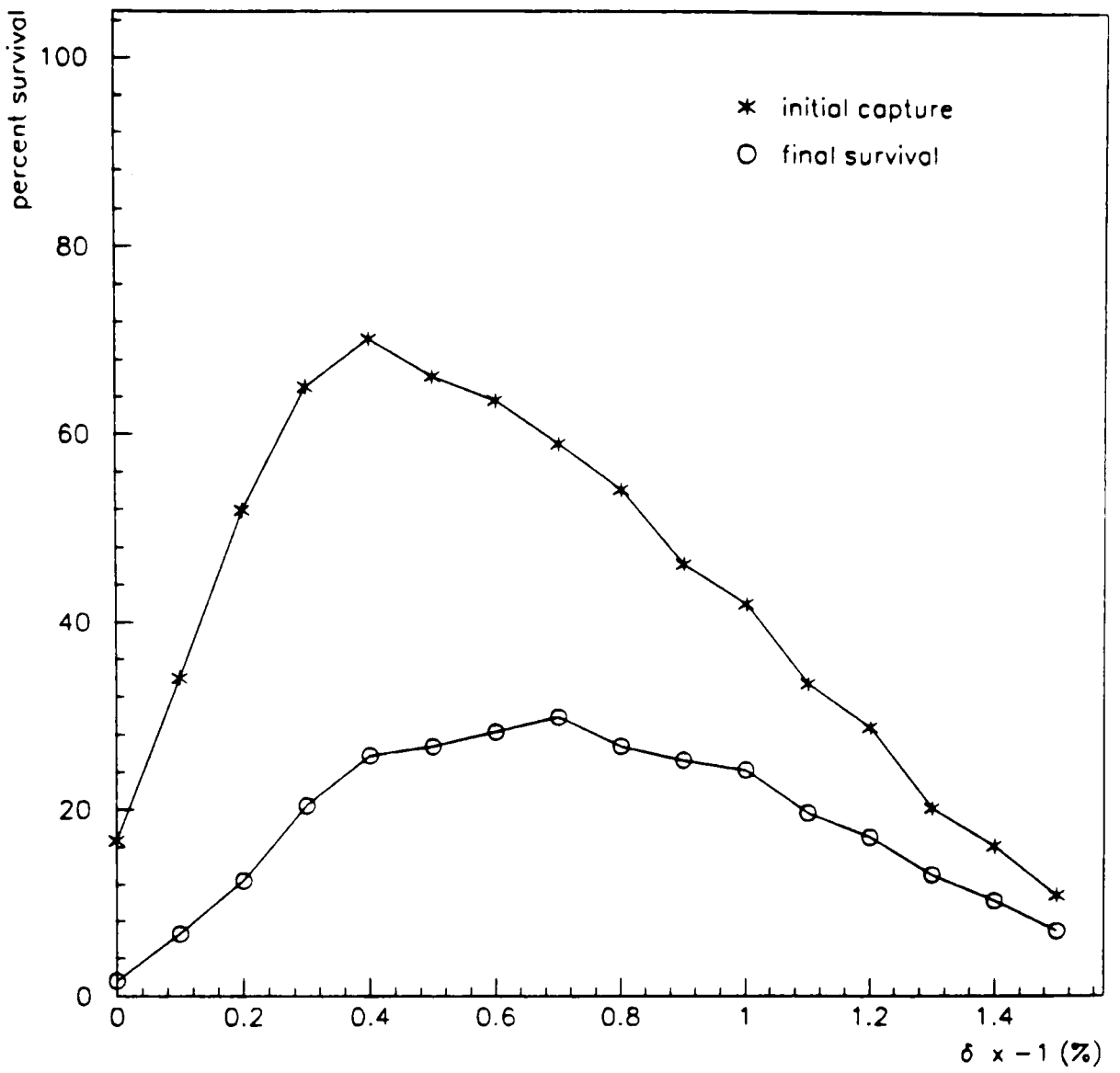


Figure 4.21: The variation of the capture percentages with the relative energy deviation of the injected beam as calculated for MAX.

HELIOS in figure 4.19, the final survival percentage already reaches its maximum around $g = 30$ %.

In general the injection efficiencies are smaller for MAX at 100 MeV than they are for HELIOS at 50 MeV, although the radiation damping times are shorter. This is probably caused by the much longer kicker pulse (injection takes place over 10 turns instead of 3), which excites the previously injected beam much more strongly than at HELIOS. Figure 4.22 shows the injection efficiencies as a function of the timing of the injected beam relative to the kicker pulse, using a very short injector pulse. It it interesting that the optimum injection efficiency is obtained before the kicker pulse has reached its maximum strength. There is also a large decrease in efficiency for electrons injected with a relative kicker timing between 1700 and 2100 ns. This

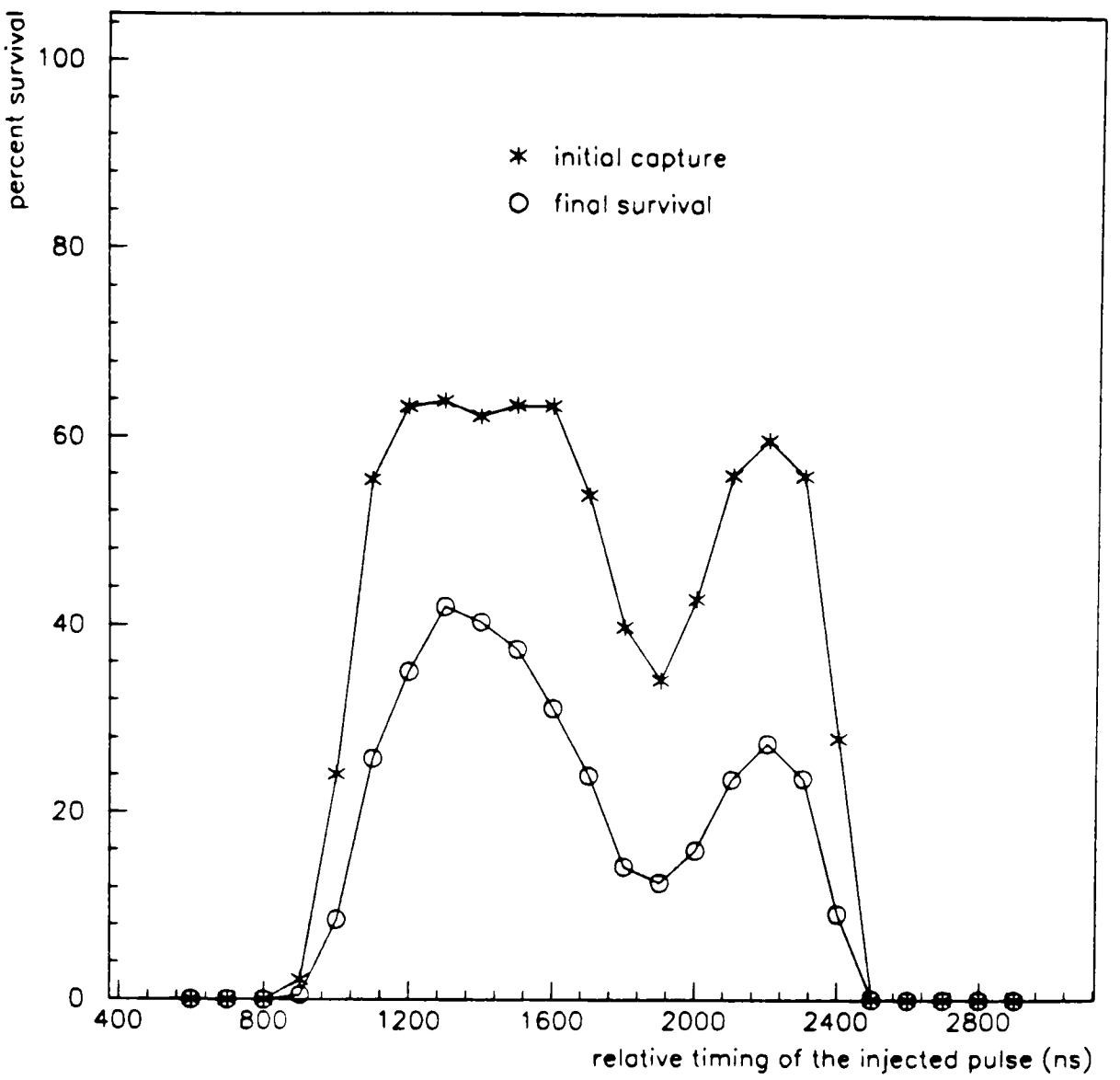


Figure 4.22: Injection efficiencies for a 1 ns long injector pulse, scanning the timing of injection. The calculations are made for MAX.

dip in the injection efficiency is not fully understood yet. It is also seen at the tail of the injected pulse in HELIOS (see figure 4.17), but it is less significant because of the shorter kicker pulse.

The presented calculations for HELIOS and for MAX result in realistic standard settings for both accelerators. If any of the variables is changed, the result agrees with the physical understanding of the injection process. This is a good starting point for chapter 5, where MCIS calculations are compared with experimental results.

Chapter 5

Experimental Results

Removed, see volume II.

5.4 Results from other Machines

There are two other machines within Europe which operate with a low-energy injection system. These are the MAX storage ring in Sweden and the compact synchrotron COSY in Berlin. Their injection results, as reported by their laboratories, are briefly discussed below.

5.4.1 Experimental Results MAX

The MAX accelerator is described in section 4.2.3. In the same section results of MCIS simulations for the operational injection energy of 100 MeV are presented. Without taking into account any coupling between the different phase spaces, the final survival percentage resulting from the simulations is only 2 %, which in practise would make the injection process very difficult. Introducing full coupling between all three phase spaces increases this to 57 %. At 100 MeV the damping times are $\tau_x = 2.8$ s, $\tau_y = 2.9$ s and $\tau_\varepsilon = 1.5$ s, and the injection takes place with a repetition rate of 10 Hz.

Routine injection at MAX is very fast: a 200 mA - 300 mA beam can be injected in about 10 s. But assuming that injection takes place over 10 turns, with an average microtron current of 8 mA, the injection efficiency is only 3 %. This is measured for operation without a pre-buncher and theoretically 5/6 of the injected beam is lost in longitudinal phase space after injection. Taking this into account, results in an effective injection efficiency of 18 %. With the use of the pre-buncher, which bunches the electrons in a bunch that can be injected at the centre of a ring RF-bunch at the synchronous phase ϕ_s (see figure 3.7), it is experimentally found that the stack rate increases by almost the expected factor 6 and in practice the injected current has to be reduced to prevent fatal beam loading of the ring RF-cavity.

No skew quadrupoles are used during injection, but the tune point is close to a coupling resonance ($\nu_x = 3.11$ and $\nu_y = 1.16$). It is possible that some coupling is introduced by ions: the stack rate is found to depend on the amount of ion clearing applied and is also larger if the ring vacuum is not at its best, which can also be an ion effect. It is possible that ions stabilise multi-particle instabilities, because

of the resulting beam blow-up, and/or give the necessary coupling between the two transverse phase spaces which theoretically improves the injection efficiency. The fast stacking does not occur in single-bunch mode; this is possibly a multi-particle instability or an ion effect.

Experiments with injection at lower energies, down to 65 MeV, have been performed. Injection at the lower energies is slightly more difficult but still very good. The main difference could be caused by having spent less time optimising the system at lower energies. At 65 MeV the damping times for MAX are $\tau_x = 10.1$ s, $\tau_y = 10.7$ s and $\tau_\epsilon = 5.5$ s

No detailed measurements have been performed to prove the presence of off-energy injection or the coupling between the two transverse phase space. Calculations with MCIS give only 1.6 % final survival if no coupling, with either longitudinal or transverse phase space, is present, but good survival if coupling is introduced (see table 4.4). This leads to the conclusion that there must be some coupling present. The measured survival percentage is higher than the theoretical results for only transverse coupling, so it is very likely that off-energy injection takes place.

5.4.2 Experimental Results COSY

COSY is a COmpact SYnchrotron, similar to HELIOS, with two 180° super conducting dipoles. The lattice differs in having one focusing and one defocusing quadrupole in each straight. The final energy is 592 MeV and a 50 MeV race-track microtron is used as injector. The circumference is 9.6 m, which is exactly the same as for HELIOS. The injection is also multi-turn and multi-shot, but takes place in the vertical direction. It is chosen to be vertical because the dispersion at the septum position is around 1.8 m and even larger in the focusing quadrupoles. This makes the horizontal orbit very sensitive to energy deviations in the beam and if injection would take place in the horizontal plane, the variation in energy of the injected particles could be critical and cause beam loss. There are three fast pulsed kicker magnets situated in the injection straight available for injection, but successful injection has been obtained with only one kicker magnet.

Currents up to 95 mA have been stored at injection energy, but no information is available about the stack rate. The damping times for COSY at 50 MeV are around 3 s, while the kicker magnet is pulsed at 10 Hz [HOL88]. Ions seem to play an important role during injection and have a large effect on the beam life time. The machine and the first injection results, using normal conducting magnets, are described in more detail in [WEI88].

Because COSY has synchrotron radiation damping times much longer than the injection interval, it is difficult to understand the injection results without including coupling between the radial and vertical phase space in the model. Considering the MCIS results for HELIOS, including coupling between the two transverse phase spaces only, the fact that COSY can inject is an indirect proof of the validity of MCIS and the underlying theories.

Chapter 6

Summary, Discussion and Conclusions

The work presented in this thesis is summarised in section 6.1. A brief discussion of some topics takes place in section 6.2, after which the final conclusions are made in section 6.3.

6.1 Summary

Studies of multi-shot injection in electron synchrotrons normally consider only the phase space in which the beam is injected and separate calculations are made for the newly injected beam and the previously stored beam. According to these calculations injection at low energies, where the synchrotron radiation damping times are much larger than the injection interval, is impossible. It also has to be considered that in this situation the separation of injected and stored beam is not valid and the modelling of the injection process using this conventional method is incorrect.

In this work a new approach to injection calculations for low energies is introduced: synchrotron radiation damping is simulated, integrating the calculations for the injected beam and the stored beam, and successful injection at low energies is explained by taking into account the coupling between the different phase spaces. A statistical approach to the problem is used, in which many particles with different starting conditions are generated. After each damping period the parameters are partially randomised.

Off-energy injection improves the injection efficiency significantly because it introduces coupling between the longitudinal and radial phase space. This is only true if there is horizontal dispersion at the septum position. The coupling with the longitudinal phase space is extremely effective in HELIOS because the radiation damping time τ_ϵ is much smaller than either τ_x or τ_y ($\tau_\epsilon = 1.3$ s, $\tau_x = 5.4$ s and $\tau_y = 3.2$ s at 50 MeV).

Besides the shorter damping time there is also an advantage in introducing coupling with the longitudinal phase space because of the random behaviour of the beam. Relative to the synchrotron tune of the electrons, the kicker is pulsed at a random time. If at this moment the energy deviation of a certain electron is negative, the centre of the horizontal phase space ellipse is displaced away from the septum (assuming that injection takes place from the outside and the dispersion is positive at the septum position). In this situation it is less likely that the kicker pulse has a fatal effect on the 'stored' electron than without any significant energy oscillation and the chances for survival are increased.

The coupling of the horizontal phase space with the vertical phase space can be modelled by the introduction of a skew quadrupole magnet. For HELIOS the advantage of coupling with the vertical phase space is not caused by the smaller vertical synchrotron radiation damping time ($\tau_y \approx \tau_x$). The positive effect of the coupling is caused by a similar process to that which takes place in longitudinal phase space: relative to the beating of the emittance between the horizontal and vertical phase space, the kicker magnet is pulsed at a random time. If at that moment the horizontal particle emittance is small (it is largely coupled into the vertical plane), it is very unlikely that the particle will be lost because of the kicker magnet pulse.

The program MCIS has been developed to quantify these new theories. Results of calculations are presented for both HELIOS and MAX. In the 'classical model', without coupling between the phase spaces, injection in HELIOS at 50 MeV and a repetition rate of 10 Hz is practically impossible: the calculated final survival percentage is only 3 %. This is relatively obvious considering that the radial synchrotron radiation damping time $\tau_x = 5.4$ s. Introducing coupling with the longitudinal phase

space by injecting electrons with an energy 1.0 % larger than the ring energy, and also taking into account that the beam has an energy spread $\sigma_\epsilon = 0.25\%$, increases the modelled efficiency to 39 %. The effect of full coupling with the vertical phase space is indeed less strong: the final survival percentage increases to 23 %. Including coupling of all three phase spaces gives the maximum survival percentage of 73 %.

The calculations for MAX, at the actual injection energy of 100 MeV, show a very similar behaviour: without introducing any coupling injection is virtually impossible. The inclusion of coupling results in good injection efficiencies; again coupling with the longitudinal phase space is most effective because of the shorter longitudinal damping time. The injection efficiencies for MAX are smaller than for HELIOS, although the damping times for MAX are shorter. This can be explained by the much longer kicker pulse used in MAX, which excites the previously injected beam more strongly, resulting in particle loss. There is a minimum in the injection efficiency at the middle of the injected beam pulse which is not fully understood.

Several parameter scans for HELIOS are presented in chapter 4. They all confirm the expected smooth behaviour of the survival percentages as a function of the scanned parameters. From these scans the hardware requirements for injection of all the essential elements involved in the process can be determined. A few of them are listed.

- The lowest possible injection energy, using the present multi-shot injection method, is around 35 MeV. Off-energy injection is necessary to achieve this. Additional coupling with the vertical phase space can be useful, but does not reduce the lower limit on the injection energy if longitudinal coupling is already present, because below 35 MeV the synchrotron radiation damping times are too long to damp the excitation of the beam by the kicker magnet. If no coupling with the longitudinal phase space has been included, the coupling with the vertical phase space does significantly reduce the lower limit on the injection energy.

- Calculations show that the requirements on beam size and divergence for 50 MeV injection are that σ_x is smaller than 1 mm and $\sigma_{x'}$ is smaller than

2 mrad. The energy spread of the beam should not exceed $\sigma_\epsilon \approx 0.5\%$. These values are well within the specification of a microtron injector, but not of a linac. The presently used 100 ns pulse length of the injected beam, which results in injection over 3 turns, is almost ideal.

- For a 100 ns injector pulse length, the kicker pulse length has to be about 250 ns, measured from zero to zero strength. The maximum kick at the top of the sinusoidal pulse has an optimum strength of - 9.0 mrad, assuming off-energy injection at 50 MeV with a repetition rate of 10 Hz and a radial tune $\nu_x = 1.54$. Small variations in either the length or the strength of the kicker pulse have no strong effect on the injection efficiency. Operation at higher radial tunes needs a stronger kicker magnet pulse because of the sensitivity of the closed orbit distortion to tune. At higher radial tunes the injection efficiency increases because of a smaller radial damping time τ_x.

The presented model as quantified with the program MCIS is compared with experimental results. For MAX and COSY the model confirms that injection at the present low energies is possible, using a multi-shot injection method. To the author's knowledge, no quantitative explanation of their injection mechanism has been published and no accurate measurements of the injection process for these accelerators have been carried out in order to prove the coupling between the different phase spaces.

Removed, see volume II.

6.2 Discussion

In HELIOS the dispersion η at the septum is around 1 m. This is almost an ideal value for introducing coupling with the longitudinal phase space: a larger dispersion at the septum will make the injection process very sensitive to any energy deviation within the injected beam; if on the other hand the dispersion at the septum is smaller, the energy deviation of the injected beam relative to the accelerator has to be larger to have any effect on the injection efficiency, which has the danger that the particle is lost in longitudinal phase space because of a limited energy acceptance of the accelerator. This situation where the horizontal dispersion is too large is seen at COSY, and as a consequence injection has to take place in the vertical direction. For vertical injection there is no beneficial effect of coupling with longitudinal phase space, because of the lack of vertical dispersion.

If coupling with the vertical phase space is introduced, the physical aperture in the vertical direction can become restricting. This is not included in the MCIS simulation, which makes it possible to study the underlying physics without including any hardware limitations. For HELIOS the critical position of the vertical aperture is in the middle of the dipoles where the vertical beta-function has its maximum and at the pulsed magnets where the physical aperture is small. To consider the vertical aperture problem for HELIOS in more detail, the total particle emittance is calculated for several particles, some turns after injection has taken place. This is justified because the large peaks in emittance caused by the kicker magnet are only present in the horizontal phase space (see figure 4.6) and after this 'kick' the total particle emittance is constant. The total emittance is smaller than can be expected from straight forward calculations because of coupling with the longitudinal phase space. For the standard conditions with coupling as used in chapter 4, the averaged total emittance $\mathcal{E}_T = 67$ mm mrad and the spread within the data is $\sigma_{\mathcal{E}_T} = 27$ mm mrad. Using the average value for $\mathcal{E}_T$ and the local beta-functions, there is only about 0.5 mm difference between the maximum particle position and the limiting aperture at both the pulsed magnets and the dipoles. This means that

considering the spread in $\mathcal{E}_T$, the vertical aperture is critical and including this in the model will reduce the efficiency for full coupling with the vertical phase space significantly. The calculations presented in chapter 4 indicate that it is not necessary to have full coupling to substantially increase the final survival percentage, which limits the effect of a critical vertical aperture. To quantify the effect of a critical physical aperture in more detail, MCIS has to be extended to check the vertical particle position against the critical aperture.

The coupling with the vertical phase space can only be modelled exactly within the program MCIS at a coupling resonance. Away from the resonance the skew quadrupole has to be stronger to give the desired coupling, but for stronger skew quadrupole fields the method used for calculating the particle emittance is not valid any more. Using a different method to calculate the particle emittance (for example by describing the motion of the electron in the normal planes of the coupled motion, see [GUI76, EDW73, TEN88]) can make the program valid at any combination of horizontal and vertical betatron tune. This more general approach of calculating the particle emittance is not used because it is more complicated and it is believed that the desired insight into the effect of coupling between the two transverse phase spaces can be obtained by the described calculations on a coupling resonance. Similar behaviour is expected for tune points not too far away from a coupling resonance, where the total particle emittance is conserved. If the tune point is closer to a sum resonance and the total emittance is not constant (see section 2.3), injection will be worse because of the emittance blow up. This states the obvious advice not to inject near a sum resonance if significant coupling with the vertical phase space is present.

The coupling with the vertical phase space can be caused by a skew quadrupole magnet, as in the model, but it is also possible that it is caused by the electric field of the ions in the residual gas which focuses the beam. The transverse coupling not only has a positive effect on the stack rate, but can also increase the beam life-time: because the beam volume is increased through the coupling, the beam density

decreases which can limit the effect of some multi-particle instabilities (Touschek effect). Also the tune spread caused by the nonlinear effects of the ion potential can counteract instabilities in the beam (Landau damping). On the other hand, ions increase the effective pressure as seen by the beam, which reduces the beam lifetime determined by scattering on residual gas molecules. All three accelerators considered show a strong dependence of the stack rate on the ion clearing applied, which is used to reduce the number of ions in the beam. The beam lifetime in COSY strongly depends on the amount of ion clearing applied. This indicates the presence of a significant amount of ions, so the success of low-energy injection at 50 MeV might be explained through coupling between the two transverse phase spaces. In MAX the injection stack rate depends critically on the amount of ions present; there seems to be an *optimum* amount of ions resulting in the largest stack rate. Considering the different positive and negative effects of ions, this is not impossible.

Some general theories of ions affecting the beam can be found in [BAC85, PON90], and studies of the effect of ions in compact synchrotrons can be found in [TAK90, GOM89]. Because the effect of ions is stronger at lower energies, it plays an important role in low-energy injection systems. A further study of the effect of ions during injection will be very useful.

Calculations for HELIOS at 35 MeV result in an injection efficiency of 9 %, including coupling with the longitudinal phase space only. This energy is assumed to be about the lower limit on the injection energy for HELIOS, considering that this percentage is possibly reduced because of multi-particle instabilities. At lower energies the injection efficiency drops sharply, because the excitation of the beam by the kicker pulse can not be damped by the synchrotron radiation damping. This means that no particle is safely trapped and the injection efficiency is zero. The mentioned injection efficiencies are all calculated for a repetition rate of 10 Hz. Repetition rates below 10 Hz result in a reduced lower limit on the injection energy, but because the radiation damping times vary with energy as $1/E^3$ this is not very effective: reducing the repetition rate by a factor of 2 allows the injection energy to be decreased by only a factor of $\sqrt[3]{2} = 1.26$. These simple assumptions agree

with simulations at 25 MeV, which result in 10 % final survival for a repetition rate of 3.5 Hz (injecting off-energy but no coupling with the vertical phase space). Extending this to lower energies: injection at 15 MeV needs a repetition rate of less than 0.8 Hz to obtain the same survival percentage (the emittance blow up of the injected beam is not taken into account). At these low energies and long times necessary for injection one seriously has to consider instabilities (ions) and other beam lifetime effects. It can be concluded that reducing the injection repetition rate is not a very effective way of lowering the limit of the injection energy.

There are several suggestions for further experimental verification of the model. Measurements of δ_m could be made for different values of the ring dipole field, using the same method as presented in chapter 5, while simultaneously measuring the stack rate. Also the repetition of these measurements at lower injection energies would be interesting. Measurements of the stack rate for different fields of the skew quadrupole magnet, and also studying the beam sizes on the synchrotron light monitor at the same time, can experimentally quantify the effect of coupling between the horizontal and vertical phase space. Detailed quantifying experiments at other electron synchrotrons, including the ones using a multi-kicker injection system, would be useful to give further proof of the presented model.

6.3 Conclusions

- Off-energy injection is a very effective method of increasing the injection efficiency at low energies for a multi-shot injection system. Coupling with the vertical phase space also increases the injection efficiency, but the effect is generally less strong.

- The general behaviour of injection as a function of several parameters is reasonably consistent with the MCIS simulation. In particular the agreement between calculated and measured optimum values of the kicker strength $\Delta x'$ and especially of the energy deviation of the injected beam relative to the ring energy δ_m give confidence in the model presented. The existence and strength

of the coupling between longitudinal and radial phase space is proven by the measurement of δ_m. The belief in the general validity of the model is reinforced by its agreement with the overall injection behaviour of accelerators other than HELIOS. These accelerators inject successfully at low energies; this can not be explained without taking into account the coupling between the different phase spaces.

- The simulation predicts a lower limit for the injection energy of HELIOS of about 35 MeV, using the present multi-shot injection method. The injected beam has to be of good quality. The required standards are generally met by a microtron injector.

Chapter 7

Experimental Background

Removed, see volume II.

Appendix A

Equations of Motion up to Second Order

In chapter 2 the differential equations for the motion in the x and y direction are derived up to first order in x, x', y, y' and δ. In this appendix this derivation is extended up to second order, including magnetic field terms up to sextupole order.

Equations 2.11 and 2.12 are generally valid and are taken as a start of the second order derivation. For the magnetic field the following expansion is taken (note that the symbol K used in chapter 2, is now replaced by the small letter k):

$$\frac{q}{p_0}B_x = ky + m_1xy \tag{A.1}$$

$$\frac{q}{p_0}B_y = h + kx + \frac{1}{2}m_1x^2 - \frac{1}{2}m_2y^2 \tag{A.2}$$

$$\frac{q}{p_0}B_s = h'y \tag{A.3}$$

where

$$h = \frac{q}{p_0}B_0 = \frac{1}{\rho} \tag{A.4}$$

$$k = \frac{q}{p_0}\frac{\partial B_y}{\partial x} \tag{A.5}$$

$$m_1 \approx \frac{q}{p_0}\frac{\partial^2 B_y}{\partial x^2} \tag{A.6}$$

$$m_2 \approx \frac{q}{p_0}\frac{\partial^2 B_x}{\partial y^2} \tag{A.7}$$

The approximately equal sign in equations A.6 and A.7 indicates that the effects of higher than sextupole order terms are neglected.

In the curvilinear coordinate system Maxwell's equations give the relations between the different components of the magnetic field [CAS85]. This results for example in the relation between the two different sextupole coefficients:

$$\frac{\partial^2 B_y}{\partial x^2} = \frac{\partial^2 B_x}{\partial y^2} + \frac{\partial^2 B_0}{\partial s^2} + \frac{1}{\rho}\frac{\partial B_y}{\partial x} \tag{A.8}$$

Expanding the square root in equations 2.11 and 2.12 and truncating at second order in x, x', y, y' and δ leads to the equations of motion of interest. The off-energy terms are again included by introducing $p = p_0 + \Delta p$ and $\delta = \Delta p / p_0$.

$$x'' + (h^2 + k)x - \delta h + \delta^2 h - \delta(2h^2 + k)x =$$
$$h'(xx' + yy') - (\frac{1}{2}m_1 + 2hk + h^3)x^2 + \frac{1}{2}m_2 y^2 + \frac{1}{2}h(x'^2 - y'^2) \tag{A.9}$$

$$y'' - ky + \delta ky = h'(xy' - yx') + (m_1 + 2hk)xy + hx'y' \tag{A.10}$$

These equations of motion have several terms depending on the bending radius ρ which are normally neglected. The significance of these terms for accelerators with a small bending radius is shown in [ARC91], both by an estimation of the size of some of the terms and the effect of them on the results of tracking calculations.

Appendix B

Input and Output Parameters of MCIS

B.1 Input Parameters

The input list of MCIS can be divided into four sections:

1. The first line.

2. Definition of the different element types used in the lattice representing the accelerator.

3. Definition of the order of the element types in the lattice.

4. All other parameters defining the simulation.

Each section will now be described in more detail:

Section 1: The First Line

The first line consists of:

$NCELL \qquad NEL \qquad NTYP \qquad E$

where

$NCELL$ = number of unit cells in the machine (the periodicity of the lattice).

NEL = total number of elements in the lattice (maximum 500).

$NTYP$ = number of different elements types in the lattice (maximum 150).

E = energy of the accelerator [GeV].

Section 2: The Different Element Types

The second section consists of $NTYP$ lines, defining the different element types. Each line defines one element type and consists of seven different parameters:

A B C D E F G

The last parameter is a possible division of the element in sub-elements. This has no effect on the injection calculations, so one can always take $G = 1$. The different groups of elements with their parameters are:

$A = 1$: Sector bending magnet

B = element length, C = entrance angle, D = radius of curvature, E = exit angle, F = sextupole gradient.

$A = 2$: Gradient bending magnet

B = element length, C = magnetic field index n, D = bending radius, E = entrance and exit angle, F = sextupole gradient.

$A = 3$: Horizontally focusing quadrupole and also $A = 4$: Vertically focusing quadrupole

B = element length, C = quadrupole gradient [T/m], $D = 0, E = 0, F = 0$.

$A = 5$: Straight section, drift

B = element length, $C = 0, D = 0, E = 0, F = 0$.

$A = 8$: Thin lens skew quadrupole

B = magnetic field gradient multiplied by the element length [T], $C = 0, D = 0$, $E = 0, F = 0$.

$A = 10$: Thin lens kicker magnet

B = maximum angular kick by kicker magnet $\Delta x'_{\mathbf{max}}$ [mrad], C = period of the half-sine pulse [ns], $D = 0, E = 0, F = 0$.

Section 3: The Order of the Element Types

This is a free format list of NEL elements, defining the order of the previously defined elements. It is possible to use one element several times.

Section 4: All Other Parameters

The other parameters necessary to define the simulation are:

ν_x *el*1 ν_y *el*2

h $\hat{V}_{rf}$

Nmicro

RR

Npart Nturn Nkick

x_m x'_m y_m y'_m δ_m

σ_x $\sigma_{x'}$ σ_y $\sigma_{y'}$ σ_δ

BS BE

g

Wsum Wlos Wdamp Wturn Wtwiss

Aout Ain

The symbols represent: ν_x, ν_y: horizontal and vertical betatron tune; $el1, el2$: the number of the two types of element which are used to set the tune; h: harmonic number; $\hat{V}_{rf}$: amplitude of the RF-voltage [kV]; *Nmicro*: micro-bunch structure number, either 1 or 3; *RR*: injection repetition rate [Hz]; *Npart*: number of particles for which the simulation takes place; *Nturn*: number of turns over which the particles are tracked between the damping simulations; *Nkick*: number of simulated kicker pulses; x_m, x'_m: centre of the injected beam in horizontal phase space[mm, mrad]; y_m, y'_m: centre of the injected beam in vertical phase space [mm, mrad]; δ_m mean value of the energy deviation of the injected beam [%]; $\sigma_x, \sigma_{x'}, \sigma_y, \sigma_{y'}, \sigma_\delta$: standard deviations of the normal distributions from which the initial coordinates of the injected beam are generated; BS, BE: Start and End of the injected Beam pulse relative to the start of the kicker pulse at t_0 [ns]; g: the coupling strength used in the damping routine [%]; *Wsum*: if equal to 1, for every particle a summary of the simulation is written to file, listing the initial and final parameters and the number of turns after which the particle is lost (if it is lost); *Wlos*: if equal to 1, an array with the rate of particle loss S_{NK} is written to a separate file; *Wdamp*:

if equal to 1, the coordinates of all particles in all three phase spaces is written to separate files each time synchrotron radiation damping is simulated; *Wturn*: the same as *Wdamp*, but now for every turn during the tracking; *Wtwiss* if equal to 1, a list of the Twiss parameters and the dispersion function as a function of position is written to a separate file; *Aout*: the outer limiting aperture [mm]; *Ain*: the inner limiting aperture [mm].

B.2 Output Parameters

Besides the extra options listed in section B.1, the program always generates a summary file. The summary file for the standard settings for HELIOS, which includes full coupling with the vertical phase space, is given in figure B.1.

B.3 CPU-time

The required CPU-time for one simulation depends linearly on the number of particles in the simulation and almost linearly on the survival percentage. For the standard settings, as given in figure B.1, the required CPU-time on an Apollo DN10000 workstation is about 20 minutes. On a VAX 8700 mainframe the required CPU-time is close to one hour.

```
**************************************************************
*   This is the Monte Carlo Injection Simulation program     *
*                          MCIS                              *
*                   version 3.2 (06/06/90)                   *
**************************************************************

ENERGY =  0.050 GEV
UNIT CELL LENGTH =    9.600 M
QH =  1.53999  QV =  0.53996 AFTER  3 ITERATIONS

MOMENTUM COMPACTION FACTOR      : 0.2475D+00
ENERGY LOSS / TURN (KEV)        : 0.1000D-02
RADIAL OSCILLATION DAMPING TIME : 0.5414D+01
VERT.  OSCILLATION DAMPING TIME : 0.3201D+01
ENERGY OSCILLATION DAMPING TIME : 0.1329D+01
SIGMAE/E0                       : 0.5330D-04
RADIAL EMITTANCE                : 0.2773D-08

PEAK RF VOLTAGE     :  0.2000D+06 V
HARMONIC NO.        :   16
OVERVOLTAGE         :  0.1999D+06
SYNCHROTRON TUNE    :  0.5021D-01
BUNCH LENGTH        :  0.1339D-11 s
EMAX / E0           :  0.2536D-01

INJECTION FREQUENCY                                 :   10.00 Hz
NUMBER OF PARTICLES IN EACH LINAC SHOT              :  2000
NUMBER OF TURNS OVER WHICH PARTICLES ARE TRACKED:   500
NUMBER OF LINAC SHOTS                               :     1
NUMBER OF KICKER SHOTS AFTER LINAC OFF              :    15
DEMAGNINFICATION OF RUNGE-KUTTA STEP SIZE           :    10

MICROBUNCH STRUCTURE NUMBER      :  1

MEAN VALUE OF POSITION X         :    27.50 mm
              ANGLE    X1        :     3.00 mrad
              POSITION Y         :     0.00 mm
              ANGLE    Y1        :     0.00 mrad
              ENERGY DEVIATION   :     1.00 %
STANDARD DEVIATION IN POSITION X :     0.50 mm
              ANGLE    X1        :     0.50 mrad
              POSITION Y         :     0.50 mm
              ANGLE    Y1        :     0.50 mrad
              ENERGY DEVIATION   :     0.25 %
TIMING INJECTION FKT - MIN       :   125.00 ns
                 FKT - MAX       :   225.00 ns

SKEW QUADRUPOLE STRENGTH         :   0.0005 T
COUPLING INPUT PARAMETER         :   100.00 %

MAXIMUM KICK BY KICKER IS        :    -9.00 mrad
KICKER PULSE LENGTH IS           :   257.00 ns

TRACKING WITH OUTER LIMITING X APERTURE =  25.00 mm
              INNER LIMITING X APERTURE =  23.00 mm

**************************************************************
*                                                            *
* PERCENTAGE SURVIVING AFTER    1 LINAC SHOTS IS             *
*                 96.95 %                                    *
*                                                            *
* AFTER ADDITIONAL   15 KICKER PULSES, SURVIVAL IS           *
*                 73.30 %                                    *
*                                                            *
**************************************************************
```

Figure B.1: MCIS summary file for the standard settings for HELIOS, including full coupling with the vertical phase space.

Appendix C

List of HELIOS Notes and Publications

A list of HELIOS project notes and other articles, written by the author over the last three years (as single author or co-author), is given below.

Title	Date	No.
Magnetic field expansion in the dipoles	Nov.'88	HUH 78/1
Using sextupole settings for zero chromaticity in tracking calculations	Dec.'88	HUH 84/1
Design parameters of a compact 50 MeV transport line	Dec.'88	HJH 35/1
Changes to the tracking routines of the accelerator program ORBIT	Feb.'89	HAH 21/1
Linac emittance measurements	Feb.'89	HJH 36/1
Data and programs to be used for tracking calculations using the measured superconducting dipole fields	Mar.'89	HUH 89/1
Electron beam injection in the compact synchrotron HELIOS and related topics	May '89	HAH23/1
Commissioning of the 200 MeV injector linac for the Oxf.Instr. – I.B.M. synchrotron light source	'89 Particle Acc. Conf. Chicago	
Injection in HELIOS – effects due to kicker and other parameters	Jul.'89	HJH38/1

continued on next page...

... continued

Title	Date	No.
Quadrupole settings and beam parameters for the transport line	Sep.'89	HJH 37/2
Low-energy injection	Jan.'90	HAH30/1
Injection process in HELIOS 2	Mar.'90	H2AH2/1
Results of 200 MeV injection studies for HELIOS and new computer codes for commissioning	May '90	HJH51/1
Summary of the accelerator physics on the commissioning of HELIOS 1	June '90 - Oct.'90	HAC1/1 - HAC11/1
Beam sizes and divergence: acceptable?	Nov.'90	HAH40/1
Closed orbit correction to be made before shipping	Nov.'90	HAH41/1
New version of the program tune	Dec.'90	HAH43/1
Tracking studies for the Oxford Instruments compact synchrotron	'91 Particle Acc. Conf. S.Francisco	

Bibliography

[ARC91] C.N. Archie, **J.A. Uythoven**. *Tracking studies for the Oxford Instruments compact electron synchrotron.* To be presented at the 1991 IEEE Particle Accelerator Conference, San Francisco.

[BAC85] Y. Baconnier. *Neutralization of accelerator beams by ionisation of the residual gas.* CERN accelerator school, general accelerator physics, P. Bryant, S. Turner. (edt.), CERN 85 – 19 (1985).

[BAR90] M.Q. Barton, private communication.

[BEL87] J.S. Bell. *Hamiltonian mechanics.* Proceedings CERN Accelerator School advanced accelerator physics, S. Turner (edt.), CERN 87 – 03 (1987).

[BOT86] J.I.M. Botman, H.L. Hagedoorn. *Lecture notes particle accelerators.* Eindhoven University of Technology (1987).

[BRO80] K.L. Brown, D.C. Carey, Ch. Iselin, F. Rothacker. *Transport, a computer program for designing charged particle beam transport systems.* CERN 80 – 04 (1980).

[BRU66] H. Bruck. *Accélérateurs circulaires.* Presses Universitaires de France, Paris (1966).

[BRY89] P.J. Bryant. *A simple theory for weak betatron coupling.* CERN accelerator school, third general accelerator physics course, S. Turner (edt.), CERN 89 – 05 (1989).

[CAS85] edt. P. Bryant, S. Turner. *CERN accelerator school, general accelerator physics.* CERN 85 - 19 (1985).

[COU58] E.D. Courant, H.S. Snyder. *Theory of the alternating gradient synchrotron.* Ann.Phys. 3, 1 - 48 (1958).

[CUL87] E. Cullmann, T. Künneth, W. Neff, K.H. Stephan. *Comparison of different X-ray sources using the same printing process parameters.* J.Vac.Sci.Technol. B 5(3) (1987).

[EDW73] D.A. Edwards, L.C. Teng. *Parametrization of linear coupled motion in periodic systems.* IEEE Transactions on Nuclear Science (1973), Vol. NS-20, Number 3.

[EIN87] D. Einfield, P.R.W. Henkes. *The reduction of betatron oscillations by the kicker pulse of a one-kicker injection system.* Nuclear Instruments and Methods in Physics Research A267 (1988) 547 - 550.

[ELL90] P. Ellaume. *Theory of undulators and wigglers.* Proceedings CERN accelerator school on synchrotron radiation and free electron lasers, S. Turner (edt.), CERN 90 - 03 (1990).

[ERI82] M. Eriksson. *The accelerator sytem MAX.* Nuclear Instruments and Methods 196 (1982) 331 - 340.

[ERI87] M. Eriksson. *Race-track microtron injectors for SR-sources.* Nuclear Instruments and Methods in Physics Research A261 (1987) 39 - 42.

[ERI90] M. Eriksson. *Low-energy injection rings.* Nuclear Instruments and Methods in Physics Research A291 (1990), Proceedings of the 6. National Conference on Synchrotron Radiation Instrumentation, Berkeley 1989.

[GIB91] E.P. Gibbons. *Variations in cavity matching with matcher plate position.* Helios project note, Oxford Instruments, HRH16/2 (1991).

[GOM89] Y. Gomei, K. Nakayama, K. Fukushima, S. Sukenobu. *Ion trapping in a superconducting circular electron storage ring.* Nuclear Instruments and Methods in Physics Research A278 (1989) 389 – 393.

[GRO83] W.D. Grobman. *Synchrotron radiation X-ray lithography.* Handbook on synchrotron radiation, Vol. I, E.E. Koch (edt.), North-Holland Publishing Company (1983).

[GUI76] G. Guignard. *The general theory of all sum and difference resonances in a three-dimensional magnetic field in a synchrotron.* CERN 76 – 07 (1976).

[HAE89] E. Häbel. *Superconducting cavity matching and the Robinson instability limit.* CERN/EF/RF 89 – 2.

[HEU86] A. Heuberger. *X-ray lithography.* Solid State Technology, February 1986.

[HIR90] H. Hirabayashi. *Survey of compact storage rings in Japan.* Nuclear Instruments and Methods in Physics Research A291 (1990) 493 – 498.

[HOF90] A. Hofmann. *Characteristics of synchrotron radiation.* Proceedings CERN accelerator school on synchrotron radiation and free electron lasers, S. Turner (edt.), CERN 90 – 03 (1990).

[HOL88] N. Holtkamp. *Eine Darstellung des Projektes COSY vor dem Umbau auf die supraleitende Dipole.* Technischer Bericht BESSY TB 126/88 COSY (1988).

[JAC75] J.D. Jackson. *Classical electro dynamics.* John Wiley & Sons, Inc. (1975).

[LEP84] *LEP design report , Vol. I and II.* CERN-LEP/TH/83-29 (1983) and CERN-LEP/84-01 (1984).

[LAC80] J.L. Laclare. *Bunched-beam Instabilities.* 11th Conference on high energy accelerators, Geneva July 1980, Publ. Berkhäusier, Bâle.

[LAC85] J.L. Laclare. *Introduction to coherent instabilities – coasting beam case.* CERN accelerator school, general accelerator physics, P. Bryant, S. Turner. (edt.), CERN 85 - 19 (1985).

[LET89] P. Letellier, G. Meyrand, C. Perraudin, A. Setty, D.T. Tran, D. Tronc, V.C. Kempson, **J.A. Uythoven**. *Commissioning of the 200 MeV injector linac for the Oxford Instr. – IBM synchrotron light source.* Proceedings of the 1989 Particle Accelerator Conference, Chicago.

[LIN83] L.J. Lindgren, M. Eriksson. *Injection and extraction at MAX.* Nuclear Instruments and Methods 214 (1983) 179 - 187.

[MOZ58] R.F. Mozley, R.C. Smith, R.E. Taylor. *Multiple scattering of 600 MeV electrons in thin foils.* Physical Review, Vol. 111, Number 2 (1958).

[PAN62] W.K.H. Panofsky, M. Philips. *Classical electricity and magnetism.* Addison-Wesley Publishing Company (1962).

[PAW89] R. Brun, O. Couet, C. Vandoni, P. Zanarini. *PAW, Physics Analysis Workstation, user manual version 1.07.* CERN computer center, program library (1989).

[PHYa] *Review of particle properties.* Physics Letters B239, April 1990, as corrected by later erratum.

[PHYb] *Review of particle properties.* Physics Letters B239, April 1990.

[PIW85] A. Piwinski. *Beam losses and lifetime.* CERN accelerator school, general accelerator physics, P. Bryant, S. Turner. (edt.), CERN 85 – 19 (1985).

[PON90] A. Poncet. *Ion trapping and clearing.* CERN accelerator school, third advanced accelerator physcis course, S. Turner. (edt.), CERN 90 – 04 (1990).

[RIN85] T. Ring. *Beam Position Monitiors for the high brightness lattice.* Internal report SRS Daresbury, RING–85/134 (1985).

[ROB64] K.W. Robinson. *Stability of beam in radiofrequency system.* Internal report Massachusetts Institute of Technology and Harvard University CEAL 1010 (1964).

[ROS87] M.C. Ross, N. Phinney, G. Quickfall, H. Shoaee, J.C. Sheppard. *Automated emittance measurements in the SLC.* SLAC - PUB - 4278 (1987).

[SAN70] M. Sands. *The physics of electron storage rings.* SLAC-121, UC-28 (AOC) (1970).

[SOK66] A.A. Sokolov, I.M. Ternov. *Synchrotron Radiation.* Pergamon Press (1966).

[SUL73] V.P. Suller. *Comparative synchrotron radiation spectra.* Daresbury report SRS/NS/75/67 (1975).

[SUL90] V.P. Suller. *Temporal aspects of the beam in electron accelerators.* Proceedings CERN accelerator school on synchrotron radiation and free electron lasers, S. Turner (edt.), CERN 90 - 03 (1990).

[TAK90] H. Takada, Y. Tsutsui, T. Tomimasu. *Ion effects in a compact electron storage ring.* Nuclear Instruments and Methods in Physics Research A294 (1990) 373 - 381.

[TAK87a] N. Takahashi. *Compact superconducting SR ring for X-ray lithography.* Nuclear Instruments and Methods in Physics Research B24/25 (1987) 425 - 428.

[TAK87b] T. Takayama. *Resonance injection method for the compact superconducting SR-ring.* Nuclear Instruments and Methods in Physics Research B24/25 (1987) 420 - 424.

[TEN88] L.C. Teng. *Coupled transverse motion.* Lecture notes in physics Vol.343, M.Month, S. Turner (edt.). Proceedings frontiers of particle beam observation, diagnostics and corrections. Springer Verlag (1988).

[TOM56] D.H. Tomboulian, P.L. Hartman. *Spectral and angular distribution of ultra-violet radiation from the 300 MeV Cornell synchrotron.* Phys.Rev. 102, 1423 (1956).

[TOS88] *The TOSCA Reference Manual.* Vector Fields Ltd., England. VF068814 (1988).

[UYT89] **J.A. Uythoven**. *Electron beam injection in the compact synchrotron radiation source HELIOS and related topics.* First year report Department of Nuclear Physics, Oxford University; also HELIOS project note HAH23/1 (1989).

[WEI88] E. Weihreter, W. Anders, et. al. *COSY a compact electron storage ring for synchrotron radiation.* European Particle Accelerator Conference 1988, Rome, June 7 – 11, World Scientific Publishing Co.Pte.Ltd (1989).

[WEI90] E. Weihreter. *Compact superconducting synchrotron radiation sources.* Proceedings CERN accelerator school on synchrotron radiation and free electron lasers, S. Turner (edt.), CERN 90 – 03 (1990).

[WIL84a] E. Wilson. *Linear coupling.* CERN accelerator school, general accelerator physics, P. Bryant, S. Turner. (edt.), CERN 85 – 19 (1985).

[WIL84b] E. Wilson. *Transverse beam dynamics.* CERN accelerator school, general accelerator physics, P. Bryant, S. Turner. (edt.), CERN 85 – 19 (1985).

[WIL85] A.D. Wilson. *X-ray lithography: can it be justified?* SPIE Vol.537 Electron-Beam, X-Ray, and Ion-Beam Techniques for Submicrometer Lithographies IV (1985).

[WIL90] M.N. Wilson. *Compact synchrotron X-ray sources.* Proceedings of the second European Particle Accelerator Conference, Nice (1990), Editions Frontières B.P.33.

Summary in Dutch

Samenvatting

In dit proefschrift wordt de injectie van elektronen in een synchrotron opslagring bij lage energieën nader beschreven. Het accent ligt op het gebruik van een multi-puls injectiemethode over meerdere omlopen in de radiële faseruimte, met het gebruik van slechts één kicker magneet. Een nieuw model is beschreven, waarin koppeling tussen de verschillende faseruimten de injectieefficiëntie significant verhoogt. De koppeling tussen de radiële en de longitudinale faseruimte is het meest effectief, doordat in het algemeen de dempingstijd voor de synchrotron oscillaties korter is dan de dempingstijden voor de radiële en vertikale oscillaties. Het onvoorspelbaar gedrag van de deeltjes in de verschillende faseruimten over het grote aantal omlopen tussen opeenvolgende injectiepulsen verhoogt de injectieefficiëntie zowel in het geval van koppeling van de radiële met de longitudinale faseruimte als in het geval van koppeling van de radiële met de vertikale faseruimte. Koppeling met de longitudinale faseruimte wordt verkregen door te injecteren met een energie die verschilt van de evenwichtsenergie in de ring en de aanwezigheid van dispersie op de injectiepositie. Koppeling met de verticale faseruimte kan worden geïntroduceerd door gebruikmaking van een quadrupool magneet geroteerd over 45°.

Een computerprogramma, MCIS, is geschreven om dit model quantitatief te testen. Berekeningen zijn gepresenteerd voor het 700 MeV supergeleidende synchrotron HELIOS. De huidige injectieenergie is 200 MeV, maar berekeningen met MCIS tonen aan dat de injectieenergie kan worden verlaagd tot een minimum waarde van ongeveer 35 MeV. De berekeningen zijn gebaseerd op het bundeldynamische gedrag van individuële deeltjes. Om succesvol te injecteren bij een lage energie is de koppeling met de longitudinale faseruimte essentieel; voor HELIOS moet tijdens injectie de energie van de geïnjecteerde bundel ongeveer 1 % boven de evenwichtsenergie in de ring liggen. De invloed van de meeste andere variabelen in de versneller op de injectieefficiëntie is ook berekend.

De berekeningen zijn vergeleken met de resultaten van 100 MeV injectie experimenten uitgevoerd met HELIOS. Het energieverschil tussen de geïnjecteerde bundel en de evenwichtsenergie van de versneller is nauwkerig gemeten en komt overeen met de theoretische voorspellingen. Dit bewijst de aanwezigheid van koppeling met de longitudinal faseruimte voor optimale injectie condities. De optimale sterkte van de kicker magneet komt ook overeen met de theoretische voorspelling. De variatie van de injectieefficiënte als een functie van de verschillende parameters komt overeen met het model. De resultaten van de verschillende metingen geven een hoge graad van vertrouwen in de juistheid van het gepresenteerde model.

Het model is ook vergeleken met de injectie resultaten van andere versnellers die bij een lage energie injecteren. Hoewel er geen resultaten bekend zijn van gedetailleerde experimentele injectie studies van deze versnellers, leidt de globale overeenkomst tussen het injectiegedrag en berekeningen tot de conlcusie dat het gepresenteerde model algemeen geldig is.